

Digital twins for selecting the optimal ventilated strawberry packaging based on the unique hygrothermal conditions of a shipment from farm to retailer

Chandrima Shrivastava^{1,2}, Seraina Schudel¹, Kanaha Shoji¹, Daniel Onwude¹, Fátima Pereira da Silva³, Deniz Turan⁴, Maxence Paillart³, Thijs Defraeye^{1*}

¹ Empa, Swiss Federal Laboratories for Materials Science and Technology, Laboratory for Biomimetic Membranes and Textiles, Lerchenfeldstrasse 5, CH-9014 St. Gallen, Switzerland

² University of Bern, ARTORG Center for Biomedical Engineering Research, Murtenstrasse 50, CH-3008 Bern, Switzerland

³ Wageningen Food & Biobased Research, Bornse Weilanden 9, P.O. Box 17, 6700 AA, Wageningen, The Netherlands

⁴ Wageningen University and Research, Food Quality and Design, Department of Agrotechnology and Food Sciences, Bornse Weilanden 9, 6708 WG, Wageningen, The Netherlands

* Corresponding author, thijs.defraeye@empa.ch

Berries are one of the most challenging products to preserve after harvest due to their high perishability and short shelf life. Ventilated packaging plays a key role in maintaining fruit quality along the supply chain. However, every supply chain is composed of different unit operations, and every shipment encounters unique hygrothermal conditions such as air temperature fluctuations over time, sub-optimal humidity conditions, and the risk of condensation. Therefore, every supply chain has an optimal packaging that provides the best hygrothermal climate and ventilation to the fruit. Given the vast space of potential supply chain scenarios and packaging configurations, in-silico studies are an attractive alternative for selecting this optimal packaging.

In this study, we developed physics-based digital twins for ventilated packaging of strawberries. We utilized measured air temperature and humidity data from an actual supply chain from the farm to the retailer store. With these digital twins, we mimicked in-silico how the strawberries evolve hygrothermally, physiologically, and microbiologically along the supply chain inside 21 different types of ventilated packaging. We predicted actionable metrics of fruit quality and shelf life for these 21 packages. These metrics include total mass loss, risk of putative mold infection due to *Botrytis cinerea*, retention time of condensate, and remaining shelf life based on respiration, transpiration, and mold growth. In addition, we analyzed the impact of package-related metrics, such as total vent area, degree of filling, pressure drop across the package, and seven-eighths cooling time, on fruit quality metrics.

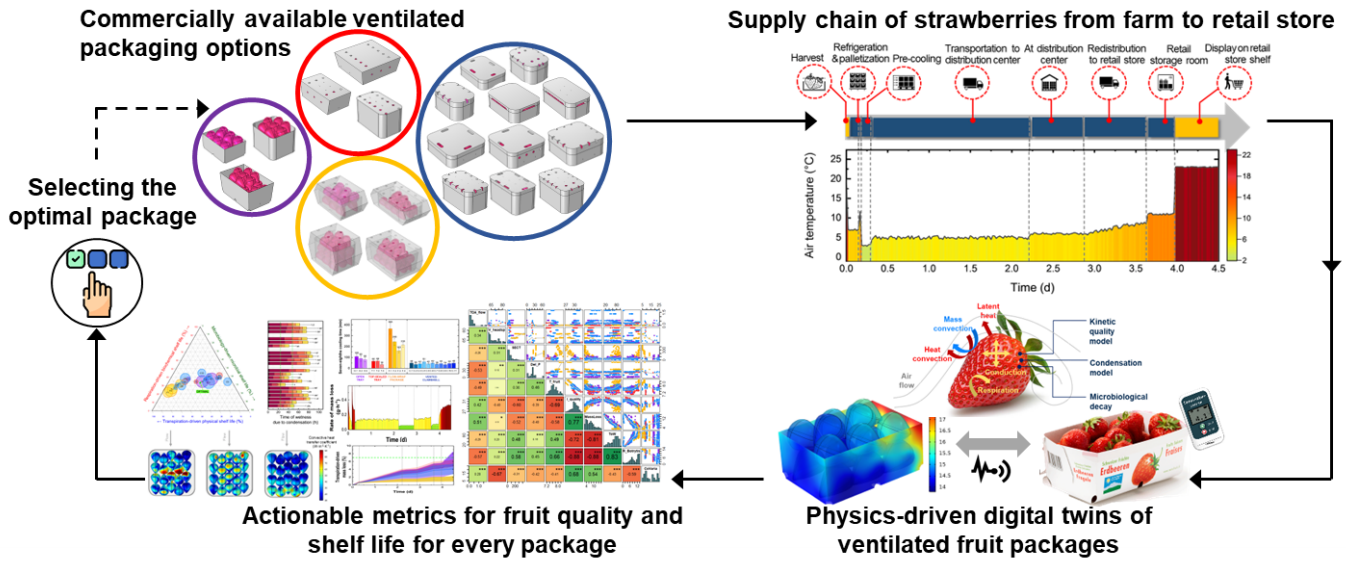
With this approach, we pinpointed the critical quality loss points in the supply chain for every package. We identified the package that performs best in balancing the three-way trade-off between the respiration-driven biochemical shelf life, transpiration-driven physical shelf life, and mold growth-driven microbial shelf life of fruit. Our findings showed that the performance of open trays is comparable to ventilated clamshells, as long as a high humidity is maintained along the supply chain. Flow-wrapped packages presented the highest risk of condensation and microbial growth. We also quantified the spatial heterogeneity in fruit quality within the packages and highlighted the most vulnerable locations for quality loss inside each packaging type. Our study presents a novel, holistic approach to select the optimal ventilated packaging of strawberries from farm to retailer based on its measured hygrothermal fingerprint. This approach can help reduce food loss and contribute towards making supply chains smart and efficient.

Keywords: multiphysics; sensor; cold chain; food loss; mechanistic modeling; ventilated packaging; condensation; clamshell; soft fruit; *Botrytis cinerea*.

Highlights

- Analyze complex trade-offs in package performance through a holistic evaluation
- Quantify hygrothermal, biochemical, and microbiological metrics for fruit quality
- Requirement-driven approach for package selection based on the intended supply chain
- Pinpoint the most vulnerable locations for the risk of condensation and mold growth
- Identify the spatial variability in fruit quality within the package

Graphical abstract



1 INTRODUCTION

Strawberries (*Fragaria x ananassa*) are one of the most challenging fresh foods to preserve along the supply chain (Ramirez et al., 2020). Postharvest losses can be as high as 40% (Porat et al., 2018; Siu, 2014; Trinetta et al., 2020). Strawberries have a high respiration rate, due to which strawberries can only be stored for 1–2 days at room temperature (Wang et al., 2019). Even under optimal conditions, viz. 0 °C at 90-95% relative humidity, the shelf life is only about 8-12 days, depending on the cultivar (Nunes, 2009; Tano et al., 2009). Due to the lack of a protective peel, strawberries are also prone to mechanical damage and moisture loss. Additionally, since strawberries are non-climacteric fruits, they are harvested almost fully ripe when they have a high water activity (~0.997), high sugar content (~7-8%), and low *pH* (~3.84) (Caner et al., 2008; Chirife and Fontan, 1982; Manteau et al., 2003). This makes strawberries particularly susceptible to spoilage by yeast and mold (Tournas and Katsoudas, 2005). *Botrytis cinerea* (or grey mold) is the most common fungal pathogen infecting strawberries (Tournas and Katsoudas, 2005; Trinetta et al., 2020). The conidia (or spores) of *B. cinerea* are omnipresent in fields and dispersed by wet splashes or air currents on the fruit surface (Ciliberti et al., 2016). These spores remain dormant until the ripened berries encounter conditions feasible for spore germination, such as elevated humidity (Abd-Elkader et al., 2021). Substantial mycelium growth is often noticeable only in the later stages of the supply chain. A very low grey mold infection level (<0.5%) is acceptable for the retail and import of strawberries, making mold growth the most frequent reason for the rejection of strawberries at retail levels (Trinetta et al., 2020; Zoffoli et al., 1999).

A good packaging strategy, coupled with maintaining an optimal hygrothermal window around the fruit, slows down the physiological and biological processes in the fruit, thus extending their shelf life. Strawberries are packed in a range of ventilated packaging in several different designs, sizes, and materials. The most commonly employed packages are ventilated clamshells. These are transparent lidded plastic boxes with vents made of (recycled) polyethylene terephthalate (PET) (Cagnon et al., 2013). Other forms of packaging include unlidded (open) punnet trays made of paperboard or plastic that may be flow-wrapped with polyethylene films or top-sealed with re-closable polypropylene films (Matar et al., 2018). These packages usually have vents on the top, bottom, and/or lateral surfaces to improve the cooling efficiency of the package and lower the risk of in-package condensation. However, the precise number, size, shape, and locations of these vents are still often determined arbitrary and designed by trial-and-error approaches (Cagnon et al., 2013). Moreover, packaging materials such as PET have high water vapor barrier properties, therefore the relative humidity in the package headspace tends to attain high values (>94%) (Bai et al., 2019; Bovi et al., 2019). High relative humidity is linked with the risk of condensation of water on fruit surfaces or package walls, which can stimulate mold growth (Linke and Geyer, 2013).

In the last decades, there has been a vast amount of research on package design in postharvest supply chains. Several studies have employed computational fluid dynamics (CFD) modeling techniques to evaluate the impact of total vent area on the cooling efficiency of different fruit packages (Ferrua and Singh, 2011a, 2009a; Mercier et al., 2017; Nalbandi et al., 2016; Nalbandi and Seiedlou, 2020; Pathare et al., 2012). Most of these studies target one unit operation in the entire supply chain, for instance, pre-cooling (Ferrua and Singh, 2011b), or quantify the cooling behavior but leave aside the impact to any fruit quality attribute. Few studies focus on the risk of condensation due to temperature fluctuations at high relative humidity or when a cooled fruit package is rewarmed to ambient temperatures (Gottschalk et al., 2007; Linke et al., 2021). Additionally, while many studies have attempted the experimental characterization of condensation (Lufu et al., 2021), the authors have reported the challenges in quantifying the spatial distribution of the risk of condensation or residence time of the condensate for several fruit in a package (Bovi et al., 2019; Linke et al., 2021). So far, very few studies have analyzed the spatio-temporal occurrences of condensation, its comparative risk amongst different packages, and the resulting impact on the microbiological quality of fruit. Moreover, every supply chain comprises a different combination of unit operations, and every shipment encounters unique logistic and environmental boundary conditions (Jalali et al., 2020). In this sense, every supply chain has different packaging requirements for providing the optimal hygrothermal climate and ventilation to the product (Cagnon et al., 2013; Defraeye et al., 2015). As such, every supply chain has its own optimal packaging design, depending, among others, on the temperature profile over time throughout all unit operations. Current approaches for packaging design do not take into consideration the whole length of unit operations along the supply chain, or the full breadth of relevant physical processes influencing fruit quality and marketability.

In this study, we developed a physics-driven digital twin of strawberries in 21 different commercially available ventilated packages, including ventilated clamshells, cardboard punnet trays, top-seal trays, and trays flow-wrapped in film packaging. A digital twin employs mechanistic simulations to mimic the hygrothermal, physiological, and microbiological evolution of the fruit in-silico (Defraeye et al., 2021, 2019; Verboven et al., 2020). It is linked with sensor data of the hygrothermal environmental conditions in an actual supply chain. We linked these twins with air temperature and humidity sensor data obtained from over 30 actual shipments of inland-transported strawberries from the farm to the retail store for a specific supply chain. With this digital twin, we predicted actionable metrics of fruit quality and shelf life for fruit in each simulated package. These metrics include total mass loss, risk of putative mold infection due to *B. cinerea*, retention time of condensate, and the remaining shelf life based on respiration, transpiration, and mold growth. For every type of package, we pinpointed the critical unit operations in the supply chain where losses are aggravated. We explored how the aerodynamic and thermodynamic metrics of the package, such as total vent area, degree of filling, pressure drop across the package, and seven-eighths cooling time, impact fruit quality attributes. We also analyzed the spatial heterogeneity within these packages and highlighted the most vulnerable locations within selected packages. Ultimately, we compared the physical, biochemical, and microbiological shelf life of berries in the 21 packages to identify the optimal ventilated package for the supply chain from the farm to the retail store. To the best of our knowledge, such a comprehensive and holistic analysis of packaging strategies in postharvest supply chains for a wide range of package types is unique and is therefore the main merit of this research.

2 MATERIALS AND METHODS

2.1 Simulated supply chain

The hygrothermal profile of the strawberry postharvest supply chain from the farm to the retail store was reconstructed based on actual measured data. We used a stochastic approach to compute air temperature and relative humidity based on the mean and variability in this segment of the measured values, using the 'rand' function for a specific range, implemented in Microsoft Excel 2016. From pack-house to retail stores, our values were derived directly from measured data for inland-transported berries from over 30 shipments from Spain to Switzerland, reported in (Shoji et al., 2022). For other segments of the supply chain, we used data from literature (Collins and Perkins-Veazie, 1993; Ferrua and Singh, 2009a; Kuchi and Sharavani, 2019; Shoji et al., 2022). The complete simulated supply chain is depicted in Figure 1. The typical air speed for every unit operation, based on the typical flow rates, are also indicated in this figure (Han et al., 2017; Li et al., 2021; Opara and Zou, 2007; Thompson et al., 2008a; Wu et al., 2019).

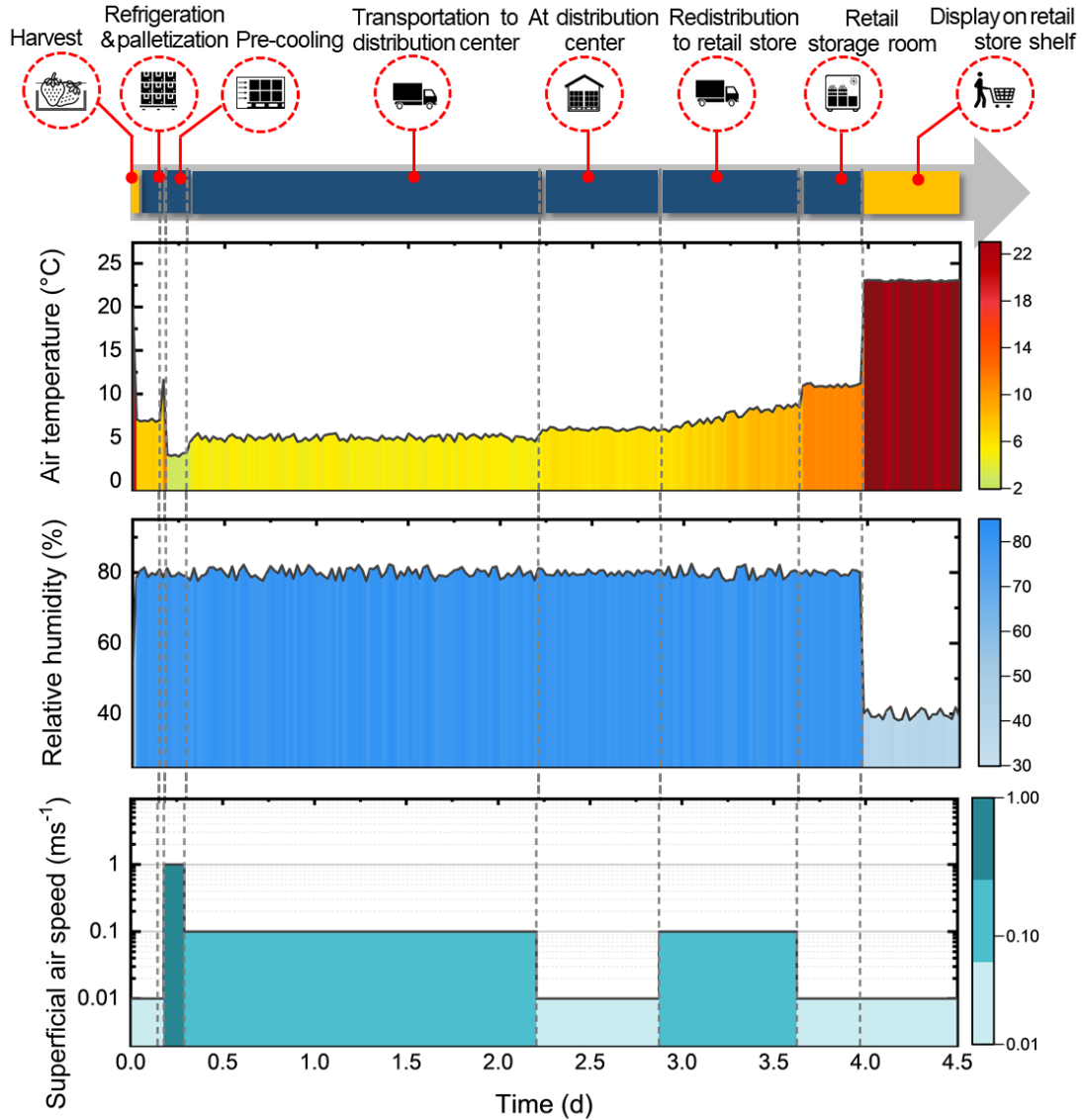


Figure 1: The simulated profile for the temperature, relative humidity, and superficial air speed of the air delivered to the packaged fruit in a typical supply chain of strawberries in-land transported from Spain to Switzerland (Collins and Perkins-Veazie, 1993; Ferrua and Singh, 2009a; Kuchi and Sharavani, 2019; Shoji et al., 2022). **These data were used as input for the physics-based digital twins. Image credits: This figure has been designed using resources from Flaticon.com.**

In a typical supply chain, strawberries are collected at harvest (at 20 °C) and field-packed in individual packages stacked in standard reusable packaging crates (Ferrua and Singh, 2009a; IFCO, 2022). These packed berries are then stored in a cold chamber (6-8 °C) for 1-6 hours. Following this, they are palletized and pre-cooled in a forced-air cooling tunnel (2-4 °C for 3 h) (Kuchi and Sharavani, 2019). The berries are then loaded into refrigerated trailers and transported from the pre-cooling facility in Spain to the distribution center in Switzerland (~ 2-day journey). It is recommended that temperatures should be as low as possible (0-4 °C), but in a previous study, our analysis showed that the air temperature is in the range of 5-6 °C during transport (Shoji et al.,

2022). One of the reasons for transporting at a higher temperature range is to reduce the risk of top freezing as the cold air entering the trailer is often not exactly at the set air temperature. Large retailers often have their own distribution centers (or warehouses) where the fruit are delivered and then redistributed to retail stores in the region. At the distribution center, the fruit spend anywhere between 12 and 18 hours (Shoji et al., 2022). Air temperatures are relatively stable (6 ± 1 °C) (Shoji et al., 2022). The berries are then redistributed from the regional warehouse/distribution center to the retail store, lasting about 18 hours. In order to lower the risk of condensation, the air temperature is often gradually increased (or ramped up) in this segment. From our measurements, we find that the air temperature increases linearly over time, for the ramp-up from 6 °C to 10 °C (Shoji et al., 2022). Our measurements revealed that the ambient relative humidity during refrigerated transport and storage is $80\pm 3\%$ from the pack house up to the retail store. On arriving at a retail store, the fruit are stored overnight (~ 8 h) in the cold storage room where air temperatures are usually 9-11 °C as the fruit are stored along with other fresh produce. Following this, we reconstructed a retail period of 8 h, when the fruit are displayed on retail store shelves at standard ambient temperatures (23 °C, 40% relative humidity) (The British Standards Institution, 2017). This is because strawberries are most often displayed on retail store shelves with no refrigeration (Collins and Perkins-Veazie, 1993). In total, a supply chain of 4.5 days is simulated with this digital twin. Since the strawberries are transferred from one unit operation to another, there is often an abrupt change in the environmental conditions. These rapid changes during handling are a result of different unit operations concatenating to compose the supply chain.

2.2 Continuum multiphysics model for a package of strawberries

2.2.1 Computational system configuration

The computational domain comprises a ventilated package filled with strawberries in an air channel without bypass, as shown in Figure 2. The fruit are modeled explicitly since the package-to-product length ratio is in the range of 2-3 (so < 10), implying the fruit in a single package cannot be modeled as porous media (Dehghannya et al., 2010; Ferrua and Singh, 2009a; Nalbandi et al., 2016). Each package is filled with equi-sized strawberries (equatorial fruit diameter = 30 mm, mass = 16.30 g, surface area = 33.06×10^{-4} m², volume = 16.9×10^{-6} m³, equivalent spherical diameter = 31.84 mm). The size is in accordance with the Class I commercial grade of berries imported to Switzerland (Schweizer Obstverband (Fruit-Union Suisse), 2005). Every individual strawberry is modeled as a three-dimensional geometry created by axi-symmetrically rotating a contour of a strawberry fruit (cv. *Fortuna*). The number of strawberries in every package varies depending on the intended weight of the stock-keeping unit, *i.e.*, 250 g (16 berries), 300 g (20 berries), 400 g (25 berries), or 500 g (31 berries). The packages are filled with fruit in 4-7% excess of the intended weight to account for the reduction in saleable weight due to moisture loss along the supply chain. The berries are stacked in a regular arrangement such that their longest edge rests on the base of the package with a net-zero torque about the center of gravity. Horizontal airflow in a no bypass channel through a single package is modeled for the different packaging configurations. The reason is that typically horizontal flow is encountered in a pre-cooling tunnel and also to some extent in a refrigerated trailer (Ambaw et al., 2021; Ferrua and Singh, 2009b; Getahun et al., 2017; Wu et al., 2019). Most packages also have vent-hole configurations that are designed for promoting horizontal airflow ventilation rather than vertical airflow ventilation. The sections upstream and downstream of the package are taken sufficiently large (~ 30 cm) to avoid an influence of the inlet and outlet boundary conditions on the airflow and heat transfer inside the package. All the selected packages are ventilated, *i.e.*, these packages had vents or macro-perforations (diameter 8-12 mm) to enable the transfer of O₂ and CO₂ at rates much higher than the fruit's respiration. Therefore, modified atmosphere packaging or the O₂ and CO₂ composition inside the package are not modeled (Paul and Clarke, 2002; Sousa-Gallagher and Mahajan, 2013).

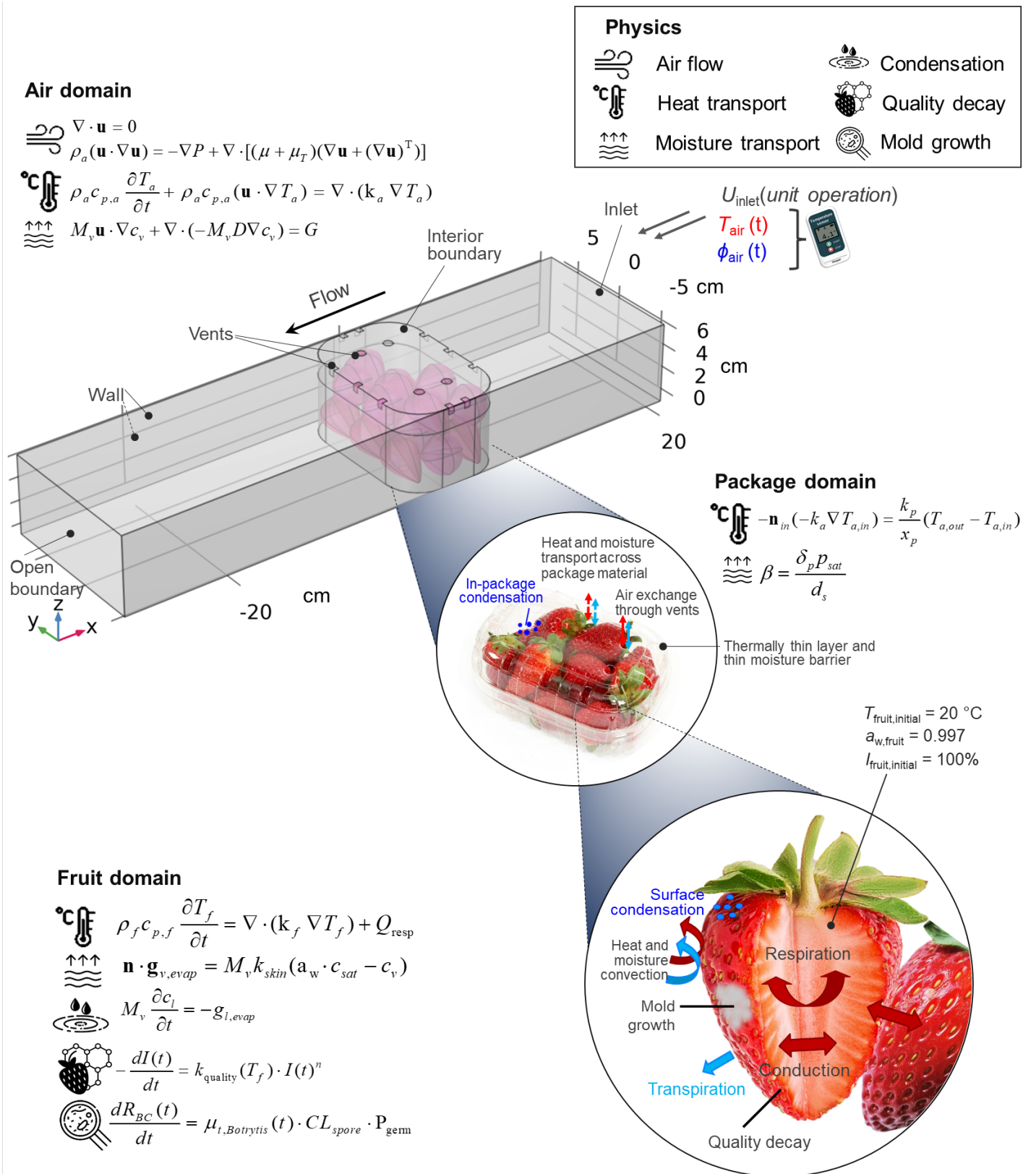


Figure 2: A schematic overview of the continuum multiphysics model depicting the computational system configuration, governing equations, and implemented boundary conditions for the air, package, and fruit domains for a representative ventilated package. The equations corresponding to the air, package, and fruit domains have been described in the text and the nomenclature is elaborated at the end of this study. Image credits: This figure has been designed using resources from Flaticon.com and Adobe Stock (AdobeStock_49352459, AdobeStock_214803643).

2.2.2 Airflow

A uniform upstream velocity (U_{inlet} , $\text{m}\cdot\text{s}^{-1}$) is defined at the inlet for airflow, based on the superficial air speed of the unit operation (Figure 1). This value is set to $0.01 \text{ m}\cdot\text{s}^{-1}$ for retail and refrigerated storage, $0.1 \text{ m}\cdot\text{s}^{-1}$ for refrigerated transport, and $1.0 \text{ m}\cdot\text{s}^{-1}$ for pre-cooling (Han et al., 2017; Li et al., 2021; Opara and Zou, 2007; Thompson et al., 2008a; Wu et al., 2019). Note that these ranges are indicative for the superficial air speeds in these unit operations. For our conceptual study, such indicative ranges of air speed are sufficient to draw relevant conclusions with respect to relative differences between packaging performances. The convective heat transfer coefficients and Biot numbers corresponding to these ranges of superficial air speed are presented in the Supplementary materials, Section A.1. A turbulence intensity of 0.05% is assumed for the flow entering the computational domain (Berry et al., 2016). An open boundary condition is defined for the outlet in the downstream section. As the contribution of moisture added due to evaporation from the fruit surface is small, a no-slip boundary condition is applied to all solid surfaces, including all surfaces of the package and fruit.

We model incompressible flow, thus the continuity equation takes the form presented in Eq. 1.

$$\nabla \cdot \mathbf{u} = 0 \quad (1)$$

where \mathbf{u} is the velocity field vector and ∇ is the vector differential operator.

The Navier Stokes equations take the form presented in Eq. 2.

$$\rho_a(\mathbf{u} \cdot \nabla \mathbf{u}) = -\nabla P + \nabla \cdot [(\mu + \mu_T)(\nabla \mathbf{u} + (\nabla \mathbf{u})^T)] \quad (2)$$

where ρ_a is the density of air ($\text{kg}\cdot\text{m}^{-3}$), P is the atmospheric pressure (Pa), and $(\mu + \mu_T)$ represents the effective viscosity ($\text{Pa}\cdot\text{s}$). Buoyancy was not considered, as analysis of the Richardson number showed that buoyancy-driven flow is only significant at superficial air speeds below $0.05 \text{ m}\cdot\text{s}^{-1}$. Note also that modeling buoyancy would significantly extend the computational cost of the simulations as, for changing thermal environments, this would require recalculating the flow field every time step. This is a reason why it is rarely accounted for in CFD simulation studies in postharvest science.

For a typical package, the flow regime is mostly laminar around the package, but turbulent at the vents (Ferrua and Singh, 2009a). Therefore, Eq. 2 is solved in the turbulent regime using the Reynolds-averaged Navier–Stokes (RANS) equations, which account for turbulence effects on the mean flow field through time averaging. To this end, we use a k - ε turbulence model with wall functions. This approach describes turbulence by an increase in effective fluid viscosity ($\mu + \mu_T$) (Norton et al., 2012). The turbulent component of viscosity (μ_T , $\text{Pa}\cdot\text{s}$) is computed using the turbulent kinetic energy (k_T), and the rate of dissipation of the turbulent kinetic energy (ε), expressed in Eq. 3.

$$\mu_T = \frac{\rho_a C_\mu k_T^2}{\varepsilon} \quad (3)$$

Here, C_μ is the turbulence model constant. The turbulence variables are solved in the whole air domain. The no-slip boundary condition is implemented at the walls. We used wall functions to model the near-wall regions and built a corresponding mesh with a desired y^+ value of 1.

As the thickness of the package is significantly smaller than the length scales of the adjacent domains, the walls of the package are modeled as interior boundaries, so a two-dimensional plane. This allows discontinuity in velocity, pressure, and turbulence variables across the package walls. We assume that the flow field is independent of the air temperature and moisture content, and therefore calculate the flow field in advance and then use it as input for the heat and moisture transport equations.

2.2.3 Heat transport

Heat transfer in the air domain

The heat transfer equation for the air domain is presented in Eq. 4. This equation describes how the air temperature (T_a , K) changes with time, based on conduction and convection terms.

$$\rho_a c_{p,a} \frac{\partial T_a}{\partial t} + \rho_a c_{p,a} (\mathbf{u} \cdot \nabla T_a) = \nabla \cdot (k_a \nabla T_a) \quad (4)$$

where $c_{p,a}$ is the specific heat capacity of air ($c_{p,a} = 1006 \text{ J}\cdot\text{kg}^{-1}\cdot\text{K}^{-1}$), and k_a is the thermal conductivity of air ($k_a = 0.024 \text{ W}\cdot\text{m}^{-1}\cdot\text{K}^{-1}$) (ASHRAE, 2010).

Heat transfer across the package walls

The walls of the package are modelled as thin layers with a thermal resistance. Since the thermal conductivity of the packaging material is comparable to that of the surrounding air, a 'thermally thin approximation' is implemented. With this approximation, we assume that the heat flux across the package is proportional to the temperature difference between both sides of the package wall (Eq. 5).

$$-\mathbf{n}_{in}(-k_a \nabla T_{a,in}) = \frac{k_p}{x_p} (T_{a,out} - T_{a,in}) = \mathbf{n}_{out}(-k_a \nabla T_{a,out}) \quad (5)$$

Here, the terms $\mathbf{n}_{in}(-k_a \nabla T_{a,in})$ and $\mathbf{n}_{out}(-k_a \nabla T_{a,out})$ correspond to the flux on either side of the package wall. The terms k_p ($\text{W} \cdot \text{m}^{-1} \cdot \text{K}^{-1}$) and x_p (m) refer to the thermal conductivity and thickness of the packaging material. The corresponding thermo-physical properties for the different packaging materials employed in this study are detailed in Table 1.

Table 1: Thermo-physical properties to quantify heat and moisture transport across the packaging materials corresponding to the different packages investigated in this study.

Material	Thickness (x_p , mm)	Thermal conductivity (k_p , $\text{W} \cdot \text{m}^{-1} \cdot \text{K}^{-1}$)	Specific heat ($c_{p,p}$, $\text{J} \cdot \text{kg}^{-1} \cdot \text{K}^{-1}$)	Density (ρ_p , $\text{kg} \cdot \text{m}^{-3}$)	Vapor permeability at 25 °C, 90% RH (δ_p , $\text{kg} \cdot \text{m}^{-1} \cdot \text{s}^{-1} \cdot \text{Pa}^{-1}$)	Vapor resistance factor (μ_p , -)	References
Recycled Polyethylene terephthalate (R-PET)	0.40	0.036	1200	1350	2.8×10^{-16}	0.7×10^6	(Auras et al., 2005; Bastarrachea et al., 2011; Guidigo et al., 2017; IDMC, n.d.; Lopes and Felisberti, 2004; Ngo et al., 2016; Wu et al., 2021)
Uncoated paperboard	0.51	0.066	1355	700	4.3×10^{-13}	450	(Bastarrachea et al., 2011; Cardoso and Labuza, 1983; Etuk et al., 2011; Latif et al., 2015; Odusote et al., 2016)
Low density polyethylene film for flow- wrap packages	0.05	0.036	1200	925	7.0×10^{-17}	2.8×10^6	(Bastarrachea et al., 2011; Ngo et al., 2016; Panda et al., 2016; Wang et al., 2018; Wu et al., 2021)
Polypropylene for recloseable top-seal films	0.03	0.036	1200	900	2.3×10^{-17}	8.5×10^6	(Bastarrachea et al., 2011; Ngo et al., 2016; Sousa- Gallagher et al., 2013; Wang et al., 2018; Wu et al., 2021)

Heat transfer in the fruit domain

Equation 6 describes the heat transfer process in the fruit domain.

$$\rho_f c_{p,f} \frac{\partial T_f}{\partial t} = \nabla \cdot (k_f \nabla T_f) + Q_{\text{resp}} \quad (6)$$

where T_f is the fruit temperature (in K) at any time instant t , k_f is the thermal conductivity of strawberry ($k_f = 0.6 \text{ W} \cdot \text{m}^{-1} \cdot \text{K}^{-1}$), $c_{p,f}$ is the specific heat capacity of strawberry ($c_{p,f} = 4000 \text{ J} \cdot \text{kg}^{-1} \cdot \text{K}^{-1}$), and ρ_f is the density of the strawberry ($\rho_f = 961 \text{ kg} \cdot \text{m}^{-3}$) (ASHRAE, 2010; Becker et al., 1996; Concha-Meyer et al., 2018; Ferrua and Singh, 2009a; Xie and Zhao, 2004). Here, Q_{resp} is the volumetric heat of respiration ($\text{W} \cdot \text{m}^{-3}$). This is estimated from the CO_2 production rate of strawberries as a function of temperature (Eq. 7), such that for every mg of CO_2 produced, 10.7 J of heat is generated (Becker et al., 1996). This corresponds to approximately 40 $\text{mW} \cdot \text{kg}^{-1}$ of heat generated at 0 °C, 150 $\text{mW} \cdot \text{kg}^{-1}$ at 10 °C, and 400 $\text{mW} \cdot \text{kg}^{-1}$ at 20 °C.

$$Q_{\text{resp}} = \frac{10.7 f}{3600} \left(\frac{9\theta_f}{5} + 32 \right)^g \cdot \rho_{\text{pulp}} \quad (7)$$

Here f and g are commodity-specific respiration coefficients which are 3.668×10^{-4} and 3.0330, respectively, for strawberries (Becker et al., 1996). θ_f is the fruit temperature at any given point within the fruit (°C). The thermo-physical properties of strawberries are assumed to remain constant throughout the process. Shriveling is neglected (Defraeye et al., 2019; Ferrua and Singh, 2009a).

Initial and boundary conditions

At the fruit-air interface, the boundary condition in Eq. 8 is adopted based on continuity of flux, where both fluxes result from the calculation of conduction in the fruit domain and convection in the air domain.

$$(k_f \nabla T_f - k_a \nabla T_a) \cdot \mathbf{n} = g_v \cdot \Delta H_v \quad (8)$$

where the term $g_v \cdot \Delta H_v$ corresponds to the latent heat of evaporation, elaborated in the following section. Additionally, thermal insulation is considered at the walls of the flow channel, so the term $(k_a \nabla T_a) \cdot \mathbf{n} = 0$.

The entire system (air, fruit, and package) is assumed to be at an initial temperature of 20 °C. The air temperature upstream of the package at the inlet (T_{upstream} , K) is defined as a function of time based on measured data (Figure 1). We are aware that spatial variations in air temperature and subsequent fruit temperature can exist inside the pallets and the cargo. However, in this study, we model a strawberry packaging that is in the vicinity of the air temperature sensor placed inside the cooling tunnel, refrigerated trailer, or storage room for the respective unit operation. These are packages that are exposed rather directly to the environmental conditions of the unit operation, so for example, located at the outside of a pallet.

2.2.4 Moisture transport

Moisture transport in the fluid domain

The moisture transport in the computational domain, namely air, is described using Eq. 9.

$$M_v \mathbf{u} \cdot \nabla c_v + \nabla \cdot (-M_v D_{v,a} \nabla c_v) = G \quad (9)$$

Here M_v is the molar mass of water vapor ($= 18 \times 10^{-3} \text{ kg}\cdot\text{mol}^{-1}$), \mathbf{u} is the velocity field vector ($\text{m}\cdot\text{s}^{-1}$), c_v is the vapor concentration ($\text{mol}\cdot\text{m}^{-3}$), and $D_{v,a}$ is the water vapor diffusion coefficient of air ($\text{m}^2\cdot\text{s}^{-1}$). The source term (G , $\text{kg}\cdot\text{m}^{-3}\cdot\text{s}^{-1}$) represents the addition of moisture within the domain, which is non-zero at the fruit surface due to the contribution of the evaporative flux from transpiration as well as when the condensate evaporates.

The relative humidity (ϕ_a , -) relates the vapor concentration with the saturation concentration of vapor (c_{sat} , $\text{mol}\cdot\text{m}^{-3}$) using Eq. 10.

$$c_v = \phi_a c_{sat} \quad (10)$$

Water vapor transport across the package

The walls of the package are modeled as 'thin moisture barriers' to model discontinuous moisture content values on either side of the wall. Water vapor transport across the package walls is modeled using the thickness of the packaging material (x_p , m) and the water vapor resistance factor (μ_p , -). The water vapor resistance factor is a measure of the resistance offered by a material to let water vapor pass through and is the ratio of water vapor permeability of air (δ_{air} , $\text{kg}\cdot\text{m}^{-1}\cdot\text{s}^{-1}\cdot\text{Pa}^{-1}$) to the water vapor permeability of the material (δ_p , $\text{kg}\cdot\text{m}^{-1}\cdot\text{s}^{-1}\cdot\text{Pa}^{-1}$). Note that the packaging materials are very vapor tight. The vapor permeability of air is considered to be $1.95 \times 10^{-10} \text{ kg}\cdot\text{m}^{-1}\cdot\text{s}^{-1}\cdot\text{Pa}^{-1}$ at 23 °C (Valovirta and Vinha, 2004). The thermo-physical properties of the packaging materials are detailed in Table 1. Temperature dependence of material properties for the packaging is not considered, as these differences are negligible in the temperature range of interest (Exama et al., 1993; Sousa-Gallagher and Mahajan, 2013; Valovirta and Vinha, 2004).

Water vapor loss at the fruit surface due to transpiration

Moisture loss (water vapor) flux at the fruit surface ($g_{v, \text{evap}}$, $\text{kg}\cdot\text{m}^{-2}\cdot\text{s}^{-1}$) is computed using Eq. 11.

$$\mathbf{n} \cdot \mathbf{g}_{v, \text{evap}} = k_{skin} M_v (a_w \cdot c_{sat} - c_v) \quad \text{if } (a_w \cdot c_{sat} > c_v) \quad (11)$$

where k_{skin} is the evaporation rate factor for the strawberry accounting for the skin resistance to moisture transport ($= 1.77 \times 10^{-3} \text{ m}\cdot\text{s}^{-1}$) and a_w is the water activity at the surface of the fruit ($= 0.997$) (Becker et al., 1996).

Net mass loss in fruit

The net mass loss in the fruit is accounted for considering the combined contribution of transpiration and respiration. For the contribution of transpiration, we directly integrate the evaporation flux (g_{evap}) over time to obtain the net decrement in mass (Δm). From the stoichiometric equation of aerobic respiration, we use the mole concept to calculate that 0.068 mg dry weight is lost for every 1 mg of CO_2 produced (Jalali et al., 2017; Tano et al., 2009; Xanthopoulos et al., 2017). The temperature-dependent loss in dry weight when glucose is converted to CO_2 during respiration is calculated using Eq. 7 presented above, where the factor of 10.7 J of heat released per mg CO_2 produced is replaced by 0.068 mg of weight lost. The contribution of mass loss due to respiration is found to be significant only at ambient storage conditions.

Liquid water transport at the fruit and tray surface due to condensation

To account for condensation and evaporation of liquid water on the fruit and tray surfaces, these are modeled as a moist surface, *i.e.*, a surface partially covered with liquid water. The concentration of liquid water accumulated on the surface due to condensation (c_l , $\text{mol}\cdot\text{m}^{-2}$) is computed using Eq. 12. This term accounts for the cumulative liquid water stored on the surface due to condensation, as well as the re-evaporation of this condensed water.

$$M_v \frac{\partial c_l}{\partial t} = -g_l \quad (12)$$

The liquid water flux at the fruit and tray surface ($g_{l, \text{evap}}$, $\text{kg}\cdot\text{m}^{-2}\cdot\text{s}^{-1}$) is computed using Eq. 13. Here, we assume condensation to take place when the surface temperature of the fruit or tray is below the dew point temperature of air. Additionally, if there is liquid water present on these surfaces, it is re-evaporated.

$$\mathbf{n} \cdot \mathbf{g}_{l, \text{evap}} = M_v K (c_{sat} - c_v) \quad \text{if } (c_v > c_{sat}) \text{ or } c_l > 0 \quad (13)$$

where K is the evaporation rate factor ($= 1$ in our case) and c_l is the liquid water concentration on the surface ($\text{mol}\cdot\text{m}^{-2}$). The boundary layer resistance is accounted for in the term $g_{l, \text{evap}}$.

The latent heat term is also added to the heat transfer equation, as $g_l \cdot \Delta H_{\text{vap}}$, where ΔH_{vap} is the temperature-dependent latent heat of evaporation ($\text{J}\cdot\text{kg}^{-1}$).

Condensation-related time of wetness for microbiological risk

In our study, we evaluate the risk of microbiological growth as the time of wetness (ToW). This is computed as the integral of the time when the liquid water concentration on the fruit surface (c_l) is non-zero, or when the relative humidity at the surface of the berry is higher than 95%, as this is critical for microbiological growth (Jarvis, 1977; Lahlali et al., 2007; Linke and Geyer, 2013;

Snow, 1949; Williamson et al., 1995). The ToW is evaluated at every point of the fruit surface, as it is possible that condensation occurs simultaneously on locally different parts of the same fruit, depending on the geometry and external conditions (Linke et al., 2021).

2.2.5 Kinetic model for biochemical fruit quality

The visual, compositional, and physiological quality of strawberries changes after harvest as a consequence of biochemical and enzymatic reactions. Some of these include the development of a reddish-brown color due to anthocyanin degradation, loss of ascorbic acid, reduction in soluble solids, and changes in soluble solid content (Nunes, 2009). Strawberries are non-climacteric fruit so they do not ripen anymore after harvest. Most of these reactions can be adequately modeled using first-order kinetics (Corradini, 2018; Valentas et al., 1997). Our study models the respiration-driven biochemical fruit quality through an overall fruit quality index (I_f , %) (Tijssens and Polderdijk, 1996). We employ a first-order kinetic model, which signifies an exponential decay in fruit quality as a function of time (Eq. 14).

$$-\frac{dI_f(t)}{dt} = k_{\text{quality}}(T_f) \cdot I_f(t)^n \quad (14)$$

where $I(t)$ is the remaining biochemical fruit quality (%) at any time instant t , $k_{\text{quality}}(T_f)$ is the temperature-dependent rate constant (s^{-1}), n is the reaction order (=1 in this case). Here, T_f represents the temperature at any point in the fruit (K). The overall quality for a strawberry is averaged over the entire fruit volume.

The initial value of the fruit quality index ($I_{t=0}$) is assumed to be 100% at the time of harvest ($t = 0$ s). This quality model is calibrated based on fruit shelf-life studies in literature for strawberries. Most strawberry cultivars, such as *cv. Fortuna*, *cv. Seascape*, *cv. Chandler*, can successfully be stored at 10 °C for about 5 days, after which the symptoms of biochemical quality loss become visible (Ayala-Zavala et al., 2004; Nunes, 2008). In our calibration, we arbitrarily set this threshold as 20% ($I_{t=5d}(T=10\text{ °C}) = 20\%$). Note that the choice of threshold does not influence the predicted value of remaining shelf life. Below this threshold, more than 50% consumers would reject the product (Jalali et al., 2020).

The temperature dependence of the rate constant $k_{\text{quality}}(T)$ is accounted for by the Arrhenius equation for reaction rates, as shown in Eq. 15 (van Boekel, 2008).

$$k_{\text{quality}}(T) = k_{0,\text{quality}} \exp\left(-\frac{E_{a,\text{quality}}}{RT}\right) \quad (15)$$

where ($k_{0,\text{quality}}$, $3.55 \times 10^6 \text{ s}^{-1}$) is the pre-exponential factor, $E_{a,\text{quality}}$ is the activation energy ($65'000 \text{ J} \cdot \text{mol}^{-1}$), R is the universal gas constant ($8.314 \text{ J} \cdot \text{mol}^{-1} \cdot \text{K}^{-1}$) (Joshi et al., 2019; Leithner and Fikar, 2019). To account for the dependence of shelf life on storage temperature, a Q_{10} value of 2.75 is considered for strawberries (Hikawa-Endo, 2020; Tano et al., 2009). This Q_{10} value corresponds to the ratio between rate constants at two temperatures that are 10 °C apart and lies between 2 and 3 for most fruits and vegetables (Eq. 16) (Becker et al., 1996).

$$Q_{10} = \frac{k_{\text{quality}}(T+10)}{k_{\text{quality}}(T)} \quad (16)$$

where $k_{\text{quality}}(T+10)$ and $k_{\text{quality}}(T)$ correspond to the rate constants at temperatures $(T+10)$ and T K, respectively. This means that strawberries can be stored for about 14 days at 0 °C, for 5 days at 10 °C, and for about 2 days at 20 °C. The overall calibration is depicted in the Supplementary Materials (Section A.2).

2.2.6 Predictive model for microbiological risk due to *B. cinerea*

We develop a predictive model for microbiological risk due to mold growth, considering the three key steps for *Botrytis cinerea* infection (Petrasch et al., 2019; Sephton-Clark and Voelz, 2018), depicted in Figure 3 a. The first step is the deposition of spores present in the air on the fruit surface, for example due to wet splashes or air currents (Ciliberti et al., 2016). The next step is spore germination that is induced by environmental triggers, particularly elevated humidity or availability of free water (Jarvis, 1977; Lahlali et al., 2007; Snow, 1949; Williamson et al., 1995). The third step is hyphal extension and mycelium growth, as a function of biokinetic factors such as fruit temperature, pH , and water activity.

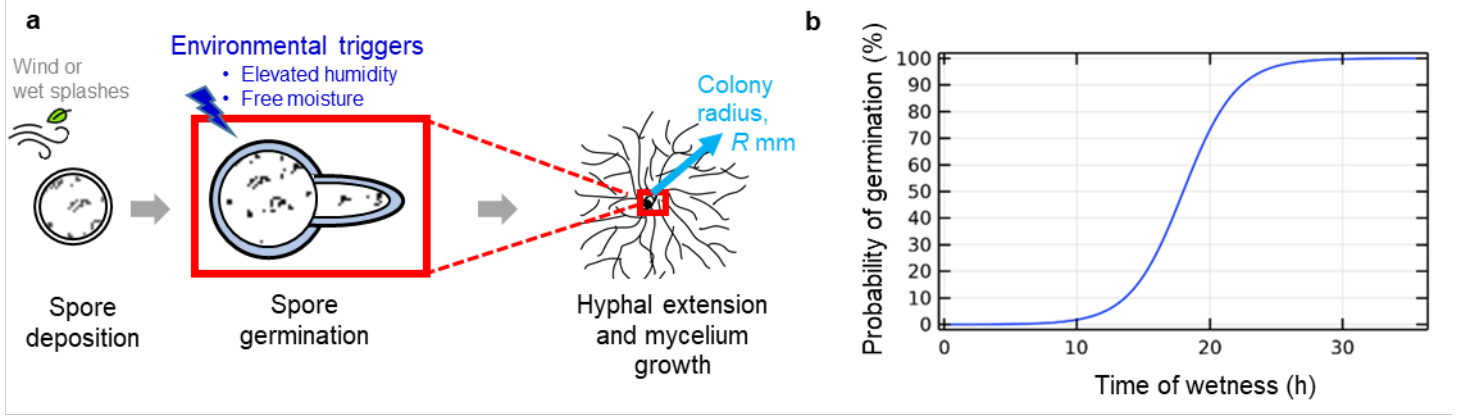


Figure 3: (a) A schematic illustration of the three critical steps for the infection of *Botrytis cinerea* on a substrate (Petrasch et al., 2019; Sephton-Clark and Voelz, 2018), depicting (1) spore deposition due to wind or wet splashes, (2) spore germination due to favorable environmental triggers such as elevated humidity or free moisture availability, when the spore swells and the hyphae emerges, and (3) hyphal growth as a function of biokinetic factors; (b) Probability of germination (P_{germ} , %) of *B. cinerea* spores as a function of time of wetness of fruit surface (ToW , h) in the temperature range of 0-25 °C. Image credits: This figure has been designed using resources from Flaticon.com.

Spore deposition

Here, we assume that the fruit are cultivated in a tunnel, hoop house or unheated greenhouse. The spores of *B. cinerea* are already present in the air inside the greenhouse and are deposited on the fruit surface prior to harvest. Therefore we do not model spore deposition explicitly. The concentration of *B. cinerea* spores in the air ($c_{spores,air}$, 0.1-0.2 spores·m⁻³) is estimated from the mean annual value based on aerobiological studies in unheated greenhouses in Western Europe (Leyronas et al., 2011; Leyronas and Nicot, 2013). In 'still' air, any suspended spore will land on the fruit with a constant and characteristic settling velocity ($u_{settling}$, m·s⁻¹), determined by Stokes' law (Den Aantrekker et al., 2003). This value is 0.00368 m·s⁻¹ for *B. cinerea* spores, computed based on the spore diameter (Boulard et al., 2006). The contamination level, *i.e.*, the number of spores deposited on the surface of berries at the time of harvest, therefore depends on the concentration of spores in the air, time of exposure from flowering, and exposed surface area of the fruit. This contamination level is computed using Eq. 17.

$$CL_{spores} = c_{spores,air} \cdot v_{settling} \cdot A_s \cdot t_{harvest} \quad (17)$$

where CL_{spores} is the contamination level of *B. cinerea* spores on the fruit surface. Here, A_s is the exposed area of the strawberry, which is assumed to be constant and estimated at the time of harvest ($A_s = 1.05 \times 10^{-3}$ m²), although in reality, this changes as the fruit matures. After blossoming, the time spent by the strawberry in the field until it is harvested ($t_{harvest}$, d) is typically between 24 - 36 days (Han et al., 2015), and is considered to be 30 days in our calculation. The resulting contamination level (CL_{spores}) is ~1-2 spores·berry⁻¹, corresponding to one infected site per fruit (Carisse, 2015).

Germination

Once the spore is deposited, it remains in a dormant state (resting spore) until it encounters the right environmental triggers for germination. The spores of *B. cinerea* can germinate over a wide range of temperatures, including temperatures as low as 0 °C (Jarvis, 1977; Liguori et al., 2021). Therefore, elevated humidity levels ($\phi_a > 95\%$) or the availability of free moisture are the prime driving forces for initiating the germination of *B. cinerea* spores and its penetration into the host epidermis (Jarvis, 1977; Lahlali et al., 2007; Snow, 1949; Williamson et al., 1995). The presence of moisture enables the spore to take up nutrients and exchange solutes with the host epidermis (Lahlali et al., 2007).

The probability of germination P_{germ} (%) is modeled as a function of the retention time of the condensate on the surface of the strawberry (ToW , h), as shown in Figure 3 b. We employ a simplified logistic function to describe P_{germ} (Eq. 17) (Dantigny et al., 2007, 2006). The temperature dependence was not considered for germination, as in the temperature range of 1-30 °C, the effect of elevated humidity on spore germination is much higher than the effect of temperature (Dantigny et al., 2007).

$$P_{germ} = \frac{P_{max}}{1 + \exp[k_{germ}(\tau - ToW)]} \quad (18)$$

Here, P_{germ} (%) corresponds to the fraction of spores germinated, and P_{max} (%) is the asymptotic maxima of P_{germ} (=100%). The germination time (τ , h) is a time constant. Its value indicates that after 18 hours of wetness (Ciliberti et al., 2015), about 50% of the spores are germinated (Dantigny et al., 2006). The slope ($k_{germ} \cdot P_{max}/4$) of the tangent at the point of inflection, τ , is calculated assuming a linear increase in P_{germ} between 12 and 24 hours (Ciliberti et al., 2015; Dantigny et al., 2007). Germination is often accompanied by a lag phase, during which sufficient water is being imbibed from the atmosphere or condensate into the spore (Jarvis, 1977). In our study, we assumed the lag time for growth, *i.e.*, when the spore adjusts to the new environment, to be zero, as a conservative estimate due to unavailability of data. Germination implies that the spore absorbs water and swells to twice its diameter, and germination culminates with the emergence of the hyphal tube (Sephton-Clark and Voelz, 2018).

Hyphal extension and mycelium growth

The hyphal tube extends and branches as hyphae (branching filaments of a fungus) and forms a circular colony of mycelium (network of hyphae). The colony diameter shows a linear increase over time due to the turgor-driven uptake of water by the hyphae (King, 2015). Therefore, the hyphal extension rate is commonly modelled as a radial growth rate ($\mu_{t,BC}$, $\text{mm}\cdot\text{d}^{-1}$) (Dantigny et al., 2002; Garcia et al., 2009; Prosser and Tough, 1991). The radius of the fungal colony (R_{BC} , mm) is modeled as a function of time t using (Eq. 18) (Dagnas and Membré, 2013).

$$\frac{dR_{BC}(t)}{dt} = \mu_{t,BC}(t) \cdot CL_{spore} \cdot P_{germ} \quad (19)$$

where optimal radial growth rate ($\mu_{opt,BC}$, $15.0 \text{ mm}\cdot\text{d}^{-1}$) is evaluated from the plot of the mean radius of the colony of *B. cinerea* as a function of time on grape juice agar medium ($pH = 4.2$, $a_w = 0.985$) (Judet-Correia et al., 2010; Saito et al., 2016; Sernaite et al., 2020; Zhou et al., 2018). The initial value of the colony radius is set to $6 \mu\text{m}$, which is equivalent to the spore diameter (Gougouli and Koutsoumanis, 2012; Saito et al., 2016).

The biokinetic effects of environmental factors (surface temperature, water activity, and pH) on the growth rate are included using the coupled γ -concept, which assumes the effects of these factors to be multiplicative (Eq. 19) (Dagnas and Membré, 2013; Ranjbaran et al., 2021; Rosso et al., 1995; Rosso and Robinson, 2001; Zwietering et al., 1996).

$$\mu_{t,BC}(t) = \mu_{opt,BC} \cdot \gamma(T_{f,surface}(t)) \cdot \gamma(a_w) \cdot \gamma(pH) \quad (20)$$

Each gamma term is parameterized such that its value ranges between 0 and 1. At $\gamma=0$, there is maximal inhibition due to this factor, whereas the proliferation rate of the mold is at its maximal value at $\gamma=1$. The individual γ -functions for surface temperature, water activity, and pH are described in Table 2.

Table 2: Values for the cardinal models for *B. cinerea* reported in literature (Fedele et al., 2020; Jarvis, 1977; Judet-Correia et al., 2010; Lahlali et al., 2007; Manteau et al., 2003; Panasencko, 1967; Ranjbaran et al., 2021; Sardella et al., 2018).

Parameter	Function	Min	Max	Opt	Strawberry
Temperature ($T_{f,surface}$, K)	$\gamma(T_{f,surface}) = \left[\frac{(T_{f,surface} - T_{max})(T_{f,surface} - T_{min})^2}{(T_{opt} - T_{min})[(T_{opt} - T_{min})(T_{f,surface} - T_{opt}) - (T_{opt} - T_{max})(T_{opt} + T_{min} - 2T_{f,surface})]} \right]$	271.15	303.15	295.15	$f(t)$
Water activity (a_w , -)	$\gamma(a_w) = \left[\frac{(a_w - a_{w,min})}{(1 - a_{w,min})} \right]$	0.930	1.000	0.990	0.997
pH (pH , -)	$\gamma(pH) = \left[\frac{(pH - pH_{min})(pH - pH_{max})}{(pH - pH_{min})(pH - pH_{max}) - (pH - pH_{opt})^2} \right]$	2.00	6.00	3.10	3.84

Min, minimal factor value; opt, optimal factor value; max, maximal factor value associated with the respective γ -functions; $f(t)$, function of time.

Each factor is characterized with three factor-value parameters - (1) minima (below which no growth occurs), (2) optima (where the growth rate has its highest value), and (3) maxima (above which no growth occurs) (Ranjbaran et al., 2021). This means that if all the factors were at their optimum value, γ would take the value of 1 for all factors, and the growth rate will attain its maximal value ($\mu_{t,Botrytis} = \mu_{opt,Botrytis}$). Here, we neglect the interactive effects between the parameters due to lack of adequate studies. The gamma-function models for growth rate have been extensively validated on several substrates with reasonable accuracy and bias factors (Belbahi et al., 2016; Gougouli and Koutsoumanis, 2010; Judet-Correia et al., 2010). The γ -functions for the influence of surface temperature, water activity, and pH on the growth rate of *B. cinerea* are plotted in Figure 4. We assumed a constant value for the pH and water activity, assuming that the changes in these parameters over time are small. Note that the digital twin enables the mold growth to be predicted based on fruit surface temperature and humidity, instead of the currently available sensor data for air temperature. The fact that the twin provides us with data on the fruit surface is a key added value of the modeling approach and leads to more representative predictions.

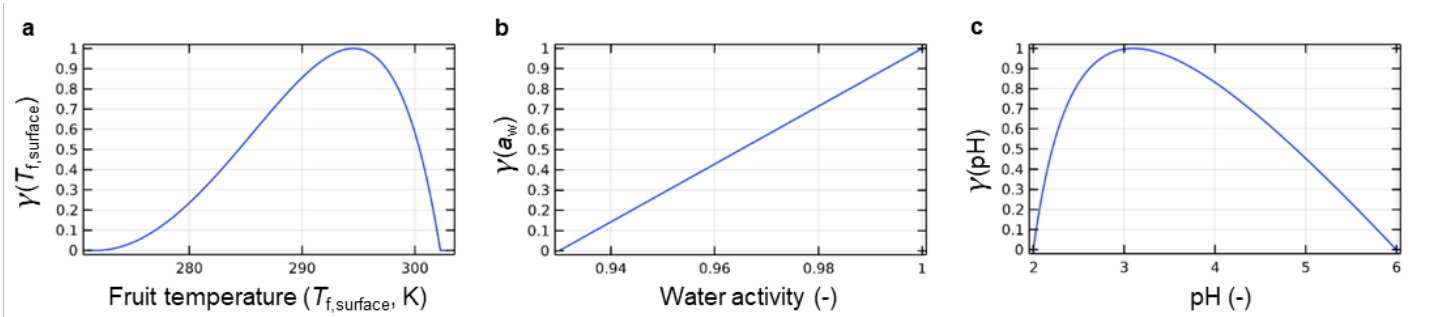


Figure 4: Gamma functions for the biokinetic effects of environmental factors, i.e., (a) surface temperature, (b) water activity, and (c) pH on the growth rate of *B. cinerea*.

2.2.7 Product-related metrics for fruit quality and marketability in every package

The physics-based model provides the following quantified actionable metrics for fruit in every package:

- volume-averaged fruit temperature (T_f , °C);
- biochemical, temperature-dependent remaining fruit quality index (I_f , %);
- total mass loss due to transpiration and respiration (ML , %);
- condensation-related time of wetness (ToW , h);
- radius of the fungal colony of *B. cinerea* (R_{BC} , mm);
- coefficient of variability (CoV , %), computed as the average of the coefficient of variability (= standard deviation/mean value) for the above metrics, indicative of the heterogeneity.

2.2.8 Multi-criteria estimation of remaining shelf life

The post-retail shelf life is simulated by placing the fruit in-silico at fixed ambient conditions that are representative of indoor conditions in Switzerland, viz. 23 °C and 40% (The British Standards Institution, 2017). We use a cut-off methodology to determine the end of the biochemical, microbial, and physical shelf life. This implies that the fruit reach the end of shelf life when at least one of the corresponding attributes attains a certain predetermined deterioration level beyond which the fruit is not saleable (cut-off point) (Giménez et al., 2012). The most widely-used approach for defining cut-off point for shelf life is the selection of an arbitrary value from literature (Hough and Garitta, 2012).

Respiration-driven biochemical shelf life

We compute the end of respiration-driven biochemical shelf life as the time remaining until the overall fruit quality index reaches a value of 20%, which was defined as the threshold for consumer acceptance in our calibration. Loss in biochemical shelf life manifests as the appearance of sunken areas and development of a reddish-brown coloration due to degradation of anthocyanins and enhanced activity of polyphenoloxidase (Nunes, 2009).

Microbial shelf life

The end of shelf life from a microbiological perspective is determined as the time until the radius of the *B. cinerea* colony attains a value of 2.5 mm (Dantigny et al., 2002; Horner and Anagnostopoulos, 1973). Beyond this value, spoilage due to mycelium growth is visible by the human eye, and therefore spoilage is visually detectable by consumers (Garcia-Gimeno et al., 2002; Gibson et al., 1994). For a package, we consider that if even a single fruit is infected and shows decay, the package of fruit is not sellable anymore.

Transpiration-driven physical shelf life

The maximum commercially acceptable moisture loss for strawberries is 6-7%, beyond which detrimental effects on the fruit's external appearance are evident (Nunes, 2009; Robinson et al., 1975). At the end of the physical shelf life, strawberries lose their turgidity and show signs of wilting and loss in stiffness (Alves et al., 2021). The transpiration-driven physical shelf life is determined as the time until the average moisture loss reaches this maximum acceptable level of 7%.

2.3 Packaging configurations

2.3.1 Packaging design space

The design space for the packages is mapped using 21 commercially-available packages that were purchased from supermarkets in Switzerland. For simplicity in some analysis, we divide the packaging into four sub-groups - (1) open (or unlidded) punnet trays, (2) top-sealed recloseable packages, (3) flow-wrapped packages, and (4) ventilated plastic clamshells. A condensed summary of the selected packages, their packaging material, as well as the nomenclature designated to them in this study, is described in Figure 5 a. A detailed summary of the packages, including dimensions, materials, vent positions, headspace volume, and volume of berries, is presented in the Supplementary Materials (Section A.3).

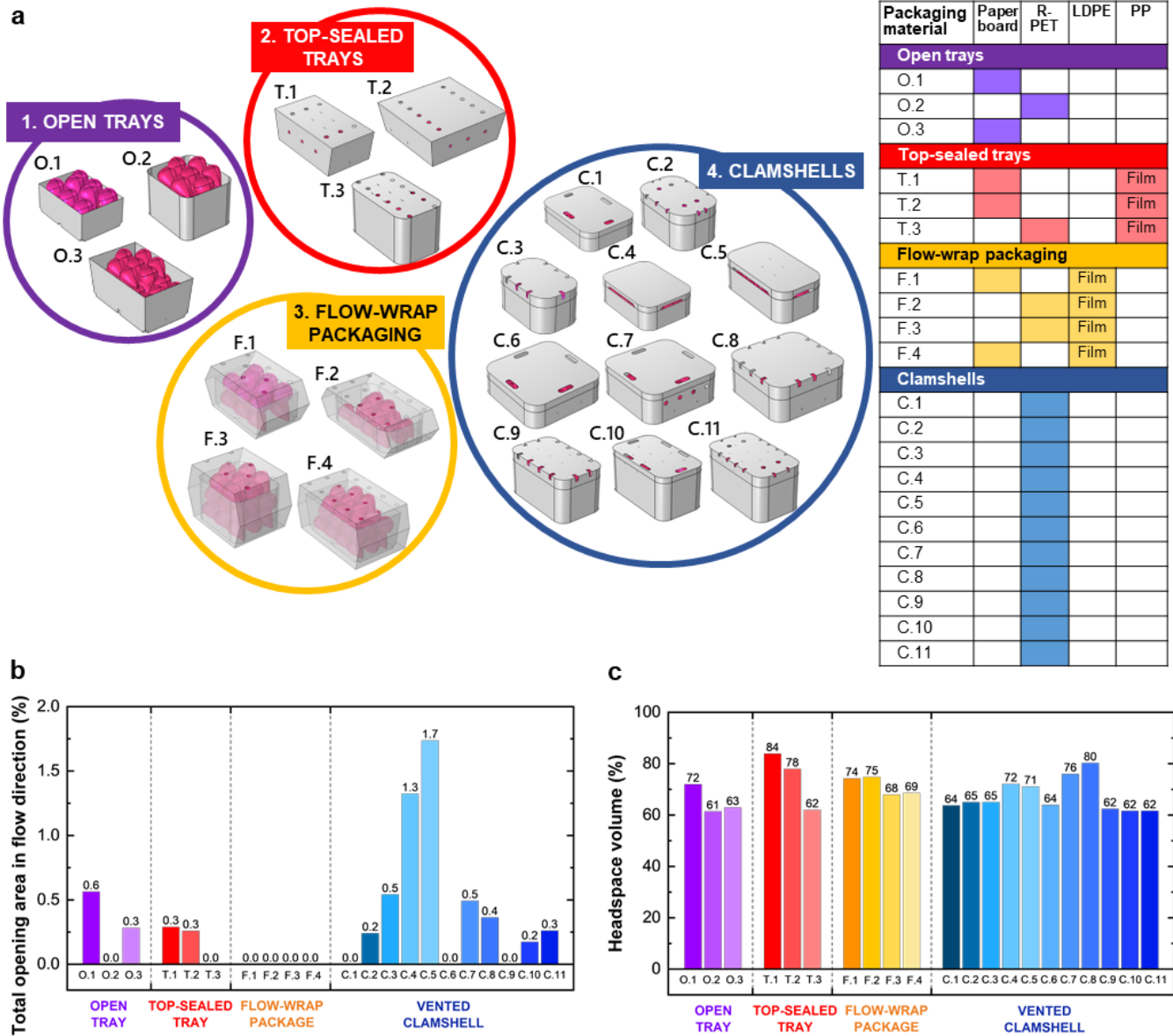


Figure 5: The 21 commercial packages investigated in this study: (a) Package sub-groups, materials, nomenclature, and color code used throughout the study; (b) Total open area in the flow direction (TOA_{flow} , %) for the packages, (c) Headspace volume ($V_{headspace}$, %) for the packages. R-PET: Recycled polyethylene terephthalate; LDPE: Low density polyethylene; PP: Polypropylene.

2.3.2 Packaging-related metrics

The 21 packages are characterized based on the following metrics (illustrated in Figure 5 b-c):

- total open area in the flow direction (TOA_{flow} , %), which is the amount of vent area in the flow direction relative to the total surface area of the package.
- headspace volume ($V_{headspace}$, %), which is the volume of air enclosed (including the air space between fruit) relative to the total package volume (air + strawberries); this is also representative of the degree of filling (DOF) of the package, as $DOF = (1 - V_{headspace})$. Note that the void space between the fruit is also included in $V_{headspace}$.

Additionally, the following metrics are computed for evaluating the aerodynamic and thermodynamic performance of the packages:

- seven-eighths cooling time ($t_{7/8}$, h), which is the time required to reduce the temperature difference between the fruit and the cooling air by seven-eighths (87.5%). This is measured for pre-cooling conditions (superficial air speed of 1 m s^{-1} to cool the fruit from $20 \text{ }^\circ\text{C}$ to $3 \text{ }^\circ\text{C}$) and the volume-averaged fruit temperature is considered.
- pressure loss coefficient (ξ , $\text{Pa}\cdot\text{s}^2\cdot\text{m}^{-6}$) as a measure of total pressure drop across the package, which is measured from the pressure drop curve for every package as a function of the superficial air speed (Supplementary materials, Section A.4).

Other metrics that were evaluated included the total open area in the lateral direction, *i.e.*, directions perpendicular to the flow (TOA_{lateral} , %), the height of the package (h_p , cm), the length-to-width ratio of the package (l_p/w_p , -), and the intended weight of fruit in the stock-keeping unit (W_t , g). Note that W_t was employed to account for the different thermal inertia of fruit in the packages, thus identifying the best-performing packaging for different quantities of fruit (250 g, 300 g, 400 g, 500 g). These values are included in Supplementary materials, Section A.5. As some of these additional metrics were redundant or did not show a correlation with any of the analyzed quality metrics, these were not reported. For example, the height of the package and the intended fruit weight in the package are already represented by the headspace volume.

2.4 Numerical implementation

We implemented the multiphysics model in the finite-element-based modeling software COMSOL Multiphysics (version 5.6). For the airflow, heat, and moisture transport models, we used the 'Turbulent Flow, k- ϵ ', 'Heat Transfer in Moist Air', and 'Moisture Transport in Air' interfaces with 'Multiphysics' coupling. All other models, including the kinetic model for biochemical quality, and microbiological growth model for mold growth, are implemented using the 'Ordinary Differential Equation' interface. The fruit and air domains were meshed as tetrahedral elements (different number of elements per configuration, $\sim 0.5 \times 10^6$ - 1.3×10^6 elements) based on a grid sensitivity analysis (Supplementary Materials, Section A.6). The elements were refined in the fruit domain and at interfaces, as strongest gradients prevail here.

This air flow study was implemented in two steps - (1) wall distance initialization, and (2) the stationary study for computing flow field. The flow field is computed as a parametric sweep for different air speeds (*i.e.*, 0.01, 0.1, and 1.0 $\text{m}\cdot\text{s}^{-1}$). A fully-coupled generalized minimal residual method (GMRES) solver was employed for wall distance initialization, and a segregated solver scheme with the MULTifrontal Massively Parallel sparse direct Solver (MUMPS) was employed for the stationary study. For the fluid flow computations, we imposed a relative solver tolerance of 0.001 and a scaled absolute tolerance of 10^{-6} for k_T and 2.5×10^{-8} for ϵ based on sensitivity analysis.

For the time-dependent study for the heat transport, moisture transport, and quality models, a segregated solver was employed with a tolerance of 10^{-4} based on sensitivity analysis. The MUMPS scheme was used for heat transport and PARALLEL DIRECT sparse Solver (PARADISO) scheme for moisture transport. The time step was determined based on the logging interval of sensor data (10 min), which provides adequate temporal sensitivity. Note that the internal time step of the solver was smaller and was determined by the tolerance. The study was implemented in successive 'steps', each corresponding to a different unit operation in the supply chain and linked with the state of the system in the preceding step. We performed the simulations on a computer with 16 GB RAM (Processor: Intel(R) Xeon(R) CPU E5-2630 V4 @ 2.20 GHz). The solution time was about 12 h for the airflow study and about 18-30 h for the time dependent study for every package, depending on the package type and number of mesh elements.

2.5 Validation and comparison with experiments

Note that the physical models are individually validated in literature and are recalibrated in our study using experimental data from literature on real strawberry fruit. The corresponding references are included in the respective sections. For further comparison with experiments, we performed experiments on actual fruit strawberry packages (clamshell C2) inside a climate chamber where we mimicked the simulated hygrothermal profile. We purchased strawberries (equatorial diameter 30-40 mm) from a local market in Switzerland. The strawberries were arranged in a clamshell (C2) in four replicates, each filled with 250 g of fruit. The packages were placed in a climate chamber to simulate the supply chain based on a realistic hygrothermal profile. The fruit core temperature was measured using temperature sensors (TinyTag Talk 2, Gemini Data Loggers, UK; accuracy ± 0.4 °C). Additionally, a sensor (SHT31, Sensirion AG, Switzerland; accuracy ± 0.2 °C and 2% RH) was placed inside the package to measure the air temperature and relative humidity in the headspace. The results are summarized in the Supplementary Materials (Section A.7). The experimental and simulated temperature and relative humidity profiles agreed well, thus the heat and moisture transport models produce realistic results.

2.6 Statistical analysis and visualization

All statistical analyses for the input parameters and output metrics are performed in the open-source software R version 3.6.3 (R Core Team, 2020). All end values are reported as mean \pm standard deviation. For all statistical analyses, we consider a significance level of 5% ($p \leq 0.05$). Statistically significant differences among different packaging are tested using one-way Analysis Of VAriance (ANOVA). The Tukey HSD (honestly significant differences) test has been used. As the sample sizes (*i.e.*, number of fruit per package) are different, the harmonic mean of the sample size is used in the Tukey HSD test (Lee and Lee, 2018). All the time series plots are visualized in the software Origin® 2022 (OriginLab, 2022). For a pairwise analysis of the degree of association between metrics, correlation analysis is performed using the 'psych' package in R 3.6.3 (R Core Team, 2020; Revelle, 2021). As all metrics are continuous, we compute the Pearson's correlation coefficient (ranging from -1 to +1, where -1 indicates a strong negative correlation, 0 indicates the absence of correlation, and +1 indicates a strong, positive correlation). A ternary plot is employed to visualize the relative contributions of the respiration-, transpiration-, and microbiology-driven shelf lives. A ternary plot uses a triangular coordinate system comprising three axes, each corresponding to the respective shelf life (Briffa et al., 2020). In this plot, we scale each axis from 0 to 100%. Every package is represented as a point in the ternary plot, and its size corresponds to the relative coefficient of variation. The ternary plot is generated using the 'Ternary' package in R 3.6.3 (R Core Team, 2020; Smith, 2017). The figures for hygrothermal evolution of fruit in the package are extracted from the models built in the software COMSOL Multiphysics® (version 5.6).

3 RESULTS AND DISCUSSION

3.1 Which unit operation is the weak link in the supply chain for every package?

In our study, we implemented a longitudinal analysis over time to compare how the fruit in different packages evolve along the supply chain. Figure 6 a-d shows that the fruit quality, mass loss, occurrence of condensation, and risk of mold growth differed considerably amongst the package sub-types. To identify which unit operations or segments of the supply chain are critical for this quality loss, we plotted the derivatives of these metrics for all the packages in Figure 6 e-h. Here, we see that every package has its own strong and weak points in different segments of the supply chain from farm to the retail store, so unit operations in which low or high loss of quality attributes occurs. Note that this analysis is performed for sub-groups of the package and corresponds to the average value for all packages within the sub-groups. The evolution of these quality metrics for individual packages is discussed in the later in this section.

Respiration-driven remaining fruit quality

The weakest link for respiration-driven quality decay is at the beginning of the supply chain prior to pre-cooling, where the rate of change in quality loss is the highest for all packages (Figure 6 e). This is in line with other studies that have reported that strawberries must be cooled within 1 hour of harvest to rapidly remove the field heat (Li et al., 2015; Nunes et al., 1995). A delay of 2, 4, 6, or 8 hours in pre-cooling can lower the marketability of strawberries by 20, 37, 50, or 70%, respectively (Mitchell et al., 1972). A commonly followed rule of thumb is that a delay of 1 hour in cooling translates into reducing the fruit shelf life by 1 day (Yahia et al., 2011). Additionally, a delay in pre-cooling can lower the level of soluble solids, ascorbic acid, and the overall brightness of strawberries (Nunes et al., 1995). For other unit operations in the cold chain, the rate of quality loss was fairly constant and in the similar range for all packages (0.5% decline in quality index per hour). The rate of quality decay increases at the end of the simulated supply chain during retail storage at ambient temperatures, so in the "last mile". However, as the fruit is at the diminishing phase of the exponential quality loss curve (of the first order kinetic model), the rate of quality loss is not as substantial as in the beginning of the cold chain.

Transpiration-driven mass loss

The rate of moisture loss shows two prominent peaks at the start of the supply chain (Figure 6 f). The first peak corresponds to the moisture loss just after harvest, prior to pre-cooling. High mass loss in strawberries due to delays before pre-cooling are also reported in other studies (Li et al., 2015; Nunes et al., 1995). The second peak corresponds to the onset of the pre-cooling phase. The air flow rates ($0.4 - 1.0 \text{ L}\cdot\text{s}^{-1}\cdot\text{kg fruit}^{-1}$), and consequently superficial air speeds are particularly high during pre-cooling (often $> 1.0 \text{ m}\cdot\text{s}^{-1}$). A higher air speed carries away the saturated layer of water vapor that has evaporated from the fruit, which is replaced by drier air. This ensures that the air near the fruit surface is not saturated with water vapor, thus increasing the driving force for transpiration (Poós and Varju, 2020). This is in line with studies reporting that hydro air cooling or mist-cooling perform better than forced air cooling by lowering the moisture loss in strawberries (Mascheroni, 2012). It is therefore also often recommended that pre-cooling should be stopped as soon as the produce is cooled, as continued airflow during pre-cooling can lead to substantial mass loss (Thompson et al., 2008a).

In the cold chain unit operations, we see a clear dependence of the rate of mass loss on the flow rate of the respective unit operations (Figure 6 f). This can be explained with the ventilation potential of the package during a certain unit operation. The volumetric flow rate is directly linked with the number of air exchanges per hour, *i.e.*, the number of times that the total volume of air is extracted out of the package and sent back in (Defraeye et al., 2016). Increasing air speed increases the transpiration rate in two ways - (1) higher convective mass transfer coefficient, and (2) higher air exchange increases the vapor pressure differential between the product surface and the air, which is the driving force for transpiration. The rate of mass loss was found to be the highest for all packages during pre-cooling ($U_{\text{upstream}} = 1.0 \text{ m}\cdot\text{s}^{-1}$), *i.e.*, about $0.015 \text{ g}\cdot\text{fruit}^{-1}\cdot\text{h}^{-1}$. For clamshells, the rate of mass loss is about $0.01 \text{ g}\cdot\text{fruit}^{-1}\cdot\text{h}^{-1}$ during transportation and redistribution ($U_{\text{upstream}} = 0.1 \text{ m}\cdot\text{s}^{-1}$), and is halved during storage at the warehouse or at the retail store cold room ($U_{\text{upstream}} = 0.01 \text{ m}\cdot\text{s}^{-1}$). Note that these values for rate of moisture loss correspond to the size of the strawberries investigated (Class I, equatorial diameter = 30 mm). For smaller berries (*i.e.*, commercial grade Class II), the rate of mass loss would be higher due to their large surface-to-volume ratio (Islam et al., 2019).

Flow-wrapped packages consistently show the lowest rate of mass loss ($< 0.005 \text{ g}\cdot\text{fruit}^{-1}\cdot\text{h}^{-1}$) throughout the cold chain. Similar studies have also reported that strawberries wrapped in packages can have up to a five times lower mass loss in comparison to unwrapped strawberries (Nunes et al., 1995). This could be because of the hygrothermal inertia as the trays are flow-wrapped in polypropylene films with no vents in the flow direction. The rate of moisture loss for open punnet trays is comparable to top-sealed trays and clamshells throughout the cold chain up to the retail store. This is mainly because our measurements show that the relative humidity in the cold chain segments is reasonably high ($80\pm 3\%$). Therefore, the absence of a lid does not drastically increase mass loss, which seems counter intuitive. The reason is that in majority of the unit operations in the supply chain, the humidity is sufficiently high to limit mass loss. However, when exposed to ambient conditions (40-50% relative humidity) during display on retail shelves, moisture loss is expedited in comparison to other packages. During retail store display in ambient conditions, the rate of moisture loss for open tray packages is almost double in comparison to ventilated packages, going as high as $0.02 \text{ g}\cdot\text{fruit}^{-1}\cdot\text{h}^{-1}$. This last unit operation severely limits the transpiration-driven shelf life of the strawberries packed in open trays. Consequently, the berries would tend to lose their firmness, appear less fresh, with a lower brightness (Alves et al., 2021; Nunes, 2009). Therefore, a short time on the shelves is key for open trays.

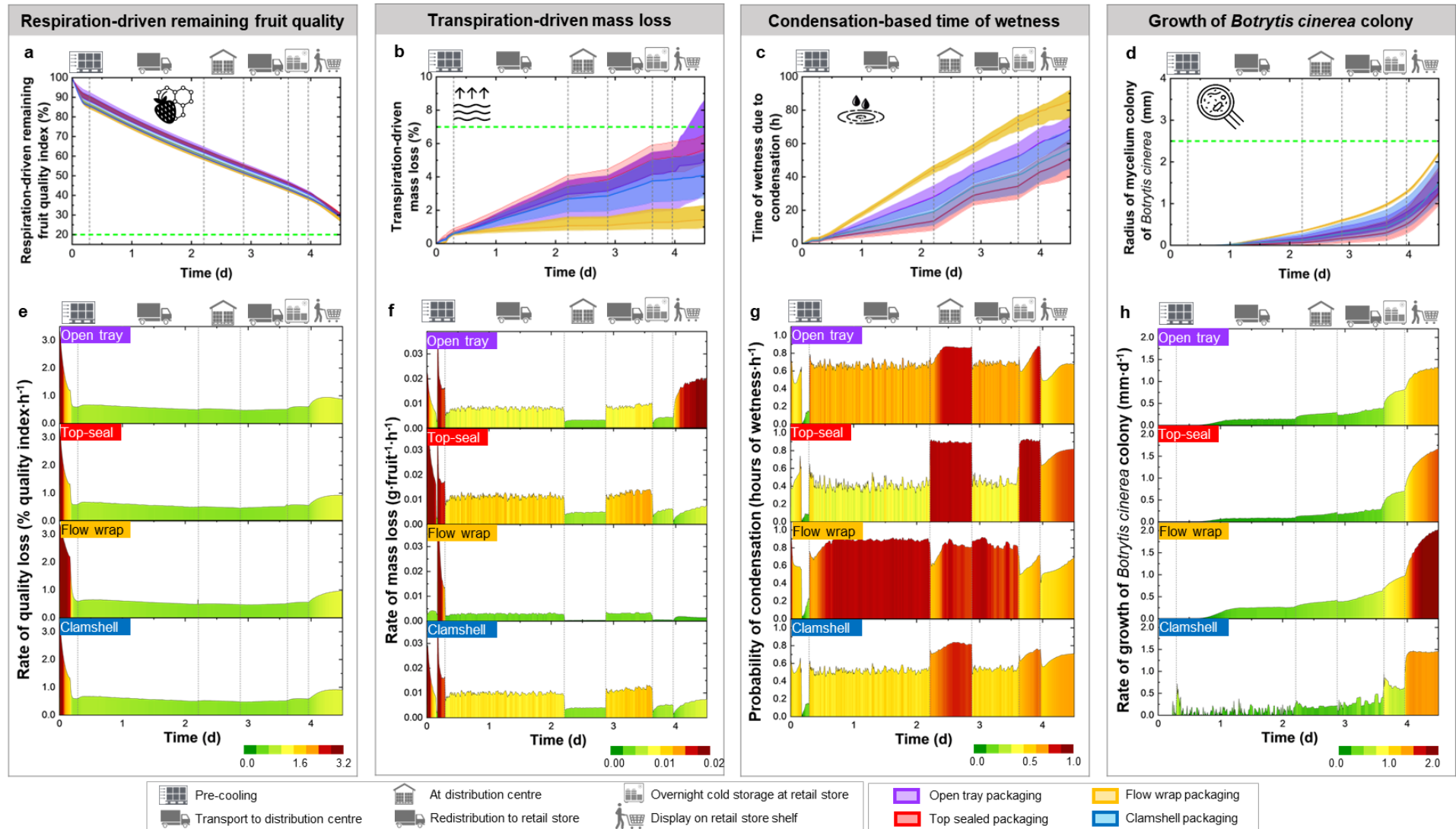


Figure 6: Plot of evolution of quality metrics (a,b,c,d) and their derivatives (e,f,g,h) across different unit operations in the supply chain: (a,e) Respiration-driven remaining fruit quality; (b,f) Transpiration-driven mass loss; (c,g) Condensation-based time of wetness; (d,h) Microbial growth of *Botrytis cinerea* colony. In a,b,c,d, the area enclosed for each package corresponds to the fruit lying within the 25th to 75th percentile considering all 21 packages grouped in their respective sub-types. The green dotted lines indicate the cut-off criteria for estimating the corresponding remaining shelf life, which is 20% for the respiration-driven quality index, 7% for mass loss, and 2.5 mm for the radius of fungal colony. Image credits: This figure has been designed using resources from Flaticon.com.

Condensation-based time of wetness and microbial growth risk

For comparing the rate of occurrence of condensation, alongside the occurrence of liquid condensate, we include the time when the relative humidity is higher than 95% at the fruit surface, as this is often sufficient for the germination of spores of *B. cinerea*. In Figure 6 c, we see that the risk of condensation occurrence is highest during storage at the warehouse and at the retail store cold room for all the packages. Under cold chain conditions (air temperature = 6-10 °C and relative humidity = 80±3%), the unit operations with the lowest air flow rate show the highest risk of condensation, for example storage at the warehouse ($U_{\text{upstream}} = 0.01 \text{ m}\cdot\text{s}^{-1}$). Here again, we see a dependence of the condensation rate on the air flow rate, and therefore ventilation potential corresponding to the unit operation. This could be due to several reasons. Firstly, low air speeds can result in stagnation of air in the package headspace, thus increasing the thickness of the boundary layer of cool air around the fruit surface. Condensation can occur not just at the fruit surface but also in its boundary layer when the air temperature falls below dew point. At higher air speeds, air movement disperses this stagnant layer, thus reducing the condensation risk. Secondly, at lower air speeds ($U_{\text{upstream}} = 0.01 \text{ m}\cdot\text{s}^{-1}$), ventilation is often inadequate to replace the humid air around the package with the drier air delivered to the pallets. Thirdly, high air speeds can rapidly dry up (or re-evaporate) the condensate or water that forms on fruit or package surfaces, thus lowering the residence time of the condensate. The risk of condensation is found to be the highest in flow-wrapped packages, due to their poor ventilation. This also favors the growth of mold, therefore flow-wrapped packages show the highest growth rate of *B. cinerea*.

When the package is shifted from the cold room to ambient retail store conditions (*i.e.*, rewarming), we see a sudden drop in the rate of condensation (Figure 6 g). This could be due to the sudden change in environment for the package, as the air in retail stores is quite dry (relative humidity of 40-50%) (The British Standards Institution, 2017). However, the rate of condensation eventually rises due to the fruit surface temperature being lower than the surrounding air. Therefore, as the fruit warms up, it cools the surrounding air, and cool air can hold less moisture, to the point that it reaches its dew point and condenses on the fruit and package surface. To mitigate this risk of condensation during rewarming, packages brought out of a cold store to be displayed on retail shelves could first be placed in front of fans that blow low-humidity, ambient air briefly through the packages. In that way, the cold surface heats up a bit and there is no risk of surface condensation in this dry environment. This practice is, however, not yet done to our knowledge and its performance in mitigating surface condensation should be tested.

Extrapolating the derivatives to evaluate fruit quality loss for every unit operation

The derivative values are almost constant for each unit operation in the cold chain, particularly for mass loss and quality loss (except pre-cooling and retail display, due to the sudden temperature change). Therefore, they can be used further and multiplied by the time length of the unit operation, to estimate the final quality metrics for any other supply chain or length of a unit operation. For example, in local supply chains, the time of transportation from pack house to distribution center is just about 6 hours, whereas for imported fruit, this can go up to 2 days. If we know that the fruit (of a certain commercial size) approximately lose moisture at the rate of $0.01 \text{ g}\cdot\text{fruit}^{-1}\cdot\text{h}^{-1}$ when packed in an open punnet tray, we can deduce that in a local supply chain, the net mass loss during transportation would be $0.06 \text{ g}\cdot\text{fruit}^{-1}$, so about 1 g in a 250 g package. As opposed to this, in an import supply chain lasting 2 days (as in our case from Spain to Switzerland), the mass loss would be $0.48 \text{ g}\cdot\text{fruit}^{-1}$, or almost 7 g in the same 250 g package. Thus, the values reported in Figure 6 are independent of the time length of the unit operation, if the hygrothermal conditions remain the same.

We extend our analysis to summarize the averaged values for the rate of loss of quality metrics for each of the 21 ventilated packages evaluated in this study across all the unit operations (Figure 7). While we observe similar trends as in Figure 6, we also observe large differences even within sub-groups, notably for top-sealed packages and ventilated clamshells. Therefore, in the Section 3.3, we analyze how packaging-related parameters, such as total open area in the flow direction, and headspace volume, influence these quality metrics.

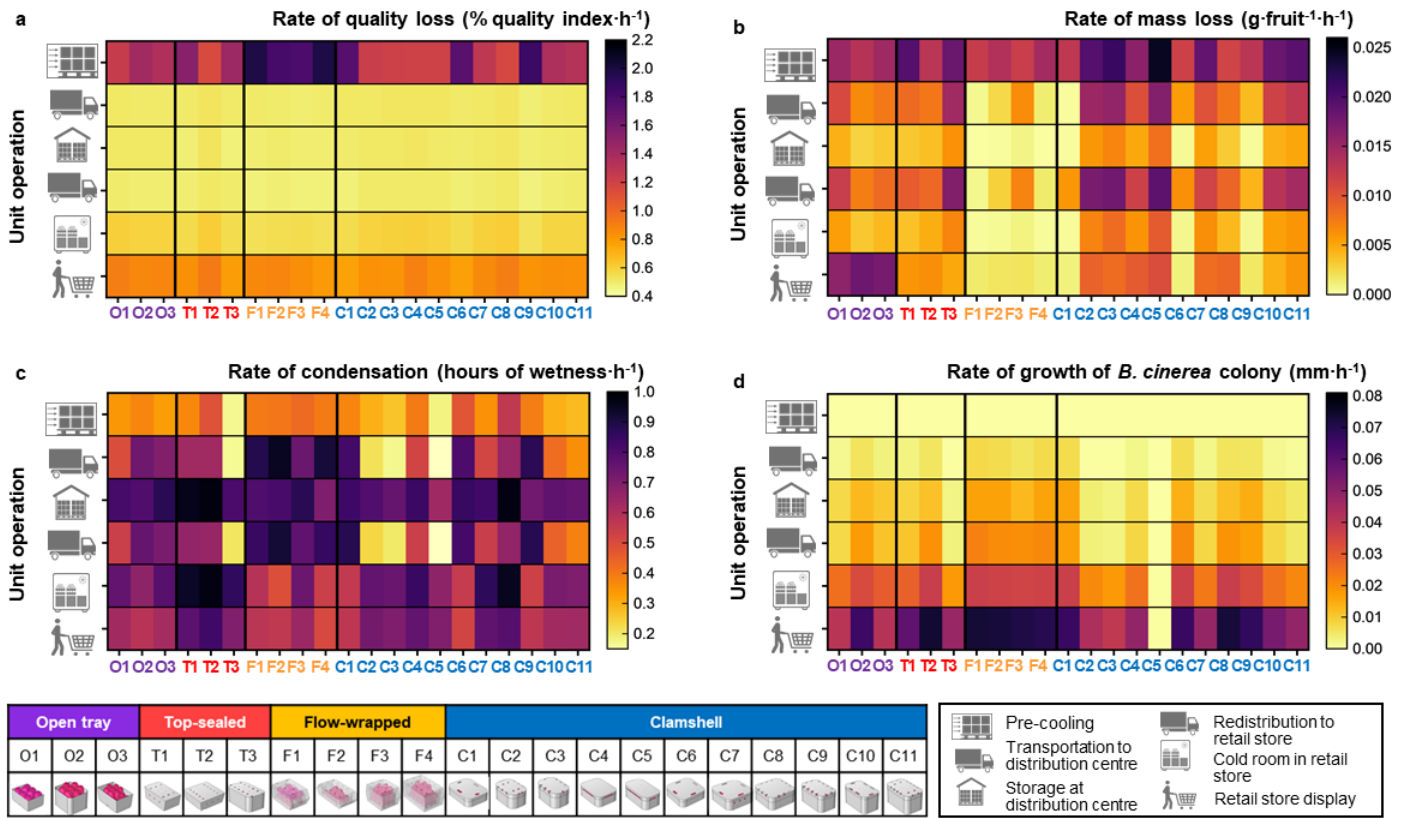


Figure 7: Plot of averaged derivatives for different unit operations corresponding to the 21 ventilated packages evaluated in this study: (a) Rate of quality loss ($\% \text{ quality loss} \cdot \text{h}^{-1}$); (b) Rate of mass loss ($\text{g} \cdot \text{fruit}^{-1} \cdot \text{h}^{-1}$); (c) Rate of condensation ($\text{hours of wetness} \cdot \text{h}^{-1}$); (d) Rate of growth of *Botrytis cinerea* colony ($\text{mm} \cdot \text{h}^{-1}$). Image credits: This figure has been designed using resources from Flaticon.com.

3.2 How does the trade-off between moisture loss and condensation evolve?

One observation that we derived from our analysis in Section 3.1 is the trade-off between condensation and moisture loss, particularly due to the influence of the flow field. Balancing the trade-off between condensation and mass loss for a package is central to maintaining strawberries fresh as well as free of mold growth. On one hand, mass loss lowers the net saleable weight of the fruit and lowers the fruit turgidity. On the other hand, condensation increases the risk of mold growth and also diminishes the external appearance by lowering the brightness of strawberries (Linke and Geyer, 2013). To pinpoint how trade-off evolves for different packages across the supply chain, we analyze the risk of condensation on the fruit surface as a function of its moisture loss for fruit in all packages in Figure 8.

Here, every single fruit in every package is located as a dot, colored by the package sub-type. We see that the curve formed by combining data for fruit in all the packages takes the shape of a trade-off frontier. The fruit on this frontier are 'efficient', implying that fruit with lower risk of condensation always have a higher mass loss. Optimizing a postharvest supply chain would entail shifting this frontier to the left, towards reducing the net mass loss and/or lowering the risk of condensation. Some practical approaches in the supply chain to shift this trade-off curve to the left include coating strawberries in the pack house to increase the resistance towards transpiration (Hosseinfarahi et al., 2020; Ribeiro et al., 2007; Wang et al., 2018), or the use of hygroscopic humidity-regulating sachets inside the package to lower the in-package headspace relative humidity (Bovi et al., 2019).

For all unit operations, the fruit in flow-wrapped packages (golden-yellow dots) are clustered at the shoulder of this trade-off curve, so in the region of high risk of condensation and low moisture loss. The fruit in other packages, including open punnet trays, ventilated clamshells, and recloseable trays are scattered across the curve. Amongst other reasons, one reason for this spread is that the fruit are stacked in layers. The fruit at the top layer of the open tray, or the fruit near the vent of a clamshell, have a higher moisture loss in comparison to other fruit within the same package.

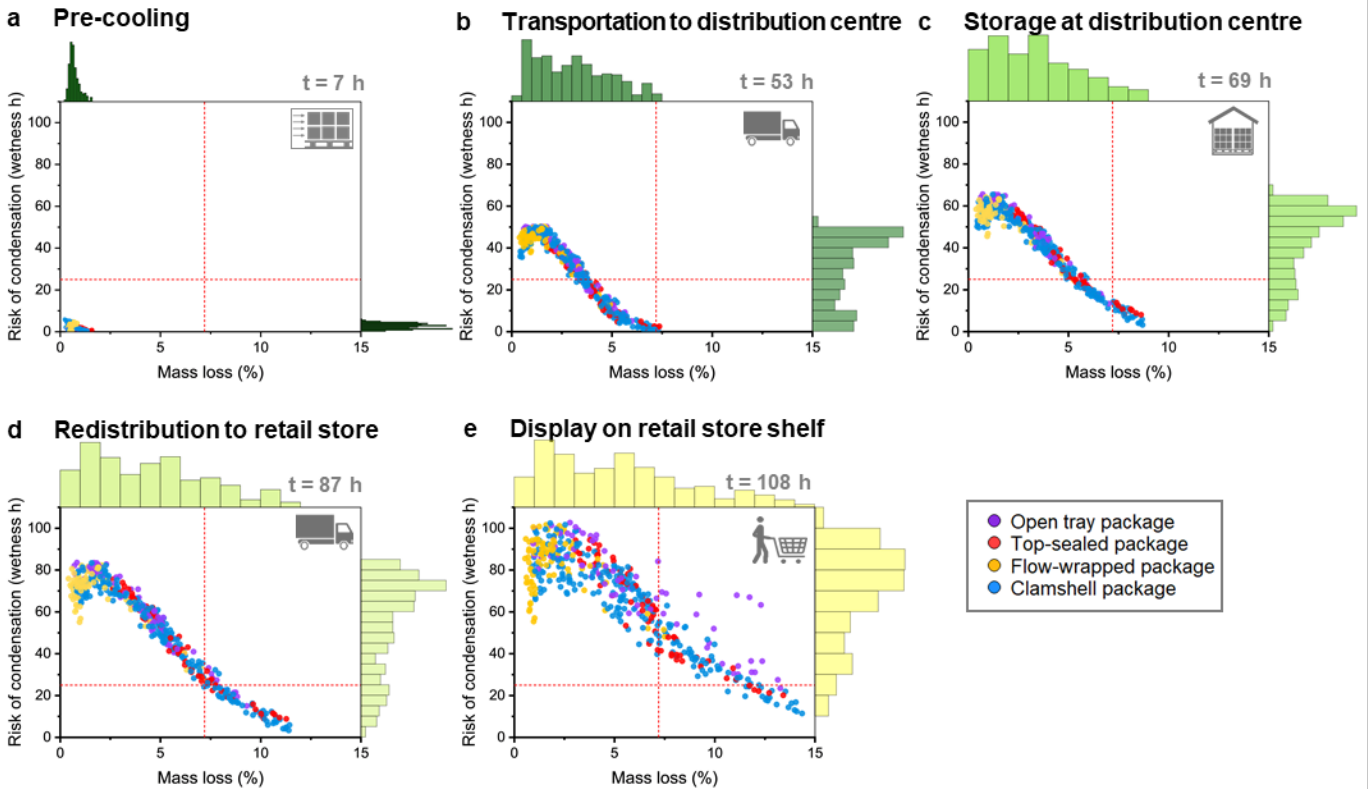


Figure 8: Trade-off between mass loss and risk of condensation: (a-e) Scatter plot for absolute values of mass loss and risk of condensation for fruit in different packages at the end of different unit operations in the supply chain. The red lines indicate the cut-off limits beyond which the metric becomes critical. For net mass loss, this is 7%, and for the risk of condensation, this is 18-24 hours. Here, each single fruit in every package is located as a dot, colored by the package sub-type. The histogram outside the scatter plot shows the frequency distribution. Image credits: This figure has been designed using resources from Flaticon.com.

The trade-off curve evolves at a near-constant rate for fruit in all the packages as we progress from pre-cooling to transportation, storage in the warehouse, and in the distribution center Figure 8 a-d. This is primarily because a high relative humidity ($80\pm 3\%$) is maintained around the package at all times, especially since the packages are stacked in pallets. However, in the unit operation of retail display, the packages show a large spread and differences become more pronounced (Figure 8 e). We also see clearly that a few berries in the open punnet tray (purple dots) deviate from this trade-off front. These correspond to the berries in the top layer of open package that lose moisture at a much higher rate in comparison to the berries in the lower layers. From a practical perspective, this could mean that open punnet trays can be used effectively for the entire duration when the fruit are in the cold chain, if a high relative humidity is maintained. However, in retail display, moisture loss is aggravated, especially for fruit in the top layer of open trays. Similar studies have reported that at 25 °C, strawberries could lose 3.1-4.3% mass per day (Rahman et al., 2016). To counter this, the open trays could be placed in refrigerated cabinets, or even cabinets with lids in retail stores. This is often not practiced by retailers due to several reasons. A key constraint is the energy and installation expense associated with these display units (Linke, 2019). Additionally, placing fruit outside cabinets stimulates impulsive purchase by consumers, as the fruit release increased volatile aromas under ambient conditions (Nunes, 2009). An added advantage is that refrigerated cabinets can maintain the fruit at a lower temperature, thus lowering the rate of respiration-driven quality loss reactions. However, such refrigerated display cabinets might not be optimal for flow-wrapped packing or clamshells with low vent area. This is mainly because frequent door opening can induce temperature fluctuations and augment the risk of condensation in these packages, particularly at the low air speeds prevalent in retail stores. Therefore, the nature of the solution to tackle this trade-off should take into focus the type of package it is designed for. Another alternative solution is to use dry misting. Here, we nebulize air into microscopic droplets. These droplets then evaporate and locally cool the air and increase the humidity (Fabbri et al., 2018).

Notably, the trade-off between moisture loss and condensation likely continues post-purchase. Some consumers tend to store their fruit in the refrigerator, while others prefer to keep them at the countertop. On one hand, low temperatures inside the refrigerator prolong the shelf life of berries and lower moisture loss. However, domestic refrigerators usually have large fluctuations in the circulating air temperature due to the compressor cycles (Laguerre et al., 2010). This can augment the risk of condensation, especially for unopened flow-wrapped packages or packages with low vent area. Studies have reported that about 50% of the consumers do not open the package before transferring it to the refrigerator (Céline et al., 2020). On the other hand, placing the strawberries at ambient temperatures expedites quality deterioration, and may also lead to excessive moisture loss if the ambient humidity is low (Porat et al., 2018).

3.3 How do package parameters influence fruit quality and marketability metrics?

In the present study, we fixed the product-related boundary conditions (such as fruit size, initial quality, and thermophysical properties), as well as process-related boundary conditions (temporal and hygrothermal profile of the supply chain). Therefore, we could isolate and analyze the differences in fruit quality and shelf life particularly due to different packaging. In Section 3.1, we reported large differences in the rate of loss of various quality metrics, even within the same sub-group of packaging. To understand how thermodynamic and aerodynamic package parameters impact the final fruit quality and marketability at the end of the simulated supply chain ($t = 4.5$ days), we performed a correlation analysis (Figure 9).

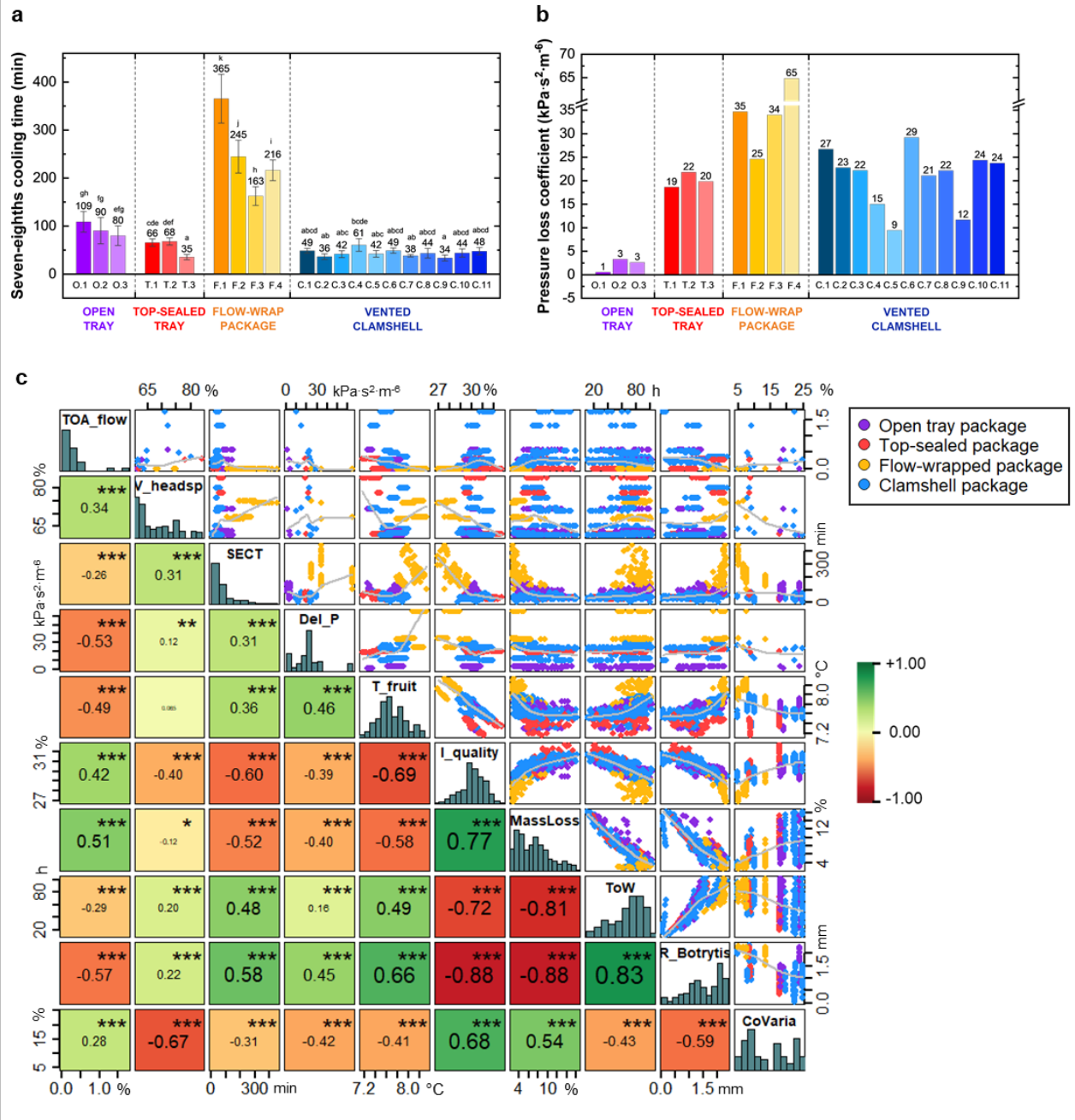


Figure 9: Relationship between metrics for packaging performance and the resulting fruit quality at the end of the supply chain, i.e., at $t = 4.5$ days: (a) Seven-eighths cooling time ($t_{7/8}$, min) for the packages during pre-cooling - here, mean values having the same alphabet do not vary significantly (Tukey HSD test, $p \leq 0.05$); (b) Pressure loss coefficient (ξ , $\text{Pa}\cdot\text{s}^2\cdot\text{m}^{-6}$) for the packages estimated from the pressure loss curve for every package as a function of the superficial air speed (Supplementary materials, Section A.4), (c) Correlation matrix depicting the pairwise scatter plot and the Pearson's correlation coefficient (ranging from -1 to $+1$, where -1 indicates a strong negative correlation, 0 indicates the absence of correlation, and $+1$ indicates a strong, positive correlation). Significance for each correlation is indicated as asterisks: * < 0.05 , ** < 0.01 , *** < 0.001 . TOA_flow: total area in the flow direction (TOA_{flow} , %); V_headsp: headspace volume ($V_{\text{headspace}}$, %); SECT: seven-eighths cooling time ($t_{7/8}$, min); Del_P: pressure loss coefficient (ξ , $\text{Pa}\cdot\text{s}^2\cdot\text{m}^{-6}$); T_fruit: volume-averaged fruit temperature ($^{\circ}\text{C}$); I_quality: respiration-driven fruit quality index (I_b , %); MassLoss: net transpiration-driven mass loss for the fruit (%); ToW: time of wetness due to condensation (h); R_Botrytis: Radius of colony of *B. cinerea* (R_{BC} , mm); CoVaria: Coefficient of variation (CoV, %).

Figure 9 a shows the seven-eighth cooling time for the fruit in different packages. The seven-eighth cooling time is the most widely used parameter to evaluate the cooling efficiency of packages, particularly during pre-cooling, since the fruit temperature reaches acceptably close (87.5%) to the target temperature of the cooling air. Several studies on packaged fresh produce have reported that the seven-eighth cooling time for strawberries lies between 1 and 6 hours, which is in agreement with our findings (Thompson, 2016). This cooling time, of course, depends on the airflow speed with which is cooled. Flow-wrapped packages show the highest values for the seven-eighths cooling time, ranging between 3 and 6 hours. This is because of the absence of any vents in the flow-direction, which results in stagnation of the air inside the package, even at high air speeds. Our findings show that during pre-cooling, flow-wrapped packages have a 5 times lower averaged convective heat transfer coefficient in comparison to ventilated clamshells (Figure 10). Flow-wrapped packages also show the largest variation in cooling time for fruit within the package (Figure 10 a). Other studies have also reported that wrapping lowers the cooling rate and increases the cooling heterogeneity within a package (Cao et al., 2020). Note that in a commercial setting, fruit are often first pre-cooled to remove field heat, after which they are flow-wrapped. On the other hand, ventilated clamshells show the shortest cooling time, so the highest cooling rates. This is because of the presence of vents in the flow direction that improve the cooling efficiency of the fruit inside the package. High-speed turbulent air jets appear and recirculation vortices promote mixing inside the packaging. Although open punnet trays have a large total open area due to the open top surface, the cooling time is higher (80-110 minutes), particularly for fruit in the middle of the package (Figure 10 b). This is due to the small vent area in the flow direction for these packages, as the direction of airflow in pre-cooling is primarily horizontal (Ambaw et al., 2021; Ferrua and Singh, 2009b; Getahun et al., 2017; Wu et al., 2019). There is little mixing, compared to the clamshells, by which the fruit at the bottom cool much slower.

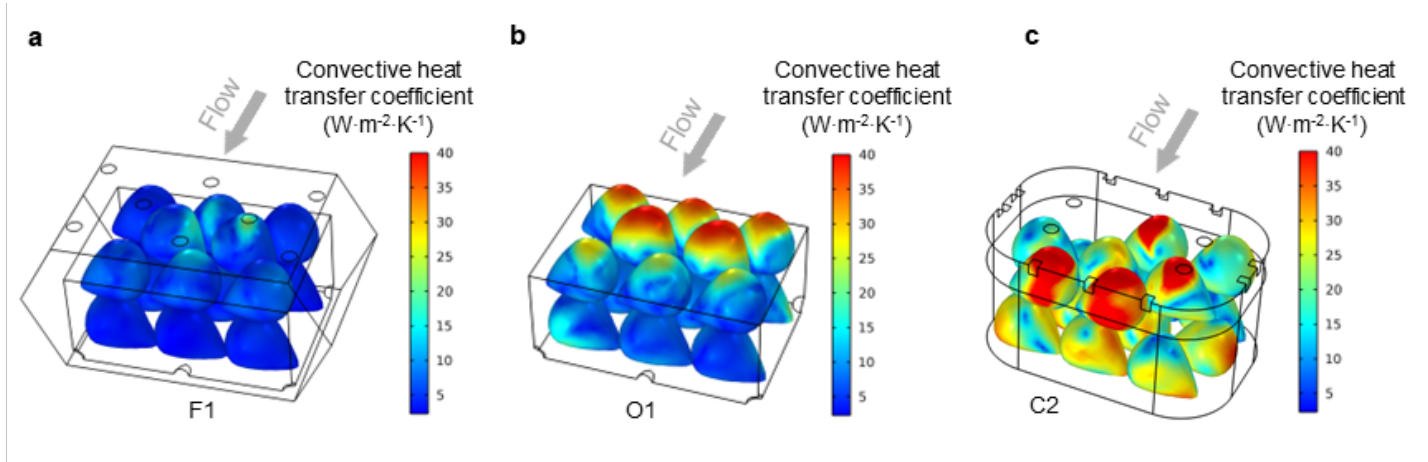


Figure 10: Convective heat transfer coefficient during pre-cooling (upstream air speed = $1.0 \text{ m}\cdot\text{s}^{-1}$) for different 250 g fruit packages: (a) flow-wrapped package (F1); (b) open punnet tray (O1); (c) clamshell (C2). The convective heat transfer coefficient is plotted to the same scale for easier comparison.

To assess the aerodynamic performance of the packages, we computed the pressure drop across the package in the flow direction, and thus estimated the pressure loss coefficient (Figure 9 b). A low pressure drop coefficient implies that the package offers less resistance to airflow. This also implies that a lower power is required to push the cooling air through the package. A low resistance to airflow improves the cooling performance of the package and also lowers the energy consumption (Getahun et al., 2017). The lowest resistance to airflow is observed for open punnet trays, as air can easily flow through the headspace of the package when it is stacked in secondary packaging inside a pallet. Flow-wrapped package have a low pressure drop across the package, due to the aerodynamic shape (*i.e.*, hexagonal cross-section) of the package, which allows air bypass from the sides. However, when accounted for the free area ratio, the pressure loss coefficient is large, as the absence of vents in the flow direction does not allow air to flow through the package.

From the correlation analysis (Figure 9 c), we find that most metrics for fruit quality and marketability show a good correlation with the total open area in the flow direction (TOA_{flow}). The vent area at the bottom surface of the packages was not considered, as the fruit itself tends to block these vents partially, or even completely. Additionally, the packages are sometimes padded with bubble wrap below the berries to minimize mechanical damage due to vibrations during transportation, thus blocking these vents. The total open area shows a good correlation with the mean fruit temperature (correlation coefficient = -0.49). The presence of vents alters the airflow distribution inside the package and in the fruit layers, thus affecting the heat transfer. Higher total open area also allows the heat or respiration to escape the package (Pathare et al., 2012). For example, in Figure 11, we compare two rounded-square clamshells with the same stacking arrangement of fruit, but different total open area in the flow direction. The package with vents in the flow direction shows a higher and more uniform distribution in the convective heat transfer coefficient. Several other studies have also reported that increasing the total open area in improves the cooling efficiency and cooling heterogeneity of a package (Getahun et al., 2017; Pathare et al., 2012).

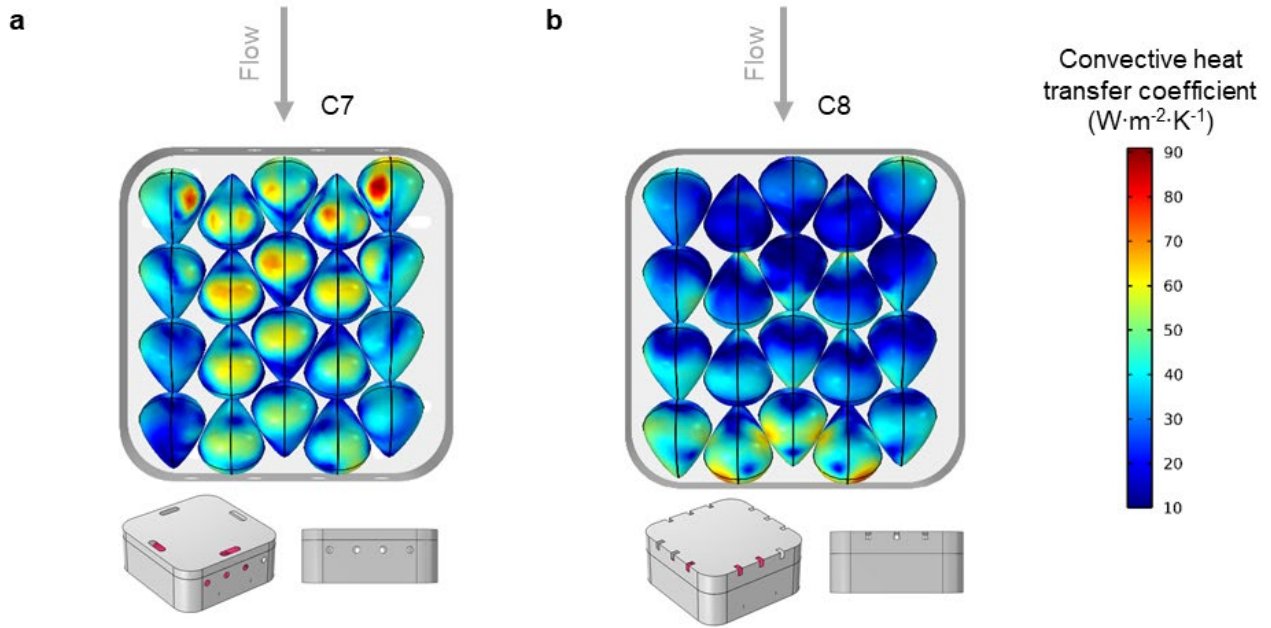


Figure 11: Convective heat transfer coefficient during pre-cooling (upstream air speed = $1.0 \text{ m}\cdot\text{s}^{-1}$) for different 250 g fruit packages: (a) clamshell (C7) with circular vents in the flow direction (net $TOA = 2.49\%$, $TOA_{\text{flow}} = 0.49\%$); (b) clamshell (C8) with no circular vents in the flow direction (net $TOA = 1.68\%$, $TOA_{\text{flow}} = 0.36\%$). The convective heat transfer coefficient is plotted to the same scale for easier comparison.

The pressure drop across the package shows a negative correlation (correlation coefficient = -0.53) with the total open area. It has widely been reported that increasing the total open area decreases the resistance to airflow offered by the package (Getahun et al., 2017). Studies have also developed models to establish a power law relationship between pressure drop as a function of the total open area of a package (Pathare et al., 2012).

The total open area in the flow direction is also correlated with the net mass loss (correlation coefficient = 0.51). This implies that the fruit inside packages with a higher vent area will have a higher mass loss. One of the reasons is that a well-ventilated package allows more air to flow through the package. This lowers the headspace humidity by constantly flushing in fresh cooling air, so higher ventilation potential. In turn, this increases the vapor pressure differential between the fruit surface and air, which is the driving force for transpiration. The total open area shows a small but significant correlation with the time of wetness due to condensation (correlation coefficient = -0.29). Therefore, if the total open area is lower, water molecules cannot escape the package. This increases the in-package relative humidity, thus increasing the risk of condensation. Consequently, the risk of mold growth is also higher, which is reflected in the correlation between TOA_{flow} and fungal colony radius (correlation coefficient = -0.57).

The packages of strawberry are not filled to the top, therefore a distinct headspace exists (Defraeye et al., 2015). The volume of this headspace ($V_{\text{headspace}}$, %) shows a good correlation with the coefficient of variation (correlation coefficient = -0.67). The headspace volume and the degree of filling (DOF) are related as $V_{\text{headspace}} = 1 - DOF$. Therefore, higher the degree of filling, higher is the overall heterogeneity within the package. This could be due to the fruit being in several layers for a package that has a higher degree of filling. In our analysis, we did not see a correlation between the headspace volume and the moisture loss. One reason could be that in the present study, the headspace volume for all the analyzed packages ranged between 60-80%, therefore the range is not large enough to capture differences introduced due to headspace volume. However, other studies have reported that the headspace volume influences the moisture lost by the fruit. For example, one study found that for the same volume of berries, doubling the headspace volume of a package increases the moisture loss by a factor of over 1.5 (Bovi et al., 2018). This is because for a package, the rate of transpiration by fruit is much higher than the rate at which moisture is exchanged across or transported outside the package. For a smaller headspace volume, water vapor saturation is reached faster, therefore moisture loss is lowered.

The product-related metrics showed a good correlation with one another and with the fruit temperature (absolute correlation coefficient > 0.5). This is because the underlying drivers responsible for these metrics are overlapping, mainly airspeed, air temperature, and relative humidity.

3.4 What is the spatial variability in fruit quality within a package?

The distribution of air temperature, relative humidity, and air speed is not uniform in the package, and this also reflects in the heterogeneity in fruit quality and marketability within the package. Ideally, we would like to have that all fruit have a rather uniform decay in fruit quality attributes within the package, and also that no distinct critical locations appear. The latter is relevant as one spoiled strawberry could make that the consumer or retailer throws away the full package, since repacking is labor intensive.

Respiration-driven remaining fruit quality

Our findings show that within the same package, the difference between fruit temperatures can be as high as 2.5 - 3 °C (Figure 12). In general, we observe that the fruit next to the vents have the lowest average temperature along the supply chain. For example, Figure 12 shows the fruit at the end of cold storage in the retail store, so just before the fruit are brought to ambient retail conditions. For open packages, we observe that the fruit at the top are the first to react to any changes in temperature (Figure 12 a). Additionally, our findings show that fruit in the bottom layer and corners (next to the vents) have the lowest average temperature along the entire supply chain. Flow-wrap packages also show a large variability in temperature, and the fruit in lower layers are at least 1.5-2 °C cooler than the fruit in the topmost layer. In contrast, the ventilated clamshell C2 has the highest temperature homogeneity as the presence of vents allows for the uniform distribution of the incoming air (Figure 12 c). Although we do observe that the fruit in the top layer are warmer than the fruit below in these packages, the difference between the highest and lowest fruit temperature within the package is very small (<1 °C).

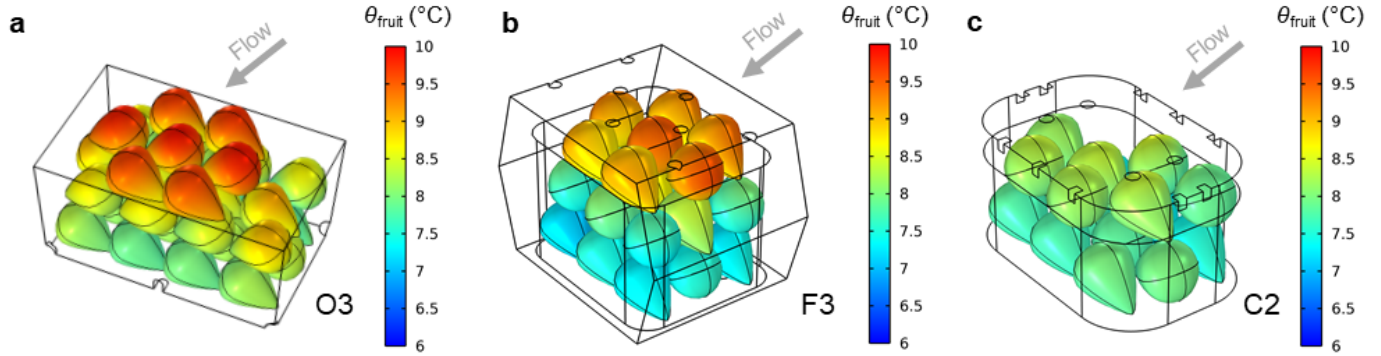


Figure 12: Spatial variability in fruit temperature (θ_{fruit} , °C) within selected packages at the end of cold storage in the retail store, i.e., just before they are brought out into ambient conditions in a retail store: (a) Open punnet tray (O3); (b) Ventilated clamshell (F3); (c) Flow-wrapped package (C2).

Transpiration-driven mass loss

The rate of moisture loss showed a large spread especially for packages with fruit stacked in multiple layers. We observe this in the violin plots in Figure 13 a, which show the net mass loss at the end of retail. The violin plots show a clear curvature corresponding to fruit in different layers of the package. This is more so for packages containing higher volume of fruit (400 - 500 g packages). Thus, in a sense, the moisture loss for a fruit depends on where in the package it is located and on the number of fruit surrounding it. Similar findings were reported in other studies, where the moisture loss was found to decrease with an increase in the number of berries in the same package. Moisture lost by a single strawberry was 2.5 times higher than of 15 strawberries (Bovi et al., 2018). This could be due to two reasons. Firstly, if a berry is surrounded by several neighboring berries, the effective surface area for transpiration is lowered. Additionally, the relative humidity in the void space between the berries is quite high as flow is restricted. A second factor, more so for closed packages, is that as the number of berries in a package is higher, the headspace of the package has a higher relative humidity, and therefore the driving force for transpiration is lowered (Bovi et al., 2018). Therefore, fruit in the topmost layer of the package lose the highest moisture, as they have fewer surrounding fruit. We see this in open punnet trays (Figure 13 b). When open (unlidded) packages are exposed to ambient conditions during retail display, the strawberries in the top-most layer lose moisture at a four times higher rate in comparison to fruit in the layers below (Figure 13 b). On the other hand, fruit in flow-wrapped packages lose moisture at much lower rates. This is because the headspace constantly has a high relative humidity, as the water molecules within the package cannot easily escape (Figure 13 c). Additionally, we observe that fruit in the middle of the package, that is surrounded by maximum neighboring fruit, have the lowest moisture loss rate.

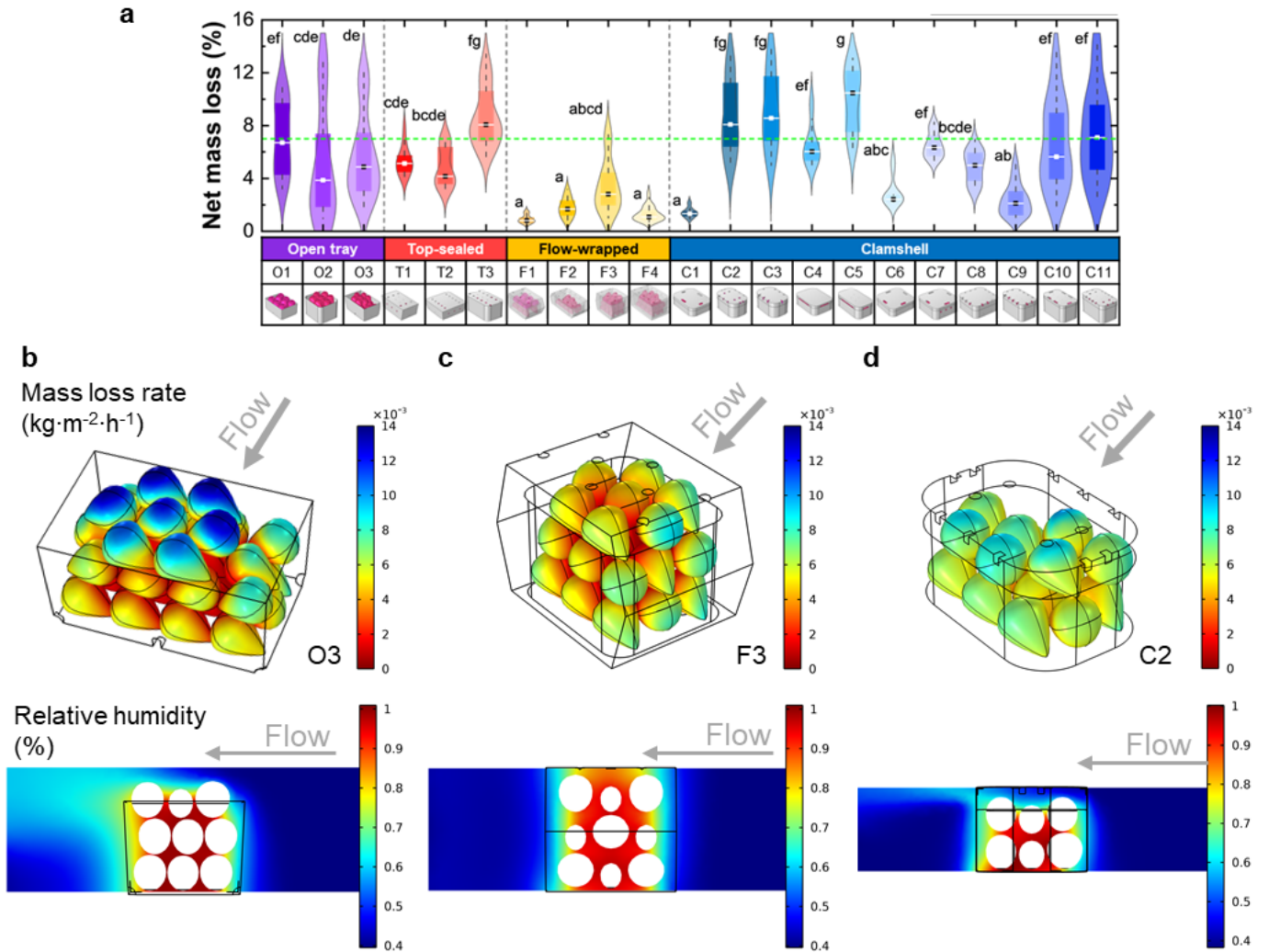


Figure 13: Net mass loss (%), spatial variability in mass loss rate ($\text{kg}\cdot\text{m}^{-2}\cdot\text{h}^{-1}$) and relative humidity distribution (%) in selected packages: (a) Violin plots showing the spread in the net mass loss within the same package at the end of the simulated supply chain ($t = 4.5$ d). The violin plot encloses a box-and-whisker plot, where the box encloses fruit in the 25-75 percentile and the whiskers represent the range within $1.5 \times$ interquartile range. The green dotted line indicates the threshold for acceptable mass loss (7%); Mass loss rate ($\text{kg}\cdot\text{m}^{-2}\cdot\text{h}^{-1}$) and relative humidity distribution (%) during retail store display under ambient conditions for: (b) Open punnet tray (O3); (c) Flow-wrapped package (F3); and (d) Ventilated clamshell (C2).

For the ventilated clamshell, we see a rather uniform mass loss rate, which is notably high. In the relative humidity distribution, we see snapshot of the relative humidity distribution when this package is brought to ambient conditions during retail. We observe that due to the vents, dry air enters the headspace of the clamshell (Figure 13 d). This was not the case in flow-wrapped packages, where the air inside the package maintains a high relative humidity due to the absence of vents. Therefore, our findings show that the position of vents plays a key role in determining the moisture lost by the fruit. This also explains the large differences amongst the net mass lost by different clamshells (Figure 13 a). Vents in a package are often designed symmetrically in the flow direction, so they mirror one another. If the package is not filled in a way that the fruit obstruct the flow, there is the risk of flow going through the package, *i.e.*, takes the direct path from inlet vents to outlet vents, often at very high air speeds. We see this specifically in clamshells C4 and C5 that have a symmetrical trapezoidal open area on the lid in the flow direction Figure 14 a-b. The placement of fruit in these packages is such that it does not completely obstruct the flow. Therefore, we see from the streamline plots that a large proportion of the air flows through, as the height of the vents is higher than the equatorial diameter of the fruit. As a result, the ventilation potential of this package is high, because a continuous stream of air is constantly flushing through this package. This is reflected in the low pressure loss coefficients of these packages. We also find that these packages, particularly C4, has the lowest risk of condensation and mold growth. However, moisture loss is expedited, particularly during unit operations where air speed is high (such as pre-cooling and transportation). In a commercial setting, there is a possibility that the flow-through of air does not happen exactly in the way we simulated it due to different stacking patterns in the pallet and the randomness in the pattern of fruit filling. Additionally, the alignment with respect to the secondary packaging will also play a role here. This work, however, highlights the role of vent positions on the package.

A similar possibility of air flowing through is also observed in packages that have vents on the lid, such as packages C2 and C3. In Figure 14 c, we see that the streamlines directly flow through the package without obstruction from the fruit. Consequently, these

clamshells have high moisture loss rates, as the headspace is occupied with drier air. Our findings show that the moisture loss rates are even comparable to open punnet trays, which are unlidded. Therefore, for the same open area, the height of the vents, as well as the filling arrangement of fruit, impact the ventilation potential of the package. This could also correspond to the size of fruit in the package. For example, in the inset in Figure 14 c, we see that small fruit have a higher surface-to-volume ratio, due to which it takes more number of fruit to fill up the package. On the other hand, the same package, when filled with larger fruit, has a larger headspace height. The size of fruit therefore define the headspace volume of the package. Based on our findings, future studies could also consider fruit size (or commercial grade) as a parameter for selecting the optimal package. Additionally, packages could consider asymmetric or staggered vent arrangement in the flow direction in order to increase the tortuosity of the air inside the package. We acknowledge here that in a real supply chain, the flow may not be perfectly horizontal due to turbulence in the incoming air stream, stacking of the packages, as well as the influence of the secondary packaging on the air flow. Therefore, evaluating different airflow scenarios might be as important as including additional details such as fruit size and tortuosity.

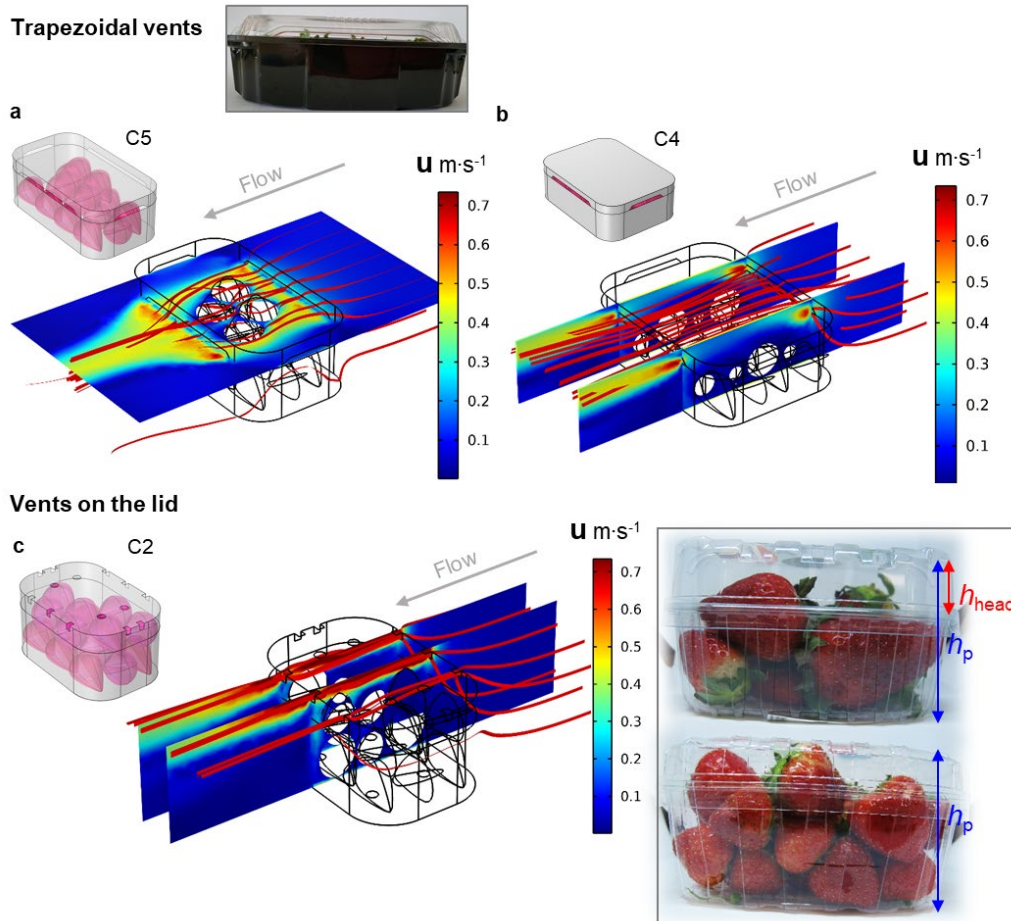
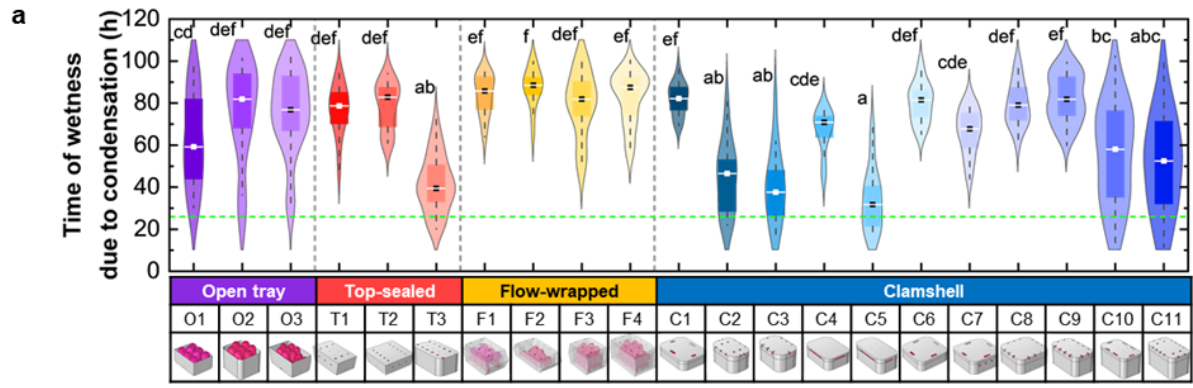


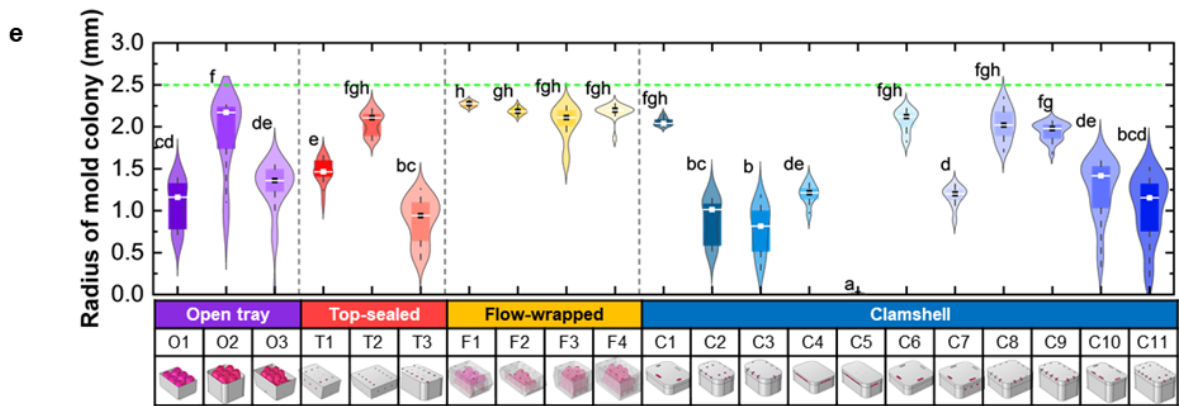
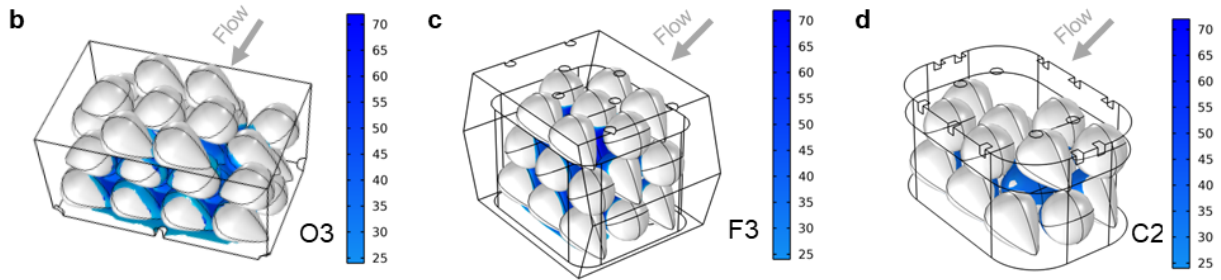
Figure 14: Impact of shape and height of vents and the absence of fruit obstructing the flow on the flow field inside the package for a superficial airspeed of $0.1 \text{ m}\cdot\text{s}^{-1}$: (a) and (b) Streamlines (red ribbons) and slice plots of the flow field as air enters the packages with trapezoidal vents (clamshells C5 and C4); (c) Streamlines (red ribbons) and slice plot of the flow field as air enters the ventilated clamshell with symmetric vents in the flow direction on the lid (clamshell C2).

Condensation-based time of wetness and mold growth risk

Through our model, we also identified regions in the package that are most prone to condensation (Figure 15). Our findings show that the middle layers and the bottom of the tray are the most critical regions for condensation, even for open (unlidded) trays (Figure 15 a). Flow-wrapped also show similar critical regions, where the fruit surrounded by maximum neighboring fruit is most prone to condensation (Figure 15 b). The risk of condensation is lower in ventilated clamshells, as the ventilation potential is higher (Figure 15 c). Therefore, drier air is constantly flushed into the package. However, for clamshells carrying larger fruit volumes (for example 500 g), fruit are often stacked in layers. As a result, the middle layers and bottom layers are prone to the risk of condensation. All the clamshells investigated in our study carrying 500 g of fruit have vents on the lid, but not on the side walls. One solution to lower the risk of condensation in such packages would be to introduce vents on the side walls, so that drier air directly hits fruit in middle layers. Additionally, vents could be in a staggered arrangement, if more than two layers of fruit are present. However, this would entail calculations to ensure that the mechanical strength of the package is not compromised. For clamshells, however, we do not expect large structural difficulties as the material and package can handle some more small perforations.



Risk of condensation (wetness hours (h) > 24 h)



Risk of mold growth (radius of *Botrytis cinerea* colony (mm))

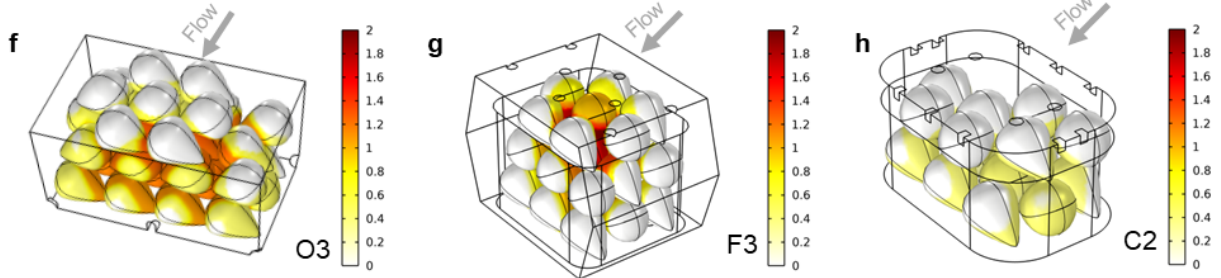


Figure 15: Spatial variability in the risk of condensation and mold growth within selected packages: (a,e) Violin plots to show the spread (variability) in risk of condensation and mold growth within the package for the 21 packages investigated in this study at the end of the simulated supply chain ($t = 4.5$ d). The violin plot encloses a box-and-whisker plot, where the box encloses fruit in the 25-75 percentile and the whiskers represent the range within $1.5 \times$ interquartile range. The green dotted line indicates the beyond which condensation and mold growth are critical; (b,f) Open punnet tray (O3); (c,g) Flow-wrapped package (F3); (d,h) Ventilated clamshell (C2). Low values and a narrow distribution of the violin plot indicates lower risk of condensation and lower heterogeneity in the risk, respectively.

The prediction of the spatial distribution of the risk of condensation is a key added value of our digital twin. As condensation is a complex spatiotemporal phenomena, it can occur simultaneously on locally different parts of the same fruit. The experimental

measurement of the condensation risk is often challenging (Linke et al., 2021). Direct methods, such as gravimetric measurements of the amount of condensate, require a very high-precision weighing scale, and do not provide a spatial risk distribution. Indirect measurements, such as the use of electric signals to measure wetness, also provide only point measurements (Linke et al., 2021). With our physics-based digital twin, we determine the intensity and retention time of the condensate. Additionally, we predict the risk of mold growth based on fruit surface temperature and humidity. This is a big step ahead of state-of-the-art, which rely only on the available sensor data that most often provide point measurements. Thus, predictions are more representative of the state of the fruit.

We found the regions within the package at a high risk of mold growth to be similar to those regions with the highest risk of condensation (Figure 15). The fruit in the middle layer of the package show the highest risk of mold growth because two drivers work in synergy: (1) temperature, as the fruit in the center of the package are often the last to reach the delivery air temperature, and (2) relative humidity, as the fruit in the center of the package have the highest relative humidity around them. We observed this previously in Figure 13 that relative humidity around these fruit can attain high values inside the package, even when the ambient relative humidity is much lower (40%). As a result, the risk of condensation and consequent mold growth is the highest. More generally, we observe that mold spread from the inside of the package towards the outside Figure 15 f-h. Most solutions aimed at lowering relative humidity in the package headspace to reduce the risk of condensation target the headspace of the package. Examples include the use of hygroscopic humidity-regulating sachets inside the package to lower the in-package headspace relative humidity (Bovi et al., 2019). Another straightforward way is to ventilate the package better by optimizing the vent hole configuration. However, our findings show that the voids between the fruit have the highest relative humidity and risk of condensation Figure 15 b-d, and therefore these regions should be the target for any solutions to lower the relative humidity inside the package. Lowering the headspace relative humidity does not necessarily imply that the humidity is lowered in the critical regions in the void space between the fruit.

3.5 Which package performs best in balancing the three-way trade-off in shelf life?

As fruit drift through a supply chain, they encounter several unit operations that influence their physical, biochemical, and microbiological quality evolution. In Figure 16, we present a summary of our analysis in the form of a packaging scorecard for all the investigated packages. Here, for every package, we can pinpoint the stage in the supply chain where losses are expedited. For example, for all the packages, the maximum respiration-driven quality is lost during transportation from pack house to the distribution center, particularly due to the time length of this segment, which can extend up to 2 days for imported fruit. Moreover, the air temperature is in the range of 5 - 6 °C, which is higher than the recommended temperature of 0 - 4 °C (Shoji et al., 2022).

We observe the largest differences in the performance of the packages for the net mass loss. Open punnet packages have a net mass loss comparable to other packages, despite being unlidded. The mass loss for these open packages is highest during retail display, at ambient conditions. On the other hand, ventilated clamshells lose the most moisture during transportation from pack-house to the distribution center, as the air flow rates are higher. As such, if the vent holes are optimally used and accessible for airflow, high airflow rates are detrimental for mass loss. Mold growth rate increases rapidly when the fruit is in the retail store, particularly due to exposure to ambient temperatures. However, our model also takes into account the risk of condensation in other segments of the supply chain, which contribute towards mold growth. Such a longitudinal analysis comprising information over the entire supply chain duration is vital to identify critical loss points in the supply chain. The latent or invisible losses incurred in the early unit operations in the supply chain can make the fruit more prone to spoilage at later stages of the supply chain, with substantial economic and environmental losses. For example, the rate of condensation for the packages is high during warehouse storage, but lowers again during redistribution to the retail store. This could mean that the condensate dries out when it reaches the retailer. However, the latent damage caused by condensation, such as aiding the germination of spores, goes unnoticed. These latent damages may only be evident until later as spoilage. This would bring retailers at the receiving end for blames or claims by consumers, when the actual cause of damage could potentially be further upstream in the preceding unit operations.

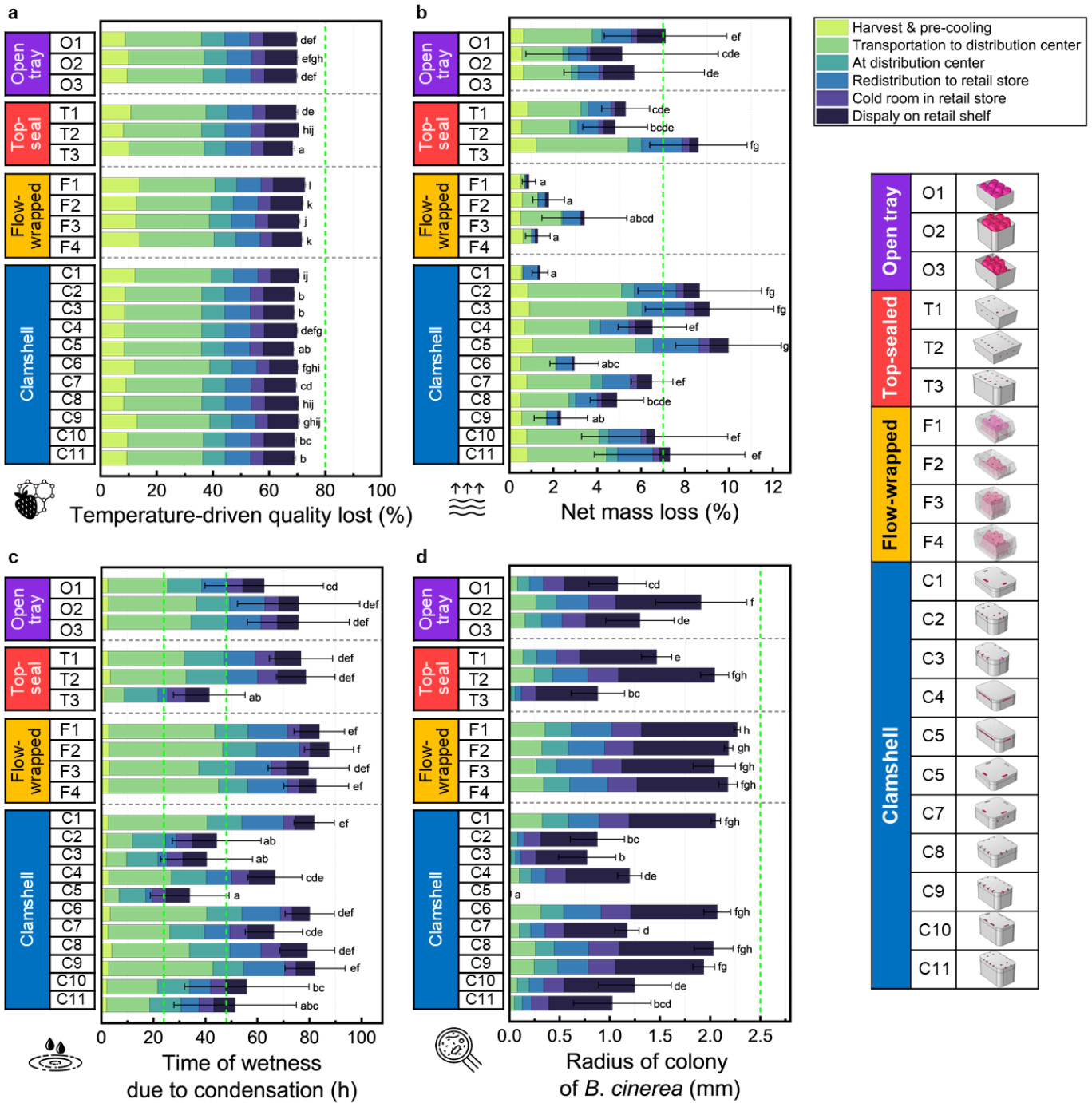


Figure 16: Packaging scorecard for evaluating the performance of different packages across the unit operations in the supply chain. For every metric, the green dotted lines indicate the cut-off point, beyond which the product is likely to get rejected by consumers. Here, the bars correspond to the mean value and the error bars denote the standard deviation as heterogeneity within the package. Mean values having the same alphabet do not vary significantly (Tukey HSD test, $p \leq 0.05$). Image credits: This figure has been designed using resources from Flaticon.com.

We combined these findings to identify the packages that maximizes the fruit shelf life. The fruit shelf life corresponds to the time, under ambient conditions, during which the fruit retains its desired biochemical, physical, microbiological, and sensory characteristics (Giménez et al., 2012). While we did not evaluate sensory characteristics, we evaluated the packages based on the fruit's temperature-driven biochemical shelf life, transpiration-driven physical shelf life, and mold growth-driven microbiological shelf life (Figure 17 a). Their unique combination determines the fruit's life expectancy and the resulting amount of food loss.

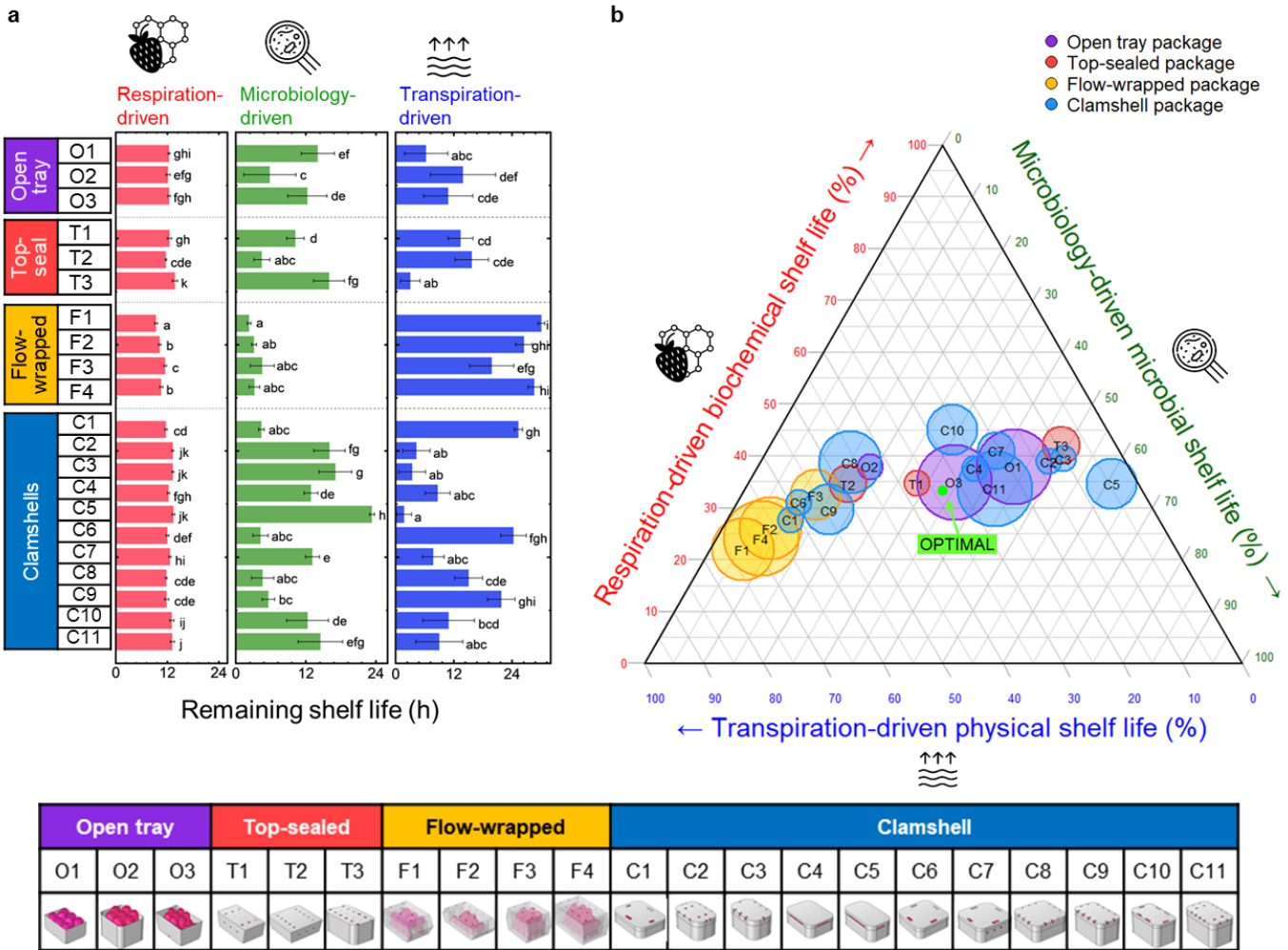


Figure 17: Three-way shelf life for fruit inside the package at the end of the simulated supply chain ($t = 4.5$ d): (a) A bar chart indicating the resulting respiration-, transpiration-, and microbiology-driven remaining shelf lives (h) for fruit in the 21 ventilated packages analyzed in this study. The shelf life was estimated using cut-off point methodology. Here, the bars correspond to the mean value and the error bars denote the standard deviation within the package. Mean values having the same alphabet do not vary significantly (Tukey HSD test, $p \leq 0.05$). (b) A ternary plot to compare the relative contributions of the respiration-, transpiration-, and microbiology-driven remaining shelf lives (%). The triangular coordinate system comprises three axes corresponding to the respective shelf life. In this plot, we scale each axis from 0 to 100%, where 0% corresponds to 0 h and 100% corresponds to 30 h. Every package is represented as a point in the ternary plot, and its size corresponds to the relative coefficient of variation. The coordinates of any point can be read by following the gridlines corresponding to the respective axes. The centroid is indicated as the green dot and corresponds to the coordinates (33.33%, 33.33%, 33.33%). Image credits: This figure has been designed using resources from Flaticon.com.

Our analysis shows that the respiration-driven biochemical shelf life of the fruit does not vary much for the packages. One of the reasons could be that strawberries have a small Biot number, particularly at lower air speeds, for all the package (Supplementary materials Section A.1). This is mainly because the fruit are small in size and rapidly equilibrate to the air temperature. Therefore, the thermal evolution of the fruit is similar in all the packages. The time scales of respiration-driven quality loss are much larger than those of heat transfer in our study. Therefore, the changes in temperature that are found between the packages do not give rise to large differences in quality attributes. On the other hand, we see that the other two driving processes, *i.e.*, transpiration and condensation-related microbial risk, show a trade-off. Flow-wrapped packages have the least moisture loss and therefore, the berries do not lose much moisture. However, these packages also have the highest risk of condensation, which is reflected in the short shelf life from a microbiological perspective.

To analyze which package(s) perform best in balancing the three-way trade-off, we created a ternary plot to capture the relative shelf life based on these three driving processes (Figure 17 b). Here, we plotted the ratios of the three shelf lives as points in a triangular coordinate system. Additionally, the radius of the points reflects the coefficient of variation, so the heterogeneity within the package. The optimal package balancing all shelf lives would ideally lie at the centroid of such a ternary plot and would have the smallest radius. In Fig. b, we see that flow-wrapped packages steer far from this balance, as the microbial shelf life is extremely small. Clamshells show a wide spread, which can be attributed to factors such as differences in their total open area in the flow direction, vent positions, and degree of filling. For example, clamshells *C1* and *C6* have the lowest total open area in the flow direction, and therefore, are aligned next to flow-wrapped packages in the ternary plot. On the other hand, clamshell *C5* has the

highest total open area (1.74%), and therefore, transpiration-driven shelf life is limiting for the fruit in this package due to expedited moisture loss.

Based on our study, for 250 g packages, the top-sealed reclosable package (*T1*, $TOA_{\text{flow}} = 0.52\%$) and the clamshell (*C4*, $TOA_{\text{flow}} = 1.06\%$) are the most consistent package from farm to fork. These packages also shows a small inter-fruit variation within the package, particularly because the fruit are arranged in a single layer. For larger fruit volumes (400 - 500 g), the inter-fruit variation within the package is much higher, evident from the larger radii of the points in the ternary plot. Amongst the three 400 g rounded-square clamshells evaluated, the clamshell with the largest total open area was the closest to the optima (*C7*; $TOA_{\text{flow}} = 0.49\%$). Amongst the analyzed 500 g packages, the open punnet tray (*O2*) performs the best in balancing the trade-off between maintaining quality, minimizing mass loss, and avoiding microbiological spoilage.

4 OUTLOOK

Selecting the optimal package, based on the supply chain that it will be used in, is an effective way to reduce food loss and waste at all stages of the supply chain with limited additional effort or cost. Changing the package is a cost-effective solution that can flexibly be implemented in commercial supply chains. From a practical standpoint, our findings about the performance of various packages in different unit operations can serve as a decision support tool for supply chain stakeholders. For example, handlers at the beginning of a supply chain, such as at the pack house, can select the most suitable packaging if they have access to product-specific or process-specific information about the supply chain. Product-specific information entails 'where are the fruit coming from'. This could include information on the fruit cultivar, growing conditions, and initial fruit quality, amongst others. In a case where strawberries were cultivated in open fields or harvested in a season with rainfall, the airborne concentration of *B. cinerea* spores is much higher and can reach up to 100 spores·m⁻³ (González-Fernández et al., 2021). In such a case, mitigating condensation-linked microbiological risk would be the main criteria that the handler should take into account when selecting the packaging. Flow-wrapped packages would not be a suitable choice here. Therefore, the packaging can be adapted based on every growing season. Process-specific information implies 'where are the fruit going to'. This implies information on the intended supply chain, the final destination to which the berries being transported, and the set of unit operations that are aligned along the supply chain. For strawberries that are transported over long distances, flow-wrapped packaging is not recommended as these packages are most susceptible to condensation during transportation and storage. Locally-produced berries can be packaged in open punnet trays or even traditional meshed berry baskets. As the supply chains are shorter and often transportation times are reduced to 4-6 hours, therefore moisture loss during transportation is small. However, we are aware that the choice of packaging is also determined by other drivers, such as the appearance in the retail stores, the prevention of damage, costs, and sustainability.

Additionally, our findings can aid interventions for designing efficient supply chains for certain batches of fruit. For instance, distributors in a warehouse can manage logistics in a way that fruit packed in open trays are delivered to large retail stores that have the infrastructure for refrigerated display cases, to reduce moisture loss during retail. Fruit in more robust packages, such as ventilated clamshells or top-sealed recloseable trays, could be distributed to smaller retail stores that lack cooling infrastructure. Future studies could include the interaction between several packages in secondary and tertiary packaging. The effect of airflow from multiple directions (vertical, horizontal, mixed) can also be investigated. Additionally, complementing this physics-based model with statistical models for biological variability would increase the relevance and application of this study, such as by considering the differences in the initial fruit quality, ripening stage, or fruit size.

5 CONCLUSIONS

In this study, we developed physics-based digital twins to mimic the complete lifecycle of strawberries from farm to the retail store for 21 ventilated packages. By identifying the weak links of the supply chain for every package, we develop a requirement-driven approach to select the optimal packaging (Cagnon et al., 2013). Our main conclusions are summarized below:

1. Packaging should be selected based on the specific supply chain it is intended for. The strengths and weaknesses of different packages are identified. Flow-wrapped packages show the highest risk of condensation, particularly during storage unit operations.
2. The total open area in the flow direction is the main package design parameter influencing fruit quality and marketability metrics. The total open area in the flow direction is positively correlated with the moisture loss, and negatively correlated with the mean fruit temperature and risk of condensation. The headspace volume is mainly correlated with the variability or heterogeneity in fruit quality within the package.
3. We observe a large variability in fruit quality metrics within the same package. The fruit in the topmost layer lose the highest moisture, whereas the fruit in the middle layers have the highest risk of condensation and mold spoilage. The fruit next to the vents have the lowest temperature. The stacking of fruit in layers also plays a key role in the packaging performance.
4. Complex trade-offs in package design require a holistic approach for selecting the package. A key trade-off is that between moisture loss and the risk of condensation. We therefore identify the optimal package for different stock-keeping units based on the respiration-driven, transpiration-driven, and microbiology-driven shelf lives. We identified that for larger fruit volumes (500 g), the open top (unlidded) package provided the best balance between these shelf lives, although the heterogeneity in fruit quality within the package was large. Future packages can therefore aim at optimizing vent positions to improve uniformity within the package.
5. The performance of open (unlidded) trays is comparable to ventilated clamshells throughout the cold chain, as long as a high relative humidity is maintained (80±3%). However, under ambient storage conditions at retail, moisture loss is aggravated in open trays, especially for the fruit in the top layers. Targeted solutions, such as dry misting, can be

implemented to mitigate mass loss at retail. In this way, we can steer towards open packages that use the least material possible (and even cardboard), while not compromising on package performance and fruit quality.

We could successfully show the added value of using simulations to evaluate package design, compared to experiments. We could test each fruit in the package virtually and have access to information of the fruit pulp and phenomena occurring at the fruit surface. By feeding our models with sensor data from real supply chains, we could, in the future, mimic how each single shipment evolves throughout the supply chain. Upon arrival at the packhouse or retailer, we then have a set of quality attributes which we can use to evaluate the shipment, in addition to the standard quality control.

Moreover, our approach of physics-based digital twins of fruit packages can expedite the process of designing new packages, enabling 'crash-testing' of solutions. Several combinations of material types, package sizes, and vent designs can be tested rapidly, thus considerably reducing the number of experimental trials needed. This is more so relevant today, as consumers and retailers are showing an increasing interest in transitioning towards sustainable packaging solutions (Fadji et al., 2018). A key question that is worthwhile to investigate is whether recyclable cardboard trays could perform equivalent to, or better than plastic punnets. Future studies could also consider the direct environmental impact of the packaging and its indirect impact of food waste reduction as performance metrics through Life Cycle Analysis (LCA) (Coffigniez et al., 2021). Altogether, we present a systemic approach to capture the complexity in selecting the optimal fruit package considering the full length of the supply chain and breadth of factors impacting fruit quality. This can contribute towards making future supply chains robust, smart, and efficient.

Acknowledgments

We thank Donato Rubinetti and Jörg Schemminger for fruitful discussions towards building the model. We acknowledge the support of Mr. Zoran Vidakovic from COMSOL Multiphysics. We would like to thank Dr. Günter Grossmann for his support in setting up the climate chamber experiments.

Funding

The authors declare that this study received funding from the *Coop Sustainability Fund* and the *Swiss National Science Foundation SNSF* (project 200021_169372). The funder was not involved in the analysis, interpretation of data, the writing of this article or the decision to submit it for publication.

Author Contributions

Chandrima Shrivastava: Conceptualization; Data curation; Formal analysis; Investigation; Methodology; Visualization; Writing - original draft.

Seraina Schudel: Conceptualization; Data curation; Writing - review & editing.

Kanaha Shoji: Data curation; Writing - review & editing.

Daniel Onwude: Writing - review & editing.

Fatima Pereira da Silva: Writing - review & editing.

Deniz Turan: Writing - review & editing.

Maxence Paillart: Writing - review & editing.

Thijs Defraeye: Conceptualization; Funding acquisition; Project administration; Supervision; Writing - review & editing.

REFERENCES

- Abd-Elkader, D.Y., Salem, M.Z.M., Komeil, D.A., Al-Huqail, A.A., Ali, H.M., Salah, A.H., Akrami, M., Hassan, H.S., 2021. Post-Harvest Enhancing and Botrytis cinerea Control of Strawberry Fruits Using Low Cost and Eco-Friendly Natural Oils. *Agronomy* 2021, Vol. 11, Page 1246 11, 1246. <https://doi.org/10.3390/AGRONOMY11061246>
- Alves, J.A.V., Steffens, C.A., Silva, J.C. da, Pansera-Espíndola, B., Amarante, C.V.T. do, Moreira, M.A., 2021. Quality of 'San Andreas' strawberries and control of gray mold with essential melaleuca oil. *J Food Process Preserv* e16130. <https://doi.org/10.1111/JFPP.16130>
- Ambaw, A., Fadji, T., Opara, U.L., 2021. Thermo-Mechanical Analysis in the Fresh Fruit Cold Chain: A Review on Recent Advances. *Foods* 2021, Vol. 10, Page 1357 10, 1357. <https://doi.org/10.3390/FOODS10061357>
- ASHRAE, 2010. Thermal properties of foods, in: 2010 ASHRAE Handbook: Refrigeration. Atlanta: ASHRAE, pp. 19.1-19.31.
- Auras, R.A., Singh, S.P., Singh, J.J., 2005. Evaluation of oriented poly(lactide) polymers vs. existing PET and oriented PS for fresh food service containers. *Packaging Technology and Science* 18, 207–216. <https://doi.org/10.1002/pts.692>
- Ayala-Zavala, J.F., Wang, S.Y., Wang, C.Y., González-Aguilar, G.A., 2004. Effect of storage temperatures on antioxidant capacity and aroma compounds in strawberry fruit. *LWT - Food Science and Technology* 37, 687–695. <https://doi.org/10.1016/J.LWT.2004.03.002>
- Bai, J., Baldwin, E., Tsantili, E., Plotto, A., Sun, X., Wang, L., Kafkaletou, M., Wang, Z., Narciso, J., Zhao, W., Xu, S., Seavert, C., Yang, W., 2019. Modified humidity clamshells to reduce moisture loss and extend storage life of small fruits*. *Food Packag Shelf Life* 22, 100376. <https://doi.org/10.1016/J.FPSL.2019.100376>
- Bastarrachea, L., Dhawan, S., Sablani, S.S., 2011. Engineering Properties of Polymeric-Based Antimicrobial Films for Food Packaging. *Food Engineering Reviews* 3, 79–93. <https://doi.org/10.1007/s12393-011-9034-8>
- Becker, B.R., Misra, A., Fricke, B.A., 1996. Bulk refrigeration of fruits and vegetables part I: Theoretical considerations of heat and mass transfer. *HVAC and R Research* 2, 122–134. <https://doi.org/10.1080/10789669.1996.10391338>
- Belbahi, A., Leguerinel, I., Méot, J.-M., Loiseau, G., Madani, K., Bohuon, P., 2016. Modelling the effect of temperature, water activity and carbon dioxide on the growth of *Aspergillus niger* and *Alternaria alternata* isolated from fresh date fruit. *J Appl Microbiol* 121, 1685–1698. <https://doi.org/10.1111/jam.13296>
- Berry, T.M., Defraeye, T., Nicolai, B.M., Opara, U.L., 2016. Multiparameter analysis of cooling efficiency of ventilated fruit cartons using CFD: Impact of vent hole design and internal packaging. *Food Bioproc Tech* 9, 1481–1493. <https://doi.org/10.1007/s11947-016-1733-y>
- Boulard, T., Chave, M., Fatnassi, H., Nieto, C., Poncet, C., 2006. Botrytis spore balance of a greenhouse rose crop. *Acta Hort* 719, 587–595. <https://doi.org/10.17660/ACTAHORTIC.2006.719.68>
- Bovi, G.G., Caleb, O.J., Rauh, C., Mahajan, P. V., 2019. Condensation regulation of packaged strawberries under fluctuating storage temperature. *Packaging Technology and Science* 32, 545–554. <https://doi.org/10.1002/pts.2470>
- Bovi, G.G., Rux, G., Caleb, O.J., Herppich, W.B., Linke, M., Rauh, C., Mahajan, P. V., 2018. Measurement and modelling of transpiration losses in packaged and unpackaged strawberries. *Biosyst Eng* 174, 1–9. <https://doi.org/10.1016/J.BIOSYSTEMSENG.2018.06.012>
- Briffa, M., Lane, S.M., Chapin, K.J., Peixoto, P.E.C., 2020. Using ternary plots to investigate continuous variation in animal contest strategies. *Anim Behav* 167, 85–99. <https://doi.org/10.1016/J.ANBEHAV.2020.06.006>
- Cagnon, T., Méry, A., Chalier, P., Guillaume, C., Gontard, N., 2013. Fresh food packaging design: A requirement driven approach applied to strawberries and agro-based materials 20, 288–298.
- Caner, C., Aday, M.S., Demir, M., 2008. Extending the quality of fresh strawberries by equilibrium modified atmosphere packaging. *European Food Research and Technology* 227, 1575–1583. <https://doi.org/10.1007/s00217-008-0881-3>
- Cao, Y., Gong, Y.-F., Zhang, X.-R., 2020. Impact of ventilation design on the precooling effectiveness of horticultural produce—a review. *Food Quality and Safety* 4, 29–40. <https://doi.org/10.1093/fqsafe/fyaa004>
- Cardoso, G., Labuza, T.P., 1983. Prediction of moisture gain and loss for packaged pasta subjected to a sine wave temperature/humidity environment. *Int J Food Sci Technol* 18, 587–606. <https://doi.org/10.1111/J.1365-2621.1983.TB00299.X>
- Carisse, O., 2015. Epidemiology and aerobiology of Botrytis spp, in: *Botrytis - The Fungus, the Pathogen and Its Management in Agricultural Systems*. Springer International Publishing, pp. 127–148. https://doi.org/10.1007/978-3-319-23371-0_7
- Céline, M., Valérie, G., Karine, G., Sandrine, C., Nathalie, G., Stéphane, G., Sébastien, G., 2020. Consumer behaviour in the prediction of postharvest losses reduction for fresh strawberries packed in modified atmosphere packaging. *Postharvest Biol Technol* 163, 111119. <https://doi.org/10.1016/J.POSTHARVBIO.2020.111119>
- Chirife, J., Fontan, C.F., 1982. Water Activity of Fresh Foods. *J Food Sci* 47, 661–663. <https://doi.org/10.1111/j.1365-2621.1982.tb10145.x>

- Ciliberti, N., Fermaud, M., Roudet, J., Languasco, L., Rossi, V., 2016. Environmental effects on the production of *Botrytis cinerea* conidia on different media, grape bunch trash, and mature berries. *Aust J Grape Wine Res* 22, 262–270. <https://doi.org/10.1111/ajgw.12217>
- Ciliberti, N., Fermaud, M., Roudet, J., Rossi, V., 2015. Environmental Conditions Affect *Botrytis cinerea* Infection of Mature Grape Berries More Than the Strain or Transposon Genotype. *Phytopathology* 105, 1090–1096. <https://doi.org/10.1094/PHYTO-10-14-0264-R>
- Coffigniez, F., Matar, C., Gaucel, S., Gontard, N., Guilbert, S., Guillard, V., 2021. The Use of Modeling Tools to Better Evaluate the Packaging Benefice on Our Environment. *Front Sustain Food Syst* 5, 111. <https://doi.org/10.3389/FSUFS.2021.634038/BIBTEX>
- Collins, J.K., Perkins-Veazie, P., 1993. Postharvest changes in strawberry fruit stored under simulated retail display conditions. *J Food Qual* 16, 133–143. <https://doi.org/10.1111/j.1745-4557.1993.tb00356.x>
- Concha-Meyer, A., Eifert, J., Wang, H., Sanglay, G., 2018. Volume estimation of strawberries, mushrooms, and tomatoes with a machine vision system. <https://doi.org/10.1080/10942912.2018.1508156> 21, 1867–1874. <https://doi.org/10.1080/10942912.2018.1508156>
- Corradini, M.G., 2018. Shelf life of food products: From open labeling to real-time measurements. *Annu Rev Food Sci Technol* 9, 251–269. <https://doi.org/10.1146/annurev-food-030117-012433>
- Dagnas, S.P., Membré, J.M., 2013. Predicting and preventing mold spoilage of food products. *J Food Prot.* <https://doi.org/10.4315/0362-028X.JFP-12-349>
- Dantigny, P., Bensoussan, M., Vasseur, V., Lebrihi, A., Buchet, C., Ismaili-Alaoui, M., Devlieghere, F., Roussos, S., 2006. Standardisation of methods for assessing mould germination: A workshop report, in: *International Journal of Food Microbiology*. Elsevier, pp. 286–291. <https://doi.org/10.1016/j.ijfoodmicro.2005.12.005>
- Dantigny, P., Marín, S., Beyer, M., Magan, N., 2007. Mould germination: Data treatment and modelling. *Int J Food Microbiol* 114, 17–24. <https://doi.org/10.1016/j.ijfoodmicro.2006.11.002>
- Dantigny, P., Soares Mansur, C., Sautour, M., Tchobanov, I., Bensoussan, M., 2002. Relationship between spore germination kinetics and lag time during growth of *Mucor racemosus*. *Lett Appl Microbiol* 35, 395–398. <https://doi.org/10.1046/j.1472-765X.2002.01214.x>
- Defraeye, T., Cronjé, P., Berry, T., Opara, U.L., East, A., Hertog, M., Verboven, P., Nicolai, B., 2015. Towards integrated performance evaluation of future packaging for fresh produce in the cold chain. *Trends Food Sci Technol* 44, 201–225. <https://doi.org/10.1016/J.TIFS.2015.04.008>
- Defraeye, T., Nicolai, B., Kirkman, W., Moore, S., Niekerk, S.V., Verboven, P., Cronjé, P., 2016. Integral performance evaluation of the fresh-produce cold chain: A case study for ambient loading of citrus in refrigerated containers. *Postharvest Biol Technol* 112, 1–13. <https://doi.org/10.1016/j.postharvbio.2015.09.033>
- Defraeye, T., Shrivastava, C., Berry, T., Verboven, P., Onwude, D., Schudel, S., Bühlmann, A., Cronje, P., Rossi, R.M., 2021. Digital twins are coming: Will we need them in supply chains of fresh horticultural produce? *Trends Food Sci Technol.* <https://doi.org/10.1016/j.tifs.2021.01.025>
- Defraeye, T., Tagliavini, G., Wu, W., Prawiranto, K., Schudel, S., Kerisima, M.A., Verboven, P., Bühlmann, A., Assefa Kerisima, M., Verboven, P., Bühlmann, A., 2019. Digital twins probe into food cooling and biochemical quality changes for reducing losses in refrigerated supply chains. *Resour Conserv Recycl* 149, 778–794. <https://doi.org/10.1016/j.resconrec.2019.06.002>
- Dehghannya, J., Ngadi, M., Vigneault, C., 2010. Mathematical Modeling Procedures for Airflow, Heat and Mass Transfer During Forced Convection Cooling of Produce: A Review. *Food Engineering Reviews* 2, 227–243. <https://doi.org/10.1007/s12393-010-9027-z>
- Den Aantrekker, E.D., Beumer, R.R., Van Gerwen, S.J.C., Zwietering, M.H., Van Schothorst, M., Boom, R.M., 2003. Estimating the probability of recontamination via the air using Monte Carlo simulations. *Int J Food Microbiol* 87, 1–15. [https://doi.org/10.1016/S0168-1605\(03\)00041-2](https://doi.org/10.1016/S0168-1605(03)00041-2)
- Etuk, S., Akpabio, L.E., Ikot, A.N., Udoimuk, A., Ekpe, S., 2011. Thermal Transport of Naturally Season Dried *Elaeis Guineensis* (Oil Plam) Tree Trunk. *Fundamental Journal of Thermal Science and Engineering* 1, 1–13.
- Exama, A., Arul, J., Lencki, R.W., Lee, L.Z., Toupin, C., 1993. Suitability of Plastic Films for Modified Atmosphere Packaging of Fruits and Vegetables. *J Food Sci* 58, 1365–1370. <https://doi.org/10.1111/J.1365-2621.1993.TB06184.X>
- Fabbi, S., Olsen, S.I., Owsianiak, M., 2018. Improving environmental performance of post-harvest supply chains of fruits and vegetables in Europe: Potential contribution from ultrasonic humidification. *J Clean Prod* 182, 16–26. <https://doi.org/10.1016/J.JCLEPRO.2018.01.157>
- Fadji, T., Coetzee, C.J., Berry, T.M., Ambaw, A., Opara, U.L., 2018. The efficacy of finite element analysis (FEA) as a design tool for food packaging: A review. *Biosyst Eng.* <https://doi.org/10.1016/j.biosystemseng.2018.06.015>
- Fedele, G., González-Domínguez, E., Rossi, V., 2020. Influence of Environment on the Biocontrol of *Botrytis cinerea*: A Systematic Literature Review, in: *Progress in Biological Control*. Springer, Cham, pp. 61–82. https://doi.org/10.1007/978-3-030-53238-3_5

- Ferrua, M.J., Singh, R.P., 2011a. Improved airflow method and packaging system for forced-air cooling of strawberries. *International Journal of Refrigeration* 34, 1162–1173. <https://doi.org/10.1016/j.ijrefrig.2011.01.018>
- Ferrua, M.J., Singh, R.P., 2011b. Improving the design and efficiency of the forced-air cooling process of fresh strawberries using computational modeling. *Procedia Food Sci* 1, 1239–1246. <https://doi.org/10.1016/J.PROFOO.2011.09.184>
- Ferrua, M.J., Singh, R.P., 2009a. Modeling the forced-air cooling process of fresh strawberry packages, Part I: Numerical model. *International Journal of Refrigeration* 32, 335–348. <https://doi.org/10.1016/j.ijrefrig.2008.04.010>
- Ferrua, M.J., Singh, R.P., 2009b. Modeling the forced-air cooling process of fresh strawberry packages, Part III: Experimental validation of the energy model. *International Journal of Refrigeration* 32, 359–368.
- Garcia, D., Ramos, A.J., Sanchis, V., Marín, S., 2009. Predicting mycotoxins in foods: A review. *Food Microbiol.* <https://doi.org/10.1016/j.fm.2009.05.014>
- Garcia-Gimeno, R.M., Sanz-Martinez, C., Garcia-Martos, J.M., Zurera-Cosano, G., 2002. Modeling Botrytis Cinerea Spores Growth in Carbon Dioxide Enriched Atmospheres. *J Food Sci* 67, 1904–1907. <https://doi.org/10.1111/j.1365-2621.2002.tb08744.x>
- Getahun, S., Ambaw, A., Delele, M., Meyer, C.J., Opara, U.L., 2017. Analysis of airflow and heat transfer inside fruit packed refrigerated shipping container: Part II – Evaluation of apple packaging design and vertical flow resistance. *J Food Eng* 203, 83–94. <https://doi.org/10.1016/j.jfoodeng.2017.02.011>
- Gibson, A.M., Baranyi, J., Pitt, J.I., Eyles, M.J., Roberts, T.A., 1994. Predicting fungal growth: the effect of water activity on *Aspergillus flavus* and related species. *Int J Food Microbiol* 23, 419–431. [https://doi.org/10.1016/0168-1605\(94\)90167-8](https://doi.org/10.1016/0168-1605(94)90167-8)
- Giménez, A., Ares, F., Ares, G., 2012. Sensory shelf-life estimation: A review of current methodological approaches. *Food Research International* 49, 311–325. <https://doi.org/10.1016/J.FOODRES.2012.07.008>
- González-Fernández, E., Kennedy, R., Osborn, R., Fernández-González, M., Rodríguez-Rajo, F.J., 2021. Botrytis cinerea airborne conidia and their germination ability assessed by immunological methods in a NW Spain vineyard. *Agronomy* 11, 1441. <https://doi.org/10.3390/AGRONOMY11071441/S1>
- Gottschalk, K., Linke, M., Mészáros, C., Farkas, I., 2007. Modeling condensation and evaporation on fruit surface. *Drying Technology* 25, 1237–1242. <https://doi.org/10.1080/07373930701438667>
- Gougouli, M., Koutsoumanis, K.P., 2012. Modeling germination of fungal spores at constant and fluctuating temperature conditions. *Int J Food Microbiol* 152, 153–161. <https://doi.org/10.1016/j.ijfoodmicro.2011.07.030>
- Gougouli, M., Koutsoumanis, K.P., 2010. Modelling growth of *Penicillium expansum* and *Aspergillus niger* at constant and fluctuating temperature conditions. *Int J Food Microbiol* 140, 254–262. <https://doi.org/10.1016/j.ijfoodmicro.2010.03.021>
- Guidigo, J., Molina, S., Adjovi, E.C., Merlin, A., André, D., Tagne, M.S., 2017. Polyethylene Low and High Density-Polyethylene Terephthalate and Polypropylene Blend as Matrices for Wood Flour – Plastic Composites. *International Journal of Science and Research (IJSR)* 6, 1069–1074. <https://doi.org/10.21275/ART20164296>
- Han, J.W., Qian, J.P., Zhao, C.J., Yang, X.T., Fan, B.L., 2017. Mathematical modelling of cooling efficiency of ventilated packaging: Integral performance evaluation. *Int J Heat Mass Transf* 111, 386–397. <https://doi.org/10.1016/j.ijheatmasstransfer.2017.04.015>
- Han, Y., Dang, R., Li, J., Jiang, J., Zhang, N., Jia, M., Wei, L., Li, Z., Li, B., Jia, W., 2015. Sucrose nonfermenting1-related protein kinase2.6, an ortholog of open stomata1, is a negative regulator of strawberry fruit development and ripening. *Plant Physiol* 167, 915–930. <https://doi.org/10.1104/PP.114.251314>
- Hikawa-Endo, M., 2020. Improvement in the Shelf-life of Japanese Strawberry Fruits by Breeding and Post-harvest Techniques. *Hort J* 89, 115–123. <https://doi.org/10.2503/HORTJ.UTD-R008>
- Horner, K.J., Anagnostopoulos, G.D., 1973. Combined Effects of Water Activity, pH and Temperature on the Growth and Spoilage Potential of Fungi. *Journal of Applied Bacteriology* 36, 427–436. <https://doi.org/10.1111/j.1365-2672.1973.tb04124.x>
- Hosseinifarahi, M., Jamshidi, E., Amiri, S., Kamyab, F., Radi, M., 2020. Quality, phenolic content, antioxidant activity, and the degradation kinetic of some quality parameters in strawberry fruit coated with salicylic acid and *Aloe vera* gel. *J Food Process Preserv* 44, 14647. <https://doi.org/10.1111/jfpp.14647>
- Hough, G., Garitta, L., 2012. Methodology for sensory shelf-life estimation: a review. *J Sens Stud* 27, 137–147. <https://doi.org/10.1111/J.1745-459X.2012.00383.X>
- IDMC, n.d. Polyethylene terephthalate .
- IFCO, 2022. Redefining the fresh grocery supply chain | IFCO [WWW Document]. URL <https://www.ifco.com/> (accessed 2.9.22).
- Islam, M.Z., Lee, Y.T., Mele, M.A., Choi, I.L., Kang, H.M., 2019. Effect of fruit size on fruit quality, shelf life and microbial activity in cherry tomatoes. *AIMS Agriculture and Food* 4, 340–348. <https://doi.org/10.3934/AGRFOOD.2019.2.340>
- Jalali, A., Linke, M., Geyer, M., Mahajan, P. V., 2020. Shelf life prediction model for strawberry based on respiration and transpiration processes. *Food Packag Shelf Life* 25, 100525. <https://doi.org/10.1016/J.FPSL.2020.100525>

- Jalali, A., Seiedlou, S., Linke, M., Mahajan, P., 2017. A comprehensive simulation program for modified atmosphere and humidity packaging (MAHP) of fresh fruits and vegetables. *J Food Eng* 206, 88–97.
- Jarvis, W.R., 1977. *Botryotinia and Botrytis species: taxonomy, physiology and pathogenicity - A guide to the literature*. Agriculture Canada.
- Joshi, K., Tiwari, B., Cullen, P.J., Frias, J.M., 2019. Predicting quality attributes of strawberry packed under modified atmosphere throughout the cold chain. *Food Packag Shelf Life* 21, 100354. <https://doi.org/10.1016/j.fpsl.2019.100354>
- Judet-Correia, D., Bollaert, S., Duquenne, A., Charpentier, C., Bensoussan, M., Dantigny, P., 2010. Validation of a predictive model for the growth of *Botrytis cinerea* and *Penicillium expansum* on grape berries. *Int J Food Microbiol* 142, 106–113. <https://doi.org/10.1016/j.ijfoodmicro.2010.06.009>
- King, R., 2015. A framework for an organelle-based mathematical modeling of hyphae. *Fungal Biol Biotechnol* 2, 5. <https://doi.org/10.1186/s40694-015-0014-2>
- Kuchi, V. S., Sharavani, C.S.R., 2019. Fruit Physiology and Postharvest Management of Strawberry, in: *Strawberry - Pre- and Post-Harvest Management Techniques for Higher Fruit Quality*. IntechOpen. <https://doi.org/10.5772/intechopen.84205>
- Laguerre, O., Benamara, S., Flick, D., 2010. Numerical simulation of simultaneous heat and moisture transfer in a domestic refrigerator. *International Journal of Refrigeration* 33, 1425–1433. <https://doi.org/10.1016/J.IJREFRIG.2010.04.010>
- Lahlali, R., Serrhini, M.N., Friel, D., Jijakli, M.H., 2007. Predictive modelling of temperature and water activity (solutes) on the in vitro radial growth of *Botrytis cinerea* Pers. *Int J Food Microbiol* 114, 1–9. <https://doi.org/10.1016/j.ijfoodmicro.2006.11.004>
- Latif, E., Lawrence, M., Shea, A., Walker, P., 2015. Moisture buffer potential of experimental wall assemblies incorporating formulated hemp-lime. *Build Environ* 93, 199–209. <https://doi.org/10.1016/j.buildenv.2015.07.011>
- Lee, S., Lee, D.K., 2018. What is the proper way to apply the multiple comparison test? *Korean J Anesthesiol* 71, 353. <https://doi.org/10.4097/KJA.D.18.00242>
- Leithner, M., Fikar, C., 2019. A simulation model to investigate impacts of facilitating quality data within organic fresh food supply chains. *Ann Oper Res* 1–22. <https://doi.org/10.1007/S10479-019-03455-0/FIGURES/8>
- Leyronas, C., Fatnassi, H., Bardin, M., Boulard, T., Nicot, P., 2011. Modelling *Botrytis cinerea* spore exchanges and production in unheated greenhouses. *Journal of Plant Pathology* 2 (93), 407-414. (2011). <https://doi.org/10.3/JQUERY-UI.JS>
- Leyronas, C., Nicot, P.C., 2013. Monitoring viable airborne inoculum of *Botrytis cinerea* in the South-East of France over 3 years: Relation with climatic parameters and the origin of air masses. *Aerobiologia (Bologna)* 29, 291–299. <https://doi.org/10.1007/S10453-012-9280-0/FIGURES/4>
- Li, C., Tang, H., Wang, J., Zhong, Z., Li, J., Wang, H., 2021. Field study to characterize customer flow and ventilation rates in retail buildings in Shenzhen, China. *Build Environ* 197, 107837. <https://doi.org/10.1016/J.BUILDENV.2021.107837>
- Li, L., Lichter, A., Kenigsbuch, D., Porat, R., 2015. Effects of Cooling Delays at the Wholesale Market on the Quality of Fruit and Vegetables after Retail Marketing. *J Food Process Preserv* 39, 2533–2547. <https://doi.org/10.1111/JFPP.12504>
- Liguori, G., Sortino, G., Gullo, G., Inglese, P., 2021. Effects of Modified Atmosphere Packaging and Chitosan Treatment on Quality and Sensorial Parameters of Minimally Processed cv. 'Italia' Table Grapes. *Agronomy* 2021, Vol. 11, Page 328 11, 328. <https://doi.org/10.3390/AGRONOMY11020328>
- Linke, M., 2019. Display cabinets for perishables with atmospheric evaporation cooling, in: *Integrated View of Fruit & Vegetable Quality*. CRC Press, pp. 259–267. <https://doi.org/10.1201/9781351073769-35>
- Linke, M., Geyer, M., 2013. Condensation dynamics in plastic film packaging of fruit and vegetables. *J Food Eng* 116, 144–154. <https://doi.org/10.1016/j.jfoodeng.2012.11.026>
- Linke, M., Praeger, U., Mahajan, P. V., Geyer, M., 2021. Water vapour condensation on the surface of bulky fruit: Some basics and a simple measurement method. *J Food Eng* 307, 110661. <https://doi.org/10.1016/J.JFOODENG.2021.110661>
- Lopes, C.M.A., Felisberti, M.I., 2004. Thermal conductivity of PET/(LDPE/Al) composites determined by MDSC. *Polym Test* 23, 637–643. <https://doi.org/10.1016/J.POLYMERTESTING.2004.01.013>
- Lufu, R., Ambaw, A., Opara, U.L., 2021. The Influence of Internal Packaging (Liners) on Moisture Dynamics and Physical and Physiological Quality of Pomegranate Fruit during Cold Storage. *Foods* 2021, Vol. 10, Page 1388 10, 1388. <https://doi.org/10.3390/FOODS10061388>
- Manteau, S., Abouna, S., Lambert, B., Legendre, L., 2003. Differential regulation by ambient pH of putative virulence factor secretion by the phytopathogenic fungus *Botrytis cinerea*. *FEMS Microbiol Ecol* 43, 359–366. <https://doi.org/10.1111/j.1574-6941.2003.tb01076.x>
- Mascheroni, R.H., 2012. Special Precooling Techniques, in: Mascheroni, R.H. (Ed.), *Operations in Food Refrigeration*. CRC Press, pp. 298–299. <https://doi.org/10.1201/B12137/OPERATIONS-FOOD-REFRIGERATION-RODOLFO-MASCHERONI>
- Matar, C., Gaucel, S., Gontard, N., Guilbert, S., Guillard, V., 2018. Predicting shelf life gain of fresh strawberries 'Charlotte cv' in modified atmosphere packaging. *Postharvest Biol Technol* 142, 28–38. <https://doi.org/10.1016/J.POSTHARVBIO.2018.03.002>

- Mercier, S., Villeneuve, S., Mondor, M., Uysal, I., 2017. Time-temperature management along the food cold chain: a review of recent developments. *Compr Rev Food Sci Food Saf* 16, 647–667. <https://doi.org/10.1111/1541-4337.12269>
- Mitchell, F.G., Guillou, R., Parsons, R.A., 1972. Commercial cooling of fruits and vegetables. *Commercial cooling of fruits and vegetables*.
- Nalbandi, H., Seiedlou, S., 2020. Exploration of heat and momentum transfer in turbulent mode during the precooling process of fruit. *Food Sci Nutr* 8, 4098–4111. <https://doi.org/10.1002/FSN3.1682>
- Nalbandi, H., Seiedlou, S., Ghasemzadeh, H.R., Rangbar, F., 2016. Innovative Parallel Airflow System for forced-air cooling of strawberries. *Food and Bioproducts Processing* 100, 440–449.
- Ngo, I.L., Jeon, S., Byon, C., 2016. Thermal conductivity of transparent and flexible polymers containing fillers: A literature review. *Int J Heat Mass Transf* 98, 219–226. <https://doi.org/10.1016/J.IJHEATMASSTRANSFER.2016.02.082>
- Norton, T., Tiwari, B., Sun, D.W., 2012. Computational Fluid Dynamics in the Design and Analysis of Thermal Processes: A Review of Recent Advances. <http://dx.doi.org/10.1080/10408398.2010.518256> 53, 251–275. <https://doi.org/10.1080/10408398.2010.518256>
- Nunes, M.C. do N., 2009. Soft Fruits and Berries, in: *Color Atlas of Postharvest Quality of Fruits and Vegetables*. Blackwell Publishing Ltd., Oxford, UK, pp. 137–189. <https://doi.org/10.1002/9780813802947.ch3>
- Nunes, M.C. do Nascimento., 2008. Color atlas of postharvest quality of fruits and vegetables. John Wiley & Sons.
- Nunes, M.C.N., Brecht, J.K., Sargent, S.A., Morais, A.M.M.B., 1995. Effects of delays to cooling and wrapping on strawberry quality (cv. Sweet Charlie). *Food Control* 6, 323–328. [https://doi.org/10.1016/0956-7135\(95\)00024-0](https://doi.org/10.1016/0956-7135(95)00024-0)
- Odusote, J.K., Onowuma, S.A., Fodeke, E.A., 2016. Production of Paperboard Briquette Using Waste Paper and Sawdust. *The Journal of Engineering Research [TJER]* 13, 80–88. <https://doi.org/10.24200/TJER.VOL13ISS1PP80-88>
- Opara, U.L., Zou, Q., 2007. Sensitivity analysis of a CFD modelling system for airflow and heat transfer of fresh food packaging: Inlet air flow velocity and inside-package configurations. *International Journal of Food Engineering* 3, 1–13. <https://doi.org/10.2202/1556-3758.1263>
- OriginLab, 2022. Origin® 2022.
- Panasenko, V.T., 1967. Ecology of microfungi. *The Botanical Review* 33, 189–215. <https://doi.org/10.1007/BF02858637>
- Panda, A.K., Goyal, R.K., Godara, A.K., Sharma, V.K., 2016. Effect of packaging materials on the shelf-life of strawberry cv. Sweet Charlie under room temperature storage. *Journal of Applied and Natural Science* 8, 1290–1294. <https://doi.org/10.31018/jans.v8i3.955>
- Pathare, P.B., Opara, U.L., Vigneault, C., Delele, M.A., Al-Said, F.A.J., 2012. Design of Packaging Vents for Cooling Fresh Horticultural Produce. *Food Bioproc Tech*. <https://doi.org/10.1007/s11947-012-0883-9>
- Paul, D.R., Clarke, R., 2002. Modeling of modified atmosphere packaging based on designs with a membrane and perforations. *J Memb Sci* 208, 269–283. [https://doi.org/10.1016/S0376-7388\(02\)00303-4](https://doi.org/10.1016/S0376-7388(02)00303-4)
- Petrash, S., Knapp, S.J., van Kan, J.A.L., Blanco-Ulate, B., 2019. Grey mould of strawberry, a devastating disease caused by the ubiquitous necrotrophic fungal pathogen *Botrytis cinerea*. *Mol Plant Pathol*. <https://doi.org/10.1111/mpp.12794>
- Poós, T., Varju, E., 2020. Mass transfer coefficient for water evaporation by theoretical and empirical correlations. *Int J Heat Mass Transf* 153, 119500. <https://doi.org/10.1016/J.IJHEATMASSTRANSFER.2020.119500>
- Porat, R., Lichter, A., Terry, L.A., Harker, R., Buzby, J., 2018. Postharvest losses of fruit and vegetables during retail and in consumers' homes: Quantifications, causes, and means of prevention, *Postharvest Biology and Technology*.
- Prosser, J.I., Tough, A.J., 1991. Growth mechanisms and growth kinetics of filamentous microorganisms. *Crit Rev Biotechnol* 10, 253–274. <https://doi.org/10.3109/07388559109038211>
- R Core Team, 2020. R: A Language and Environment for Statistical Computing.
- Rahman, M.M., Moniruzzaman, M., Ahmad, M.R., Sarker, B.C., Khurshid Alam, M., 2016. Maturity stages affect the postharvest quality and shelf-life of fruits of strawberry genotypes growing in subtropical regions. *Journal of the Saudi Society of Agricultural Sciences* 15, 28–37. <https://doi.org/10.1016/J.JSSAS.2014.05.002>
- Ramirez, J.A., Castanon-Rodriguez, J.F., Uresti-Marin, R.M., 2020. An exploratory study of possible food waste risks in supermarket fruit and vegetable sections. *Food Science and Technology*. <https://doi.org/10.1590/fst.27320>
- Ranjbaran, M., Carciofi, B.A.M., Datta, A.K., 2021. Engineering modeling frameworks for microbial food safety at various scales. *Compr Rev Food Sci Food Saf* 20, 4213–4249. <https://doi.org/10.1111/1541-4337.12818>
- Revelle, W., 2021. Procedures for Psychological, Psychometric, and Personality Research [R package psych version 2.1.9].
- Ribeiro, C., Vicente, A.A., Teixeira, J.A., Miranda, C., 2007. Optimization of edible coating composition to retard strawberry fruit senescence. *Postharvest Biol Technol* 44, 63–70. <https://doi.org/10.1016/j.postharvbio.2006.11.015>

- Robinson, J.E., Browne, K.M., Burton, W.G., 1975. Storage characteristics of some vegetables and soft fruits. *Annals of Applied Biology* 81, 399–408. <https://doi.org/10.1111/j.1744-7348.1975.tb01656.x>
- Rosso, L., Lobry, J.R., Bajard, S., Flandrois, J.P., 1995. Convenient Model To Describe the Combined Effects of Temperature and pH on Microbial Growth. *Appl Environ Microbiol* 61, 610–616. <https://doi.org/10.1128/AEM.61.2.610-616.1995>
- Rosso, L., Robinson, T.P., 2001. A cardinal model to describe the effect of water activity on the growth of moulds. *Int J Food Microbiol* 63, 265–273. [https://doi.org/10.1016/S0168-1605\(00\)00469-4](https://doi.org/10.1016/S0168-1605(00)00469-4)
- Saito, S., Margos, D., Michailides, T.J., Xiao, C.L., 2016. *Botrytis californica*, a new cryptic species in the *B. cinerea* species complex causing gray mold in blueberries and table grapes. *Mycologia* 108, 330–343. <https://doi.org/10.3852/15-165>
- Sardella, D., Gatt, R., Valdramidis, V.P., 2018. Modelling the growth of pear postharvest fungal isolates at different temperatures. *Food Microbiol* 76, 450–456. <https://doi.org/10.1016/j.fm.2018.07.010>
- Schweizer Obstverband (Fruit-Union Suisse), 2005. Normen und Vorschriften für Früchte - 5.
- Sephton-Clark, P.C.S., Voelz, K., 2018. Spore Germination of Pathogenic Filamentous Fungi. *Adv Appl Microbiol* 102, 117–157. <https://doi.org/10.1016/BS.AAMBS.2017.10.002>
- Sernaite, L., Rasiukeviciute, N., Valiūškaite, A., 2020. Application of plant extracts to control postharvest gray mold and susceptibility of apple fruits to *B. cinerea* from different plant hosts. *Foods* 9. <https://doi.org/10.3390/foods9101430>
- Shoji, K., Schudel, S., Onwude, D., Shrivastava, C., Defraeye, T., 2022. Mapping the postharvest life of imported fruits from packhouse to retail stores using physics-based digital twins. *Resour Conserv Recycl* 176, 105914. <https://doi.org/10.1016/J.RESCONREC.2021.105914>
- Siu, A., 2014. An Analysis of Food Waste in Ontario's Domestic Fresh Strawberry Supply Chain.
- Smith, M.R., 2017. Ternary: An R Package for Creating Ternary Plots. <https://doi.org/10.5281/ZENODO.1123463>
- Snow, D., 1949. The germination of mould spores at controlled humidities. *Annals of Applied Biology* 36, 1–13. <https://doi.org/10.1111/j.1744-7348.1949.tb06395.x>
- Sousa-Gallagher, M.J., Mahajan, P. V., 2013. Integrative mathematical modelling for MAP design of fresh-produce: Theoretical analysis and experimental validation. *Food Control* 29, 444–450. <https://doi.org/10.1016/J.FOODCONT.2012.05.072>
- Sousa-Gallagher, M.J., Mahajan, P. V., Mezdad, T., 2013. Engineering packaging design accounting for transpiration rate: Model development and validation with strawberries. *J Food Eng* 119, 370–376. <https://doi.org/10.1016/j.jfoodeng.2013.05.041>
- Tano, K., Kamenan, A., Arul, J., 2009. Respiration and transpiration characteristics of selected fresh fruits and vegetables. *Agronomie Africaine* 17, 103–115. <https://doi.org/10.4314/aga.v17i2.1662>
- The British Standards Institution, 2017. BS ISO 17772-1:2017 Energy performance of buildings — Assessment of overall energy performance.
- Thompson, J.F., 2016. Precooling and storage facilities, in: Gross, K.C., Wang, Y., Saltveit, M. (Eds.), *The Commercial Storage of Fruits, Vegetables, and Florist and Nursery Stocks*. United States Department of Agriculture, pp. 11–14.
- Thompson, J.F., Mitchell, F.G., Rumsay, T.R., 2008a. Commercial cooling of fruits, vegetables, and flowers. University of California, Agriculture and Natural Resources, p. 61.
- Thompson, J.F., Mitchell, F.G., Rumsey, T.R., Kasmire, R.F., Crisosto, C.H., 2008b. *Commercial Cooling of Fruits, Vegetables, and Flowers*, Revised. ed. University of California Department of Agriculture and Natural Resources, Oakland, California.
- Tijskens, L.M.M., Polderdijk, J.J., 1996. A generic model for keeping quality of vegetable produce during storage and distribution. *Agric Syst* 51, 431–452. [https://doi.org/10.1016/0308-521X\(95\)00058-D](https://doi.org/10.1016/0308-521X(95)00058-D)
- Tournas, V.H., Katsoudas, E., 2005. Mould and yeast flora in fresh berries, grapes and citrus fruits. *Int J Food Microbiol* 105, 11–17. <https://doi.org/10.1016/j.ijfoodmicro.2005.05.002>
- Trinetta, V., McDaniel, A., G. Batziakas, K., Yucel, U., Nwadike, L., Pliakoni, E., 2020. Antifungal Packaging Film to Maintain Quality and Control Postharvest Diseases in Strawberries. *Antibiotics* 9, 618. <https://doi.org/10.3390/antibiotics9090618>
- Valentas, K.J., Rotstein, Enrique., Singh, R.Paul., 1997. Kinetics of food deterioration and shelf-life prediction, in: *Handbook of Food Engineering Practice*. CRC Press, pp. 361–403.
- Valovirta, I., Vinha, J., 2004. Water vapor permeability and thermal conductivity as a function of temperature and relative humidity 16 p. <https://doi.org/10.2/JQUERY.MIN.JS>
- van Boekel, M.A.J.S., 2008. Kinetic Modeling of Food Quality: A Critical Review. *Compr Rev Food Sci Food Saf* 7, 144–158. <https://doi.org/10.1111/J.1541-4337.2007.00036.X>
- Verboven, P., Defraeye, T., Datta, A.K., Nicolai, B., 2020. Digital twins of food process operations: the next step for food process models? (accepted). *Curr Opin Food Sci*.

- Wang, D., Lai, Y., Zhao, H., Jia, B., Wang, Q., Yang, X., 2019. Numerical and Experimental Investigation on Forced-Air Cooling of Commercial Packaged Strawberries. *International Journal of Food Engineering* 15. <https://doi.org/10.1515/IJFE-2018-0384/MACHINEREADABLECITATION/RIS>
- Wang, J., Gardner, D.J., Stark, N.M., Bousfield, D.W., Tajvidi, M., 2018. Moisture and Oxygen Barrier Properties of Cellulose Nanomaterial-Based Films. *ACS Sustainable Chem. Eng* 6. <https://doi.org/10.1021/acssuschemeng.7b03523>
- Williamson, B., Duncan, G.H., Harrison, J.G., Harding, L.A., Elad, Y., Zimand, G., 1995. Effect of humidity on infection of rose petals by dry-inoculated conidia of *Botrytis cinerea*. *Mycol Res* 99, 1303–1310. [https://doi.org/10.1016/S0953-7562\(09\)81212-4](https://doi.org/10.1016/S0953-7562(09)81212-4)
- Wu, F., Misra, M., Mohanty, A.K., 2021. Challenges and new opportunities on barrier performance of biodegradable polymers for sustainable packaging. *Prog Polym Sci* 117, 101395. <https://doi.org/10.1016/J.PROGPOLYMSCI.2021.101395>
- Wu, W., Cronjé, P., Verboven, P., Defraeye, T., 2019. Unveiling how ventilated packaging design and cold chain scenarios affect the cooling kinetics and fruit quality for each single citrus fruit in an entire pallet. *Food Packag Shelf Life* 21. <https://doi.org/10.1016/j.fpsl.2019.100369>
- Xanthopoulos, G.T., Templalexis, C.G., Aleiferis, N.P., Lentzou, D.I., 2017. The contribution of transpiration and respiration in water loss of perishable agricultural products: The case of pears. *Biosyst Eng* 158, 76–85. <https://doi.org/10.1016/J.BIOSYSTEMSENG.2017.03.011>
- Xie, J., Zhao, Y., 2004. Physical and physicochemical characteristics of three U.S. strawberry cultivars grown in the Pacific Northwest. *J Food Qual* 27, 181–194. <https://doi.org/10.1111/J.1745-4557.2004.TB00648.X>
- Yahia, E.M., De Jesus Ornelas-Paz, J., Elansari, A., 2011. Postharvest technologies to maintain the quality of tropical and subtropical fruits. *Postharvest Biology and Technology of Tropical and Subtropical Fruits* 1, 142–195e. <https://doi.org/10.1533/9780857093622.142>
- Zhou, Y., Li, N., Yang, J., Yang, L., Wu, M., Chen, W., Li, G., Zhang, J., 2018. Contrast Between Orange- and Black-Colored Sclerotial Isolates of *Botrytis cinerea*: Melanogenesis and Ecological Fitness. *Plant Dis* 102, 428–436. <https://doi.org/10.1094/PDIS-11-16-1663-RE>
- Zoffoli, J.P., Latorre, B.A., Rodríguez, E.J., Aldunce, P., 1999. Modified atmosphere packaging using chlorine gas generators to prevent *Botrytis cinerea* on table grapes. *Postharvest Biol Technol* 15, 135–142. [https://doi.org/10.1016/S0925-5214\(98\)00078-7](https://doi.org/10.1016/S0925-5214(98)00078-7)
- Zwietering, M.H., De Wit, J.C., Notermans, S., 1996. Application-of predictive microbiology to estimate the number of *Bacillus cereus* in pasteurised milk at the point of consumption. *Int J Food Microbiol* 30, 55–70. [https://doi.org/10.1016/0168-1605\(96\)00991-9](https://doi.org/10.1016/0168-1605(96)00991-9)

Nomenclature

Symbols

a_w	water activity of strawberry [-]
A_s	surface area of strawberry fruit [m ²]
A_{channel}	cross-sectional area of channel [m ²]
Bi	Biot number [-]
c_l	concentration of liquid water [mol·m ⁻³]
$c_{p,a}$	specific heat capacity of air [J·kg ⁻¹ ·K ⁻¹]
$c_{p,f}$	specific heat capacity of strawberry fruit [J·kg ⁻¹ ·K ⁻¹]
$c_{p,p}$	specific heat capacity of packaging material [J·kg ⁻¹ ·K ⁻¹]
c_{sat}	saturation concentration of water vapor [mol·m ⁻³]
$c_{\text{spores, air}}$	concentration of spores in air [spores·m ⁻³]
c_v	concentration of water vapor [mol·m ⁻³]
C_{μ}	turbulence model constant [-]
$CHTC$	convective heat transfer coefficient on strawberry surface [W·m ⁻² ·K ⁻¹]
CL_{spores}	contamination level of spores [spores·berry ⁻¹]
CoV	coefficient of variation [%]
$D_{v,a}$	diffusion coefficient of water vapor in air [m ² ·s ⁻¹]
$E_{a,\text{quality}}$	activation energy of rate constant for kinetic quality model [J·mol ⁻¹]
f	pre-exponential respiration coefficient [-]
g	exponential respiration coefficient [-]
g_{Levap}	liquid water evaporation flux [kg·m ⁻² ·s ⁻¹]
$g_{v,\text{evap}}$	water vapor evaporation flux [kg·m ⁻² ·s ⁻¹]
G	source term for moisture transport [kg·m ⁻³ ·s ⁻¹]
h_p	height of the package [m]
I_f	biochemical respiration-driven fruit quality index [%]
k_T	turbulent kinetic energy [J·kg ⁻¹] or [m ² ·s ⁻²]
k_a	thermal conductivity of air [W·m ⁻¹ ·K ⁻¹]
k_f	thermal conductivity of strawberry fruit [W·m ⁻¹ ·K ⁻¹]
k_{germ}	rate of change of probability of spore germination [s ⁻¹]
k_{skin}	skin mass transfer resistance for strawberry [m·s ⁻¹]
k_p	thermal conductivity of packaging material [W·m ⁻¹ ·K ⁻¹]
$k_{0,\text{quality}}$	reference kinetic rate constant for respiration-driven quality loss [s ⁻¹]
k_{quality}	kinetic rate constant for respiration-driven quality loss [s ⁻¹]
K	evaporation rate factor [m·s ⁻¹]
l_p	length of the package [m]
M_v	molar mass of water vapor [kg·mol ⁻¹]
\mathbf{n}	normal vector [-]
n	order of reaction in the kinetic model
P	atmospheric pressure [Pa]
P_{germ}	probability of spore germination [%]
P_{max}	asymptotic maxima of probability of spore germination [%]
Q_{10}	van Hoff factor (or temperature coefficient) for reaction rates [-]
Q_{resp}	volumetric heat of respiration [W·m ⁻³]
R	universal gas constant [J·mol ⁻¹ ·K ⁻¹]
R_{BC}	radius of <i>Botrytis cinerea</i> colony [mm]
Re	Reynolds number [-]
Ri	Richardson number [-]
t	time [s]
$t_{7/8}$	seven-eighths cooling time [s]
T_a	air temperature [K]
T_f	fruit temperature [K]
TOA_{flow}	total open area in the flow direction [%]
TOA_{lateral}	total open area in the lateral direction, <i>i.e.</i> , perpendicular to the flow [%]
ToW	time of wetness due to condensation [h]
\mathbf{u}	velocity field vector
U_{inlet}	superficial air speed [m·s ⁻¹]
v_{settling}	settling velocity for spores [m·s ⁻¹]
$V_{\text{headspace}}$	headspace volume [%]
w_p	width of the package [m]
W_f	intended weight of the fruit in the stock-keeping unit [g]
x_p	thickness of packaging material [m]
y^+	non-dimensional distance from the wall to the first mesh node based on local fluid velocity [-]

Greek symbols

γ	gamma function parameterized between 0 and 1 for different biokinetic factors [-]
----------	---

δ_a	water vapor permeability of air [$\text{kg}\cdot\text{m}^{-1}\cdot\text{s}^{-1}\cdot\text{Pa}^{-1}$]
δ_p	water vapor permeability of packaging material [$\text{kg}\cdot\text{m}^{-1}\cdot\text{s}^{-1}\cdot\text{Pa}^{-1}$]
ΔH_v	latent heat of vaporization [$\text{J}\cdot\text{kg}^{-1}$]
ΔP	pressure loss across the package [Pa]
∇	vector differential operator
ε	rate of dissipation of the turbulent kinetic energy [$\text{m}^2\cdot\text{s}^{-3}$]
θ_f	fruit temperature [$^{\circ}\text{C}$]
μ	fluid viscosity [$\text{Pa}\cdot\text{s}$]
$\mu_{\text{opt},BC}$	optimal radial growth rate of <i>Botrytis cinerea</i> colony [$\text{mm}\cdot\text{d}^{-1}$]
μ_p	water vapor resistance factor [-]
$\mu_{t,BC}$	radial growth rate of <i>Botrytis cinerea</i> colony at a certain time instant [$\text{mm}\cdot\text{d}^{-1}$]
μ_T	turbulent component of viscosity [$\text{Pa}\cdot\text{s}$]
ξ	pressure loss coefficient [$\text{Pa}\cdot\text{s}^2\cdot\text{m}^{-6}$]
ρ_a	density of air [$\text{kg}\cdot\text{m}^{-3}$]
ρ_f	density of strawberry fruit [$\text{kg}\cdot\text{m}^{-3}$]
ρ_p	density of packaging material [$\text{kg}\cdot\text{m}^{-3}$]
τ	spore germination time [s]
ϕ_a	relative humidity of air [%]

Subscripts

0	reference conditions
a	air
BC	<i>Botrytis cinerea</i>
$evap$	evaporation
f	fruit
$germ$	germination
$harvest$	harvest
$headspace$	headspace of the package
in	in
$inlet$	inlet
l	liquid water
max	maximum
min	minimum
opt	optimal
out	out
p	package
$quality$	quality
sat	saturated
$skin$	skin
$spores$	spores of <i>B. cinerea</i>
$surface$	fruit surface
T	turbulent
t	time
v	vapor

Abbreviations

cv	cultivar
ANOVA	analysis of variance
CFD	computational fluid dynamics
DOF	degree of filling
GMRES	generalized minimal residual method
HSD	honestly significant differences
LDPE	low-density polyethylene
MUMPS	multifrontal massively parallel sparse direct solver
PARADISO	parallel direct sparse solver
PET	polyethylene terephthalate
PP	polypropylene
RANS	Reynolds-averaged Navier–Stokes
RH	relative humidity
R-PET	recycled polyethylene terephthalate
SKU	stock-keeping unit
TOA	total open area
ToW	time of wetness